Nonlinear three-dimensional waves on water of varying depth

By Joseph Mathew

B.Tech. Indian Institute of Technology, Madras
(1984)

M.S. University of Missouri–Rolla
(1986)

Submitted to the Department of Mechanical Engineering
in partial fulfillment of the requirements for the degree of

DOCTOR OF PHILOSOPHY

at the
Massachusetts Institute of Technology

June 1990

Signature of Author _____
Department of Mechanical Engineering
April 24 1990

Certified by _____
Triantaphyllos R. Akylas
Associate Professor of Mechanical Engineering
Thesis Supervisor

Accepted by _____
Ain Ants Sonin
Chairman, Departmental committee for graduate studies.

Nonlinear three-dimensional waves on water of varying depth

By Joseph Mathew

Submitted to the Department of Mechanical Engineering,
on April 24 1990,
in partial fulfillment of the requirements for the degree of
Doctor of Philosophy in Mechanical Engineering.

ABSTRACT

Nonlinear effects in three-dimensional water waves that propagate in wide channels with sloping sidewalls, and along the shoreline of a sloping beach, have been studied.

A theoretical model is presented for the propagation of long, weakly nonlinear water waves along a channel bounded by sloping sidewalls, on the assumption that $h_0/w \ll 1$, where $2w$ is the channel width and h_0 is the uniform depth away from the sidewalls. Owing to the non-rectangular cross-section, waves are three-dimensional in general, and the Kadomtsev–Petviashvili equation applies. When the sidewall slope is $O(1)$, an asymptotic wall boundary condition is derived that involves a single parameter, $\mathcal{A} = A/h_0^2$, where A is the area under the depth profile; for milder slopes that are $O(h_0/w)^{1/2}$, the corresponding wall boundary condition depends more seriously on the depth profile. The model is used to discuss the development of undular bores in channels of trapezoidal cross-section with sidewall slopes that are $O(1)$; the theoretical predictions are in close quantitative agreement with previous experiments and confirm the presence of significant three-dimensional effects, not accounted for by previous theories. Furthermore, computations show that the nature of three-dimensional upstream disturbances excited by transcritical forcing, for $-1 \leq \mathcal{A} \leq 1$, depends crucially on $\mathcal{A}$, and is closely related to the three-dimensional structure of the corresponding periodic waves of permanent form.

It is demonstrated using small-amplitude expansions that periodic edge waves, which propagate along the shoreline of a beach and are trapped in the offshore direction according to linear theory, can be attenuated by radiation of oblique waves out to sea owing to nonlinear self-interactions. Necessary conditions for such radiation to occur are obtained for a few beach profiles whose edge-wave dispersion relations are known in closed form. In particular, it is shown that quadratic nonlinear interactions cause the second edge-wave mode on a uniformly sloping beach of slope α to radiate when $\frac{1}{18}\pi < \alpha < \frac{1}{6}\pi$; a detailed derivation to find the amplitude of the radiated wave and the attendant decay rate of the edge wave is presented, using the full water-wave theory. Also, it is pointed out that a concomitant nonlinear mechanism can transfer energy from incoming oblique waves to subharmonic edge waves—a plausible mechanism for the generation of travelling edge waves in coastal waters.

Thesis Supervisor: Triantaphyllos R. Akylas
Title: Associate Professor of Mechanical Engineering

ACKNOWLEDGEMENTS

I thank Professor T. R. Akylas for investing much time and effort in directing my dissertation, and for much else that he has taught me both directly and by example.

I thank Professors D. J. Benney and D. K. P. Yue, who served on my thesis committee, for their interest, their questions and suggestions.

I am all too aware that this final degree is in no small measure due to the encouragement given by many other teachers, in three countries, the earliest of whom were my parents; I thank them all for being so inspiring.

This work was supported by the Office of Naval Research under project NR062-742 and by the National Science Foundation Grant MSM-8451154.

CONTENTS

FIGURES

TABLES

CHAPTER 1

INTRODUCTION

Water waves are among the most widely observed of natural phenomena. It is possible to study water waves in the laboratory, and some of their varied manifestations are amenable to detailed theoretical treatment. Yet, over the considerable span of research in this area, there have been some discoveries that suggest that more curious and interesting phenomena await discovery.

Water waves arise due to the restoring forces of gravity and surface tension, though the latter can usually be neglected unless the wavelengths are small (on the order of a few cm). The associated fluid motions are largest at the free surface and diminish with depth, the penetration depth being of the order of the wavelength. The classical gravity-water-wave theory neglects viscous effects, but still finds a difficult nonlinear problem. The nonlinearity is due to the free surface being an unknown boundary of the domain whose location must be determined as part of the solution. Accordingly, theoretical progress has been possible largely, though not solely, in the study of small-amplitude (linear) waves.

Some characteristics of water wave propagation can be understood from the linearized theory. For example, these are dispersive waves: linear sinusoidal wave modes that comprise surface disturbances will each travel with a slightly different group velocity so that long waves can be seen travelling ahead of short waves. Three-dimensionality is evident when the water depth is varying or when there are obstacles in the path of propagation. If the depth variation is mild, the resulting refraction may be obtained by constructing rays, borrowing from the theory of geometrical optics, and in the presence of obstacles, waves undergo scattering. Of particular relevance to this thesis is the uniquely three-dimensional feature of wave trapping in the vicinity of sloping beaches.

It has long been recognized that the linear theory must be supplemented by addressing the essentially nonlinear nature of water waves. There exist theoretical findings showing qualitative differences due to nonlinearity, and observed phenomena, such as wave breaking, cannot be explained by linear models. Stokes (see Whitham 1974, §13.13) found that

plane nonlinear periodic waves are possible and that the dispersion relation includes wave-amplitude dependence; these waves are periodic but not sinusoidal in that higher harmonics are present as in the Fourier expansion of a general periodic function. A tractable nonlinear approximation is obtained in the shallow-water limit (Whitham 1974, §13.10) which predicts wave steepening and the onset of breaking. Although the model has drawbacks in as much as it predicts that *all* wave fronts with negative slopes steepen and eventually break, and the modelling assumption of large wavelengths ceases to be valid for steep waves, nonetheless, it reveals steepening to be a uniquely nonlinear effect. By assuming both wave amplitude and water depth to be small, but finite, plane (two-dimensional) waves can be modelled by the Korteweg-de Vries equation (KdV). The KdV equation admits periodic waves called cnoidal waves, which have sharp crests and broad troughs and the solitary wave is obtained in the limit that the period becomes infinite. The latter is physically unusual in that it is a single mound of elevation, confined to a finite region, the tails decaying exponentially. More importantly, solitary waves are extremely stable states with unusual mathematical properties. In particular, their wave speed increases with amplitude, and a faster moving solitary wave can overtake one of smaller amplitude without change of form—in fact, to emphasize this particle-like behaviour of preservation during collisions, solitary waves are also referred to as solitons. Solitons continue to appear, both in water-wave theories as well as in other physical contexts (see Ablowitz & Segur 1981, for examples).

Water-wave phenomena that are three-dimensional and nonlinear are more complicated, but some theoretical understanding has been achieved. One can develop approximate theories using perturbation methods; also, as high-speed digital computers become increasingly available, it is possible to find numerical solutions. However, direct numerical solutions are not necessarily revealing, nor always feasible: three-dimensional grids that can adequately resolve the smaller scales of nonlinear problems lead to large systems of equations. So, sophisticated approaches that incorporate the expected behaviour of the solution become necessary for efficient numerical schemes. Often, periodic waves of permanent form are studied, or periodic boundary conditions are imposed, to restrict the computational do-

main. Still, in general, integration of three-dimensional, nonlinear initial-value problems remains quite an expensive task, and theoretical models that can reduce the complexity of these problems are desirable.

One area in which nonlinear three-dimensional waves have been studied with success is the propagation of long waves in a channel. The impetus for some of the recent work (see, for example, Wu 1987; Akylas 1988 and references given there) comes from experimental observations of certain forced wave phenomena. The experiments involved a forcing moving at transcritical speeds in rectangular channels. These speeds are in the neighbourhood of the phase speed, c_0, of linear long waves in water of constant depth and the forcing has been a model ship in a towing tank (Ertekin, Webster & Wehausen 1984), or a small bump on the tank bed (Lee, Yates & Wu 1989). According to linear theory (Whitham 1974 §12.3), when the forcing travels at a speed $U < c_0$, waves with phase speed equal to U will appear stationary and can be found behind the forcing; when $U = c_0$, the group velocity, which is the velocity at which the excited waves transport energy, vanishes in the frame of reference in which the forcing is stationary and therefore, the response in the vicinity of the forcing grows without bound (Akylas 1984); at higher speeds, $U > c_0$, there remains no wave disturbance for long times. In no case is a disturbance expected to propagate upstream of the forcing. Surprisingly, in the experiments, a strong upstream response is seen, consisting of a uniform train of waves of elevation. Furthermore, even when the forcing is thin, hence three-dimensional, the upstream waves are two-dimensional. Although this phenomenon has now been theoretically understood by including nonlinear effects, it is clear that if the channel cross-section is not rectangular, even the upstream waves must be three-dimensional. Accordingly, in chapter 2, a theory for long nonlinear waves in wide channels with sloping sidewalls is developed in which, the effect of the depth variation at the sidewalls is characterized by a single parameter for wall slopes that are $O(1)$. Numerical studies then show that the three-dimensional structure of the upstream waves excited by a slender pressure distribution, as well as that of the corresponding free periodic waves, depends crucially on this slope parameter. The theory can also be used

to study the development of three-dimensional, undular (laminar) bores; we have obtained results that are in close quantitative agreement with existing experimental data.

The second part of this thesis is concerned with a nonlinear effect in edge waves. Edge waves are waves trapped by a sloping beach such that they propagate along the shoreline and their amplitudes diminish in the offshore direction. As in the case of waves in channels with sloping sidewalls, the three-dimensional character of edge waves arises due to depth variation in the direction normal to that of propagation. The first known solution is due to Stokes (1846; see Lamb 1945, §260) for the fundamental edge wave on a uniformly sloping beach. Lamb had catalogued this solution but did not expect edge waves to occur in nature; after all, edge waves are markedly different from the commonly observed waves on beaches. Munk, Snodgrass & Carrier (1956) reported the first indications, from wave records, that very long edge waves (wavelength $\approx$ 200–400 km) could be present in coastal waters in the aftermath of storms. More recently, field observations (Bowen & Inman 1971; Guza & Inman 1975) and nonlinear analysis (Guza & Bowen 1976) suggest that shorter edge waves (wavelength $\approx$ 300 m) could be responsible for longshore periodic beach forms, such as crescentic sand bars on the sea bed near coastlines, and beach cusps.

The effect of nonlinearity on travelling edge waves—at least for small amplitudes—has been thought to be mild: Whitham (1976) found for the Stokes edge wave, an amplitude dependence in the dispersion relation, similar to Stokes's result for plane waves (Whitham 1974 §13.13), and like the linear mode, the higher harmonics were exponentially decaying, far out at sea. Also, it was noted that the rate at which the edge wave amplitude decayed in the offshore direction decreased with amplitude. We find, however, that in certain situations, nonlinear self-interactions of a finite-amplitude edge wave generate higher harmonics that are waves travelling out to sea; consequently, in these situations, finite-amplitude edge waves are attenuated by radiation. Moreover, a concomitant nonlinear mechanism of excitation of progressive edge waves is also possible and the details of this process are presented.

Finally, in chapter 4, a study of nonlinear shallow-water edge waves of permanent form is presented; the mechanism of radiative damping, mentioned in the previous paragraph, is

not exhibited by this model. For a beach whose slope decays exponentially so that water-depth remains small compared with wavelength everywhere, a numerical integration of the nonlinear shallow-water equations shows that the phase speed increases with amplitude, in agreement with the predictions of a perturbation approach at small amplitudes, and then departs uniformly with further increase in amplitude. The calculations were not very successful as it could not be resolved as to whether the failure in the numerical solution beyond a certain amplitude was suggestive of a physical limit: an edge wave of greatest elevation, analogous to the known limiting form for plane waves.

CHAPTER 2

WAVES IN CHANNELS WITH SLOPING SIDEWALLS

2.1 Introduction

In narrow channels of uniform, but arbitrary, cross-section—those in which the channel width is comparable with water depth—waves are quasi-two-dimensional; a relatively small spanwise variation in the wave elevation is present, but wave crests remain straight and the KdV equation is still valid to leading order (Peregrine 1968; Fenton 1973). Peregrine (1968) noted, however, that the KdV theory breaks down when the channel width is much larger than the water depth; as the channel width is increased, spanwise variations become relatively large, giving rise to non-uniformities in the perturbation expansion. This is consistent with the earlier experimental observations of Sandover & Taylor (1962), who had studied the development of undular bores in trapezoidal channels of moderately large width—about six to seven times the water depth. They pointed attention to the three-dimensional structure of wave disturbances; in particular, the presence of wave-crest curvature across the channel and the tendency for waves to have irregular forms (except at very low discharge) cannot be explained by the KdV theory (Fenton 1973).

In §2.2, a theoretical model is presented for long waves propagating along a channel of uniform non-rectangular cross-section, allowing for the presence of significant three-dimensional effects. The channel is assumed to be wide, $h_0/w \ll 1$, where $2w$ is the channel width at the undisturbed free surface and h_0 is the constant water depth away from the sidewalls. The approximate governing equations and boundary conditions are derived from the full water-wave theory, using matched asymptotic expansions: the main body of fluid, away from the sloping boundaries, forms an 'outer' region where waves satisfy the Kadomtsev–Petviashvili equation (KP), so that three-dimensional effects balance with nonlinear and dispersive effects; close to each sidewall, where the depth varies, there is an 'inner' region. Matching between the corresponding inner and outer expansions gives

the appropriate asymptotic boundary condition for the KP at each sidewall, depending on the relative size of the inner region: when the wall slope is $O(1)$, as in the experiments of Sandover & Taylor (1962), this boundary condition involves only a single parameter, $\mathcal{A} = A/h_0^2$, A being the area under the depth profile; for wall slopes $O(h_0/w)^{\frac{1}{2}}$, the inner region is relatively thicker, and the appropriate boundary condition has a different form which depends more seriously on the details of the depth profile. Finally, when the wall slope is very gentle, $O(h_0/w)$, there is no distinction between an inner and outer region any more, and one can use a KP with variable coefficients to account for depth variations; this possibility has been discussed in a number of recent studies (see, for example, Kirby, Philip & Vengayil 1987; David, Levi & Winternitz 1989) and will not be considered here.

The present theory is used, first, to discuss the development of an undular bore in channels with trapezoidal cross-sections, modelling the experimental set-up of Sandover & Taylor (1962). The theoretical predictions confirm the presence of significant three-dimensional effects, and are in quantitative agreement with experiment until wave breaking, which is not taken into account in the theory, occurs.

Next, the response to a slender pressure distribution, moving with transcritical speed at the free surface along the channel centerline is investigated. As indicated earlier, in a channel with vertical sidewalls, there is a strong upstream response that is two-dimensional, and the presence of sloping sidewalls, indeed, causes the upstream disturbance to be three-dimensional. However, quite remarkably, as the parameter $\mathcal{A}$ is increased ($0 \leq \mathcal{A} \leq 1$), the regular, periodic form of the upstream response found in a channel with vertical sidewalls ($\mathcal{A} = 0$) disappears, and then reappears, while the individual waves acquire a far more complicated, three-dimensional structure. It seemed plausible that, despite the apparent disorder in the upstream free-surface elevation for positive values of $\mathcal{A} < 1$, some average measure such as the wave-resistance coefficient might be nearly periodic. It turns out that there is a certain regularity in the variations of the drag coefficient but not the uniform periodicity found with rectangular channels. More importantly, the drag coefficient varies over a wider range in the process of generating an upstream wave compared with its values

for a channel of rectangular cross-section.

The loss and reappearance of uniformity in the upstream response seems to be related to the three-dimensional structure of periodic nonlinear waves of permanent form—numerically obtained solutions over the range ($0 \leq \mathcal{A} \leq 1$) are discussed in §2.5. Also, a perturbation study for small $\mathcal{A}$ suggests that three-dimensional waves, which correspond to the KdV solitary waves when $\mathcal{A} = 0$, are no longer localized because there are small, but finite, oscillatory tails consisting of channel cross-modes.

The parameter $\mathcal{A}$ is negative when the cross-sectional area of the channel is greater than that of a similar channel whose depth remains the same constant value h_0 even near the sidewalls. The problems studied in §§2.4, 2.5 are re-examined in §2.6 for $-1 \leq \mathcal{A} < 0$; the shape of the waves is now quite different from that obtained for $\mathcal{A} > 0$, and also, the upstream wavetrain is more nearly uniform over the entire range of values studied.

2.2 Theoretical model

Consider an infinitely long channel of uniform cross-section. Cartesian coordinates are chosen such that y is directed vertically upward, x is along, and z is across the channel. The undisturbed free surface is at $y = 0$, $0 < z < 2w$, where $2w$ is the channel width and the rigid bottom is at $y = -h(z/B)$. The cross-section is assumed to be such that the undisturbed water depth is a constant h_0 everywhere, except in the vicinity of the sidewalls where it decreases from h_0 to zero over a distance $O(B)$ with $B \ll w$ (see figure 2.1).

In setting up this asymptotic theory, it is most convenient to consider the generation of long waves by a pressure distribution moving with transcritical speed along the channel at the free surface; the propagation of free waves can then be formulated as a special case. In the frame of reference following the applied pressure p, a uniform current of speed U exists in the water. Assuming inviscid, irrotational flow, gravity waves are described in terms of the free-surface elevation $y = \eta(x, z, t)$ and the velocity potential $\Phi = Ux - \frac{1}{2}U^2 t + \phi(x, y, z, t)$. The velocity potential satisfies Laplace's equation in the fluid

$$\Phi_{xx} + \Phi_{yy} + \Phi_{zz} = 0 \quad (-h(\frac{z}{B}) < y < \eta,\ 0 < z < 2w), \tag{2.1}$$

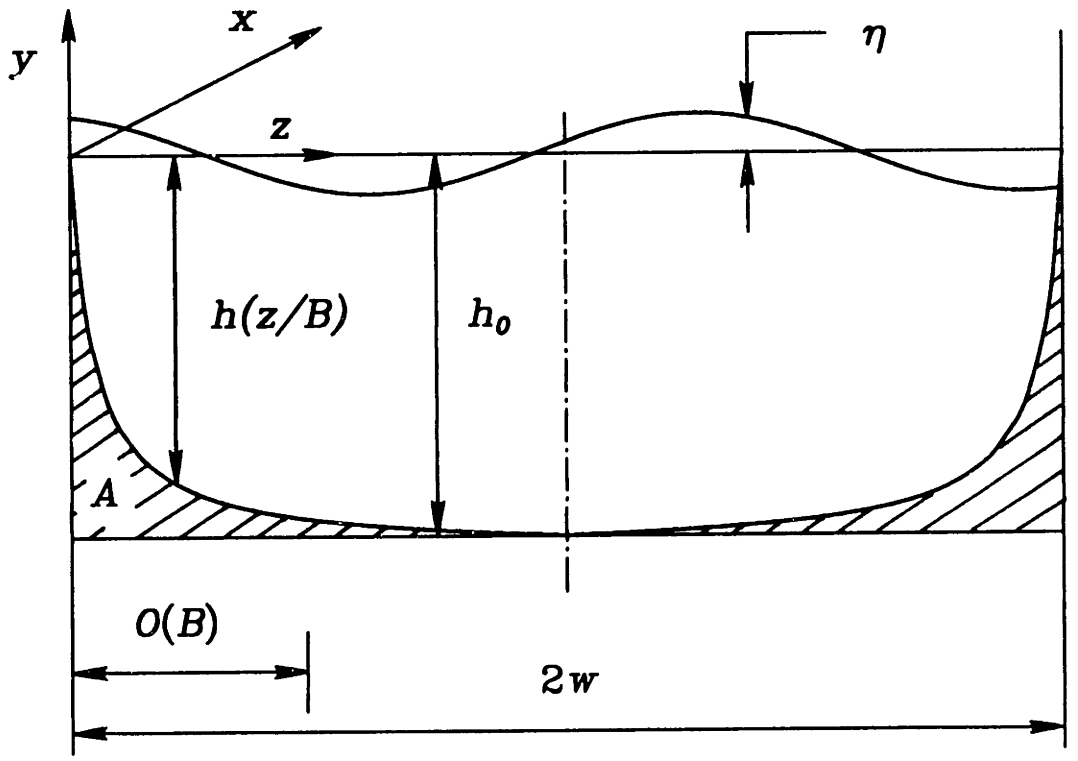

FIGURE 2.1 Channel cross-section.

subject to the kinematic and dynamic boundary conditions at the free surface

$$\eta_t + \Phi_x\eta_x + \Phi_z\eta_z = \Phi_y \quad (y = \eta), \tag{2.2a}$$

$$\Phi_t + \tfrac{1}{2}\,|\nabla\Phi|^2 + g\eta = -p/\rho \quad (y = \eta), \tag{2.2b}$$

and the kinematic condition on the channel bed and sidewalls

$$\nabla\Phi \cdot \mathbf{n} = 0 \quad (y = -h(\tfrac{z}{B})); \tag{2.3}$$

here g is the gravitational acceleration, p is the pressure in excess over the atmospheric pressure, ρ is the water density, and $\mathbf{n}$ is the direction normal to the channel walls and bed. Using a typical wavelength L, a typical wave amplitude a, and the linear long-wave speed, $c_0 = (gh_0)^{\frac{1}{2}}$, for water of uniform depth h_0, all quantities are cast in dimensionless form (primed variables),

$$x = Lx', \;\; y = h_0y', \;\; z = h_0z', \;\; t = \left(\frac{L}{c_0}\right)t', \;\; \eta = a\eta', \;\; h = h_0h',$$

$$\phi = \left(\frac{aLc_0}{h_0}\right)\phi', \;\; p = \left(\frac{a^2g\rho}{h_0}\right)p',$$

and then, for convenience, the primes are dropped. Equations (2.1)–(2.3) then read

$$\mu^2\phi_{xx} + \phi_{yy} + \phi_{zz} = 0 \quad (-h(\beta z) < y < \epsilon\eta, \;\; 0 < z < 2\sigma),$$

$$\eta_t + (F + \epsilon\phi_x)\eta_x + \frac{\epsilon}{\mu^2}\phi_z\eta_z = \frac{1}{\mu^2}\phi_y \quad (y = \epsilon\eta),$$

$$\phi_t + F\phi_x + \eta + \tfrac{1}{2}\frac{\epsilon}{\mu^2}(\mu^2\phi_x^2 + \phi_y^2 + \phi_z^2) = -\epsilon p \quad (y = \epsilon\eta),$$

$$\nabla\phi \cdot \mathbf{n} = 0 \quad (y = -h(\beta z).$$

Note that, apart from the Froude number $F = U/c_0$, the long-wave parameter $\mu = h_0/L$, and the nonlinearity parameter $\epsilon = a/h_0$, two additional independent dimensionless parameters arise:

$$\beta = \frac{h_0}{B}, \quad \sigma = \frac{h_0}{w};$$

β is a measure of the slope of the channel sidewalls, while σ measures the channel width relative to the water depth and, as will be seen shortly, also controls three-dimensional effects.

Attention is now focused on weakly nonlinear, long waves propagating along a wide channel; thus, the parameters ϵ, μ and σ are taken to be small ($\epsilon, \mu, \sigma \ll 1$). Moreover, as already indicated, it is assumed that the channel cross-section is such that depth variations are confined close to sidewalls ($\sigma/\beta = B/w \ll 1$), which then suggests the use of matched asymptotic expansions.

2.2*a* *Outer expansion*

The main part of the channel, away from the sloping boundaries ($1/\beta \ll z \ll 2/\sigma - 1/\beta$) forms an outer region where the water depth is uniform. Katsis & Akylas (1987*a*) have developed an asymptotic theory for long waves excited by a pressure distribution moving at transcritical speed on water of uniform depth; as the analysis in the outer region follows closely that of Katsis & Akylas (1987*a*), only the main results will be highlighted here.

At transcritical Froude number, $F = 1 + \lambda\mu^2$ ($\lambda = O(1)$), waves evolve on the 'slow' time $T = \mu^2 t$ owing to weak nonlinear, dispersive and three-dimensional effects, which are taken to be equally important. To include nonlinearity and dispersion at the same order, the choice $\epsilon = \mu^2$ is made; furthermore, a balance with three-dimensional effects is achieved by introducing the stretched (outer) spanwise variable $Z = \epsilon z$, so that waves propagate predominantly along the x-direction. Based on these scalings, three-dimensional effects are expected to become appreciable when the channel is sufficiently wide, such that the extent of the outer region, in terms of Z, is $O(1)$:

$$\sigma = O(\epsilon) \quad \text{or} \quad W = \epsilon \frac{w}{h_0} = O(1). \tag{2.4}$$

Now, in terms of the scaled coordinates, Laplace's equation for ϕ and the bottom boundary condition at $y = -1$ give

$$\phi(x, Z, T; y) = f(x, Z, T) - \frac{\epsilon}{2!}(y+1)^2 f_{xx} + \frac{\epsilon^2}{4!}(y+1)^4 f_{xxxx} - \frac{\epsilon^2}{2!}(y+1)^2 f_{ZZ} + \cdots. \tag{2.5}$$

The free-surface boundary conditions at $y = \epsilon\eta$ then imply that f is related to η through

$$\eta = -f_x + \epsilon\left(-p + \tfrac{1}{2} f_{xxx} - f_T - \lambda f_x - \tfrac{1}{2} f_x^2\right) + O(\epsilon^2), \tag{2.6}$$

and η satisfies the forced KP equation:

$$\eta_{Tx} + \lambda\eta_{xx} - \tfrac{3}{4}(\eta^2)_{xx} - \tfrac{1}{6}\eta_{xxxx} - \tfrac{1}{2}\eta_{ZZ} = \tfrac{1}{2}p_{xx} \quad (0 < Z < 2W). \tag{2.7}$$

In order to complete the formulation in the outer region, one needs to supplement (2.7) with boundary conditions at $Z = 0,\ 2W$. The appropriate boundary conditions will be obtained by matching the flow near the sidewalls with the outer flow. In preparation for this matching, it follows from (2.5) and (2.6) that the inner limit of the outer flow as $Z \to 0^+$ is

$$\phi \sim f(x,0,T) + \epsilon\,[zf_Z - \tfrac{1}{2}(y+1)^2 f_{xx}] + O(\epsilon^2), \tag{2.8a}$$

$$\eta \sim -f_x(x,0,T) + \epsilon\,[\tfrac{1}{2}f_{xxx} - zf_{xZ} - f_T - \lambda f_x - \tfrac{1}{2}f_x^2] + O(\epsilon^2); \tag{2.8b}$$

for simplicity, it has been assumed that $p(x, Z)$ is localized close to the channel centerline ($Z = W$), and, thus, makes no contribution to η in (2.8*b*).

2.2*b* *Inner expansion*

It turns out that the form of the inner expansion and the resulting boundary conditions depend on the magnitude of the slope parameter β. When $\beta = O(1)$, the extent of the inner region is $O(h_0)$, which is small compared with both the channel width $2w$ and the typical wavelength L. On the other hand, if $\beta = O(\epsilon^{\frac{1}{2}})$, the extent of the inner region is now comparable with L (but still small compared with $2w$); so, on physical grounds, one would expect that in the latter case, the outer flow will be affected more seriously by the details of the depth variation close to the wall, and this should show up in the corresponding boundary conditions. First, the wall boundary condition for $\beta = O(1)$, which is appropriate for comparing with the experiments of Sandover & Taylor (1962), will be derived. The case $\beta = O(\epsilon^{\frac{1}{2}})$ will follow in §2.2*c*.

For $\beta = O(1)$, the appropriate inner spanwise variable is z in the region close to the sidewall where $Z \to 0^+$. The governing equation is Laplace's equation

$$\epsilon\phi_{xx} + \phi_{yy} + \phi_{zz} = 0 \quad (-h(z) < y < 0,\ \ z > 0), \tag{2.9}$$

subject to the free-surface boundary conditions, correct to $O(\epsilon)$,

$$\phi_y = \epsilon(\eta_x + \phi_z\eta_z - \phi_{yy}\eta) \quad (y = 0), \tag{2.10a}$$

$$\phi_x + \eta + \tfrac{1}{2}(\phi_y^2 + \phi_z^2) = -\epsilon[\phi_T + \lambda\phi_x + \tfrac{1}{2}\phi_x^2 + \tfrac{1}{2}\eta(\phi_y^2 + \phi_z^2)_y + \eta\phi_{xy}] \quad (y = 0), \tag{2.10b}$$

the bottom boundary condition

$$\phi_y + h_z\phi_z = 0 \quad (y = -h(z)), \tag{2.11}$$

and the matching conditions (2.8 a, b) as $z \to \infty$. (In (2.9), the depth variation is specified as $y = -h(z)$, rather than $y = -h(\beta z)$, since $\beta = O(1)$.)

By expanding ϕ and η in powers of ϵ,

$$\phi = \phi_0 + \epsilon\phi_1 + \epsilon^2\phi_2 + \cdots, \quad \eta = \eta_0 + \epsilon\eta_1 + \epsilon^2\eta_2 + \cdots,$$

and substituting into equations (2.9)–(2.11), a hierarchy of linear problems is obtained. To $O(1)$, taking into account (2.8 a, b), it is readily found that $\phi_0 = f(x,0,T)$, $\eta_0 = -f_x(x,0,T)$. Proceeding to $O(\epsilon)$, we write

$$\phi_1 = zf_Z - \tfrac{1}{2}(y+1)^2 f_{xx} + u \quad (Z = 0), \tag{2.12}$$

so that u satisfies

$$u_{yy} + u_{zz} = 0 \quad (-h(z) < y < 0, \ z > 0), \tag{2.13}$$

$$u_y = 0 \quad (y = 0), \tag{2.14a}$$

$$u_y + h_z u_z = (1-h)f_{xx} - h_z f_Z \quad (y = -h(z)), \tag{2.14b}$$

and, in view of (2.12), the matching condition (2.8 a) becomes

$$u \to 0, \quad (z \to \infty). \tag{2.15}$$

The boundary-value problem for u, consisting of Laplace's equation (2.13) subject to the Neumann conditions (2.14) and the matching condition (2.15), has a solution if the compatibility condition

$$f_{xx}\int_0^\infty (1-h)\,\mathrm{d}z - f_Z\int_0^\infty h_z\,\mathrm{d}z = 0 \quad (Z = 0),$$

which follows from Green's theorem, is satisfied; or, in terms of $\eta = -f_x + O(\epsilon)$,

$$\eta_Z = \mathcal{A}\eta_{xx} \quad (Z = 0), \tag{2.16}$$

where

$$\mathcal{A} = \int_0^\infty (1 - h)\, \mathrm{d}z$$

is the difference in cross-sectional areas near the sidewall, between a channel of constant unit depth everywhere and a channel whose depth varies as $y = -h(z)$. So $\mathcal{A}$ can be positive or negative depending on the relative magnitudes of these cross-sectional areas. Note that the outer flow is insensitive to the exact geometry of the sidewalls; of course, if the sidewalls are vertical, $\mathcal{A} = 0$ and the familiar no-flux boundary condition used by Katsis & Akylas (1987*a*) is recovered. Condition (2.16) ensures that matching between the inner and outer flow is possible and this completes the formulation of the outer flow; it consists of the forced KP equation (2.7) subject to the boundary condition (2.16) at the two sidewalls, $Z = 0,\ 2W$.

It is worth noting that the propagation of long waves along a sloping beach (with $\beta = O(1)$) can be discussed as a special case of the present formulation; the KP equation (2.7) applies in $Z > 0$ and the boundary condition (2.16) holds at $Z = 0$. In particular, linear sinusoidal wave modes (in the absence of forcing, $p = 0$, $\lambda = 0$),

$$\eta = E(Z)\ \exp[\mathrm{i}(kx + \omega T)],$$

satisfy

$$E_{ZZ} + l^2 E = 0 \quad (Z > 0),$$

$$l^2 = 2k(\omega + \frac{1}{6}k^3),$$

subject to the boundary conditions

$$E_Z = -k^2 \mathcal{A} E \quad (Z = 0)$$

and E bounded as $Z \to \infty$. This boundary-value problem for E has two kinds of solutions: for

$$\omega = -\frac{k^3}{2}(\tfrac{1}{3} + \mathcal{A}^2), \tag{2.17 a}$$

and $\mathcal{A} > 0$, there is an edge-wave mode ($E \to 0$ as $Z \to \infty$),

$$E = \exp(-k^2 \mathcal{A} Z); \tag{2.17b}$$

for $\omega > -\frac{1}{6}k^3$ there is a continuous spectrum representing waves that are the obliquely incident and reflected waves at the beach,

$$E = \sin lZ - \frac{l}{k^2 \mathcal{A}} \cos lZ. \tag{2.18}$$

The dispersion relation (2.17a) is in agreement with the earlier work of Grimshaw (1974), who studied linear long edge waves in an ocean of finite depth; in chapter 3, the edge-wave mode (2.17) will be used to illustrate radiative damping and excitation of progressive edge waves.

2.2c *Wall boundary condition for* $\beta = O(\epsilon^{\frac{1}{2}})$

When $\beta = O(\epsilon^{\frac{1}{2}})$, the analysis presented in §2.2b needs to be modified. Here the main steps in the inner expansion which lead to the modified wall boundary condition are presented.

The wall slope being smaller, the inner region is now described in terms of a new spanwise coordinate $\tilde{z} = \epsilon^{\frac{1}{2}} z$, and the rigid bottom is at $y = -h(\tilde{z})$. In terms of the inner variables, the governing equations, correct to $O(\epsilon)$, are

$$\epsilon(\phi_{xx} + \phi_{\tilde{z}\tilde{z}}) + \phi_{yy} = 0 \quad (-h < y < 0, \ \tilde{z} > 0), \tag{2.19}$$

$$\phi_y = \epsilon(\eta_x - \phi_{yy}\eta) \quad (y = 0), \tag{2.20a}$$

$$\phi_x + \eta + \tfrac{1}{2}\phi_y^2 = -\epsilon(\phi_T + \lambda\phi_x + \tfrac{1}{2}\phi_x^2 + \eta\phi_y\phi_{yy} + \eta\phi_{xy}) \quad (y = 0), \tag{2.20b}$$

$$\phi_y = -\epsilon h_{\tilde{z}}\phi_{\tilde{z}} \quad (y = -h(\tilde{z})), \tag{2.21}$$

together with the matching conditions (2.8a, b) as $\tilde{z} \to \infty$. To solve this problem we write

$$\phi = \chi(x, \tilde{z}, T) - \epsilon v(x, y, \tilde{z}, T) + \cdots,$$

and upon substitution into (2.19)–(2.21), it is found that v satisfies

$$v_{yy} = \chi_{xx} + \chi_{\tilde{z}\tilde{z}} \quad (-h < y < 0, \ \tilde{z} > 0), \tag{2.22}$$

$$v_y = \chi_{xx} \quad (y = 0), \tag{2.23}$$

$$v_y = h_{\tilde{z}}\chi_{\tilde{z}} \quad (y = -h(\tilde{z})). \tag{2.24}$$

In addition, the matching condition (2.8*a*) implies

$$\chi \sim f + \epsilon^{\frac{1}{2}}\tilde{z}f_Z \quad (Z = 0,\ \tilde{z} \to \infty), \tag{2.25}$$

$$v \sim \tfrac{1}{2}(y+1)^2 f_{xx} - \tfrac{1}{2}\tilde{z}^2 f_{ZZ} \quad (Z = 0,\ \tilde{z} \to \infty). \tag{2.26}$$

The solution of (2.22)–(2.24), consistent with (2.26), is

$$v = \tfrac{1}{2}(y+1)^2\chi_{xx} + \tfrac{1}{2}y^2\chi_{\tilde{z}\tilde{z}} - \tfrac{1}{2}\tilde{z}^2 f_{ZZ},$$

subject to the compatibility condition

$$(h\chi_{\tilde{z}})_{\tilde{z}} + (h-1)\chi_{xx} = 0 \quad (\tilde{z} > 0). \tag{2.27}$$

Note that $h = 0$ at the shoreline $\tilde{z} = 0$, so that in general, solutions of (2.27) are expected to be singular there; requiring that χ is regular at $\tilde{z} = 0$ and imposing the matching condition (2.25) determine the desired boundary condition at $Z = 0$ for the outer flow. The details depend on the specific depth profile $h(\tilde{z})$; here, the particular case of exponential depth variation,

$$h(\tilde{z}) = 1 - \mathrm{e}^{-\tilde{z}}, \tag{2.28}$$

is worked out. Taking Fourier transforms in x, the solution of (2.27) is

$$\chi = \int_{-\infty}^{\infty} \hat{\chi}(k;\tilde{z},T)\,\mathrm{e}^{\mathrm{i}kx}\,\mathrm{d}k,$$

where $\hat{\chi}$ satisfies

$$(h\hat{\chi}_{\tilde{z}})_{\tilde{z}} + k^2(1-h)\hat{\chi} = 0 \quad (\tilde{z} > 0). \tag{2.29}$$

Now, for the exponential depth profile (2.28), the solution of (2.29) that is regular at $\tilde{z} = 0$ can be related to hypergeometric functions (Ball 1967; see also §4.2*a*), and its asymptotic behaviour as $\tilde{z} \to \infty$ is found to be

$$\hat{\chi} \sim D(1 - K(k)\tilde{z}) \quad (\tilde{z} \to \infty), \tag{2.30}$$

where D is, as yet, an unspecified constant and

$$K(k) = \frac{1}{2\gamma + \psi(a_+) + \psi(a_-)};$$

here ψ is the digamma function (Abramowitz & Stegun 1964, p. 258), γ is Euler's constant, and

$$a_\pm = \tfrac{1}{2} \pm \tfrac{1}{2}(1 + 4k^2)^{\frac{1}{2}}.$$

Comparing (2.30) with (2.25), matching is achieved if

$$\epsilon^{\frac{1}{2}} \hat{f}_Z + K(k)\hat{f} = 0 \quad (Z = 0), \tag{2.31}$$

or, equivalently in terms of $\eta = -f_x + O(\epsilon)$, if

$$\epsilon^{\frac{1}{2}} \eta_Z + \int_{-\infty}^{\infty} K(k)\hat{\eta}\, \mathrm{e}^{\mathrm{i}kx}\, \mathrm{d}k = 0 \quad (Z = 0). \tag{2.32}$$

So, when $\beta = O(\epsilon^{\frac{1}{2}})$, the wall boundary condition takes the integral–differential form (2.32). Note that dropping the $O(\epsilon^{\frac{1}{2}})$ term in (2.31), (2.32) is inconsistent close to the zeroes of $K(k)$ at

$$k = \pm(m(m+1))^{\frac{1}{2}} \quad (m = 1, 2, 3, \ldots);$$

these are the cut-off wavenumbers of edge-wave modes found by Ball (1967). The form of the boundary condition (2.32) remains valid for any depth variation $h(\tilde{z})$, but the function $K(k)$ will depend on the particular depth profile.

2.3 Undular bore

Suppose that in an infinitely long, uniform channel there is a gate that separates water at two different levels on either side. If the gate is suddenly removed, water advances into the region of lower depth forming a bore. It has been observed experimentally that, when the ratio of initial water depths exceeds a threshold value (of about 1.28), the resulting bore is short and turbulent, while below this threshold, it is laminar and consists of undulations (see, for example, Lighthill 1978, §2.12). In the latter case, one can use long-wave theory to describe the development of a bore because the undulations are long compared with the

water depth. In a channel with rectangular cross-section, where the waves are straight-crested, KdV theory predicts that an undular bore ultimately develops into a train of cnoidal waves of slowly varying amplitude and period, the leading wave being a solitary wave (Peregrine 1966; Fornberg & Whitham 1978). Three-dimensional bores were studied in the laboratory by Sandover & Taylor (1962) in channels with trapezoidal cross-sections. Here, data from their experiments are used to make some comparisons with theoretical predictions based on the asymptotic theory developed in the previous section for wall-slope parameter $\beta = O(1)$.

The formulation of the bore problem follows as a special case of the discussion in §2.2. As there is no forcing, p and λ are set equal to zero in (2.7); furthermore, assuming that the channel is symmetric, it suffices to consider half the channel, $0 < Z < W$, and in addition to the boundary condition (2.16) at $Z = 0$, impose a symmetry condition at $Z = W$:

$$\eta_{Tx} - \tfrac{3}{4}(\eta^2)_{xx} - \tfrac{1}{6}\eta_{xxxx} - \tfrac{1}{2}\eta_{ZZ} = 0 \quad (-\infty < x < \infty,\ 0 < Z < W), \tag{2.33}$$

$$\eta_Z = \mathcal{A}\eta_{xx} \quad (Z = 0), \tag{2.34a}$$

$$\eta_Z = 0 \quad (Z = W). \tag{2.34b}$$

The appropriate initial conditions are

$$\eta(x, Z, T = 0) = 0 \ \ (x < 0), \qquad \eta(x, Z, T = 0) = \eta_\infty \ \ (x \geq 0), \tag{2.35a}$$

while far upstream and downstream the conditions

$$\eta \to 0 \ \ (x \to -\infty,\ T > 0), \qquad \eta \to \eta_\infty \ \ (x \to \infty,\ T > 0), \tag{2.35b}$$

apply, where η_∞ is the initial difference in water levels.

2.3*a* *Numerical method*

The numerical integration of th initial-boundary-value problem (2.33)–(2.35), was performed using the explicit, conditionally stable finite-difference scheme of Katsis & Akylas

(1987*a*). Spatial derivatives were approximated by centred, second-order difference formulae, except for the derivative with respect to Z in the wall boundary condition (2.34*a*) which was represented by a first-order difference formula. The algorithm is described in Appendix A, but for a detailed study, the reader should consult Katsis (1986). It is noted here that Katsis (1986) had tested the scheme against an analytical, similarity solution of the KP.

Special care was taken that the necessarily finite extent of the computational domain did not affect the results presented here. The upstream boundary, $x = x_{-\infty}$, presents no difficulty—the domain can be extended to include any disturbance of appreciable amplitude. It is not feasible to extend, on the other hand, the downstream boundary of the computational domain, $x = x_{\infty}$, to include at all times the entire region wherein an appreciable disturbance exists; however, the simple device of holding η fixed at the end of a suitably large region was found to be sufficient previously (Katsis & Akylas 1987*a*), as long as the study was confined to the upstream waves: it was observed that there were large errors near the downstream boundary but that these errors remained in the neighbourhood of the downstream boundary. In the present calculations too, this same boundary treatment was found to be adequate; a graph showing the extent of the contamination—quite small—due to the artificial downstream boundary condition is included in the discussion of the algorithm in Appendix A.

In addition, it is possible to derive an integral constraint from (2.33) and (2.34) together with mass conservation:

$$\int_{-\infty}^{\infty} [\eta(x, Z, T) - \eta(x, Z, T = 0)] \, \mathrm{d}x = 0. \tag{2.36}$$

The above integral is independent of the spanwise position Z and can be interpreted as a mass conservation statement along lines of constant Z. This constraint is useful for checking solutions (see Appendix A for details).

All the results presented below are from computations on a grid with $\Delta x = 0.07$, $\Delta Z = 0.021$ and time step $\Delta T = 0.5 \times 10^{-4}$; the downstream boundary was located at $x_{\infty} = 17.5$.

2.3*b* *Comparison with experiment*

Sandover & Taylor (1968) conducted their experiments in channels with trapezoidal cross-sections, keeping the width at the bed constant at 12 in. while the sidewalls were supported at various angles θ to the vertical; also, the still-water depth was kept constant at 3 in. Thus, in terms of θ, the parameter $\mathcal{A}$ is given by

$$\mathcal{A} = \tfrac{1}{2}\tan\theta. \tag{2.37}$$

Wave-height measurements were taken for a range of different discharges, using gauges which were located at several points across the channel at a distance of 48 ft. from the inlet. The initial discharge Q, as measured in the laboratory, made dimensionless with $c_0 h_0^2$, is related to the parameters η_∞, $\mathcal{A}$, W and ϵ through

$$Q = 2W(\eta_\infty + \tfrac{3}{4}\epsilon\eta_\infty^2) - \epsilon\eta_\infty\mathcal{A}. \tag{2.38}$$

The parameter ϵ is specified by normalizing the dimensionless channel width at the free surface, $2W$, to be equal to unity; from (2.4) and the cross-section geometry, one then has

$$\epsilon = \frac{1}{2(2+\tan\theta)}. \tag{2.39}$$

Numerical computations were carried out for two sidewall inclinations $\theta = \frac{1}{4}\pi$, $\frac{1}{3}\pi$. Using (2.37) and (2.39), it is found that the corresponding values of $\mathcal{A}$ are 0.5, 0.866 and those of ϵ are 0.167 and 0.134. Figures 2.2*a* and 2.2*b*, respectively, show perspective views of the computed free surface for $\theta = \frac{1}{4}\pi$ with $\eta_\infty = 1.08$, and for $\theta = \frac{1}{3}\pi$ with $\eta_\infty = 1.13$, which correspond to the same value of $Q = 1.13$ (this gives a discharge of 90 gals/min), according to (2.38). In both cases, these snapshots are taken as the leading crest of the bore crosses the streamwise position at which the gauges were placed in the experiment; the corresponding times turn out to be $T = 12.5$, 9.5, respectively.

Initially, the step-shaped free surface fissions into a series of undulations, the extent of which increases with time. An individual wave undergoes the more rapid changes, as it matures, until the trough separating it from its downstream neighbour is at nearly the

(*a*)

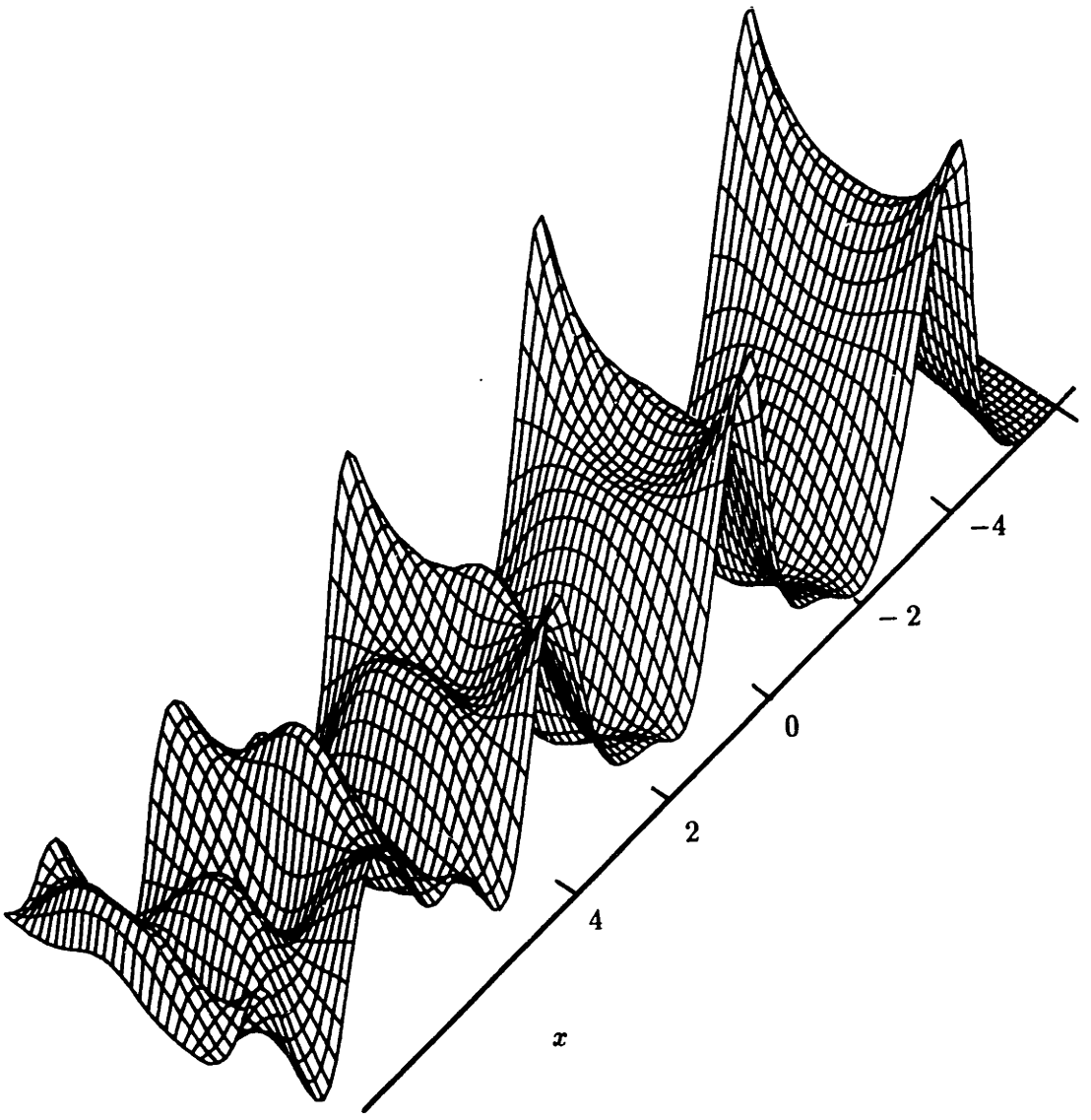

FIGURE 2.2*a* (*for caption, see following page*)

(*b*)

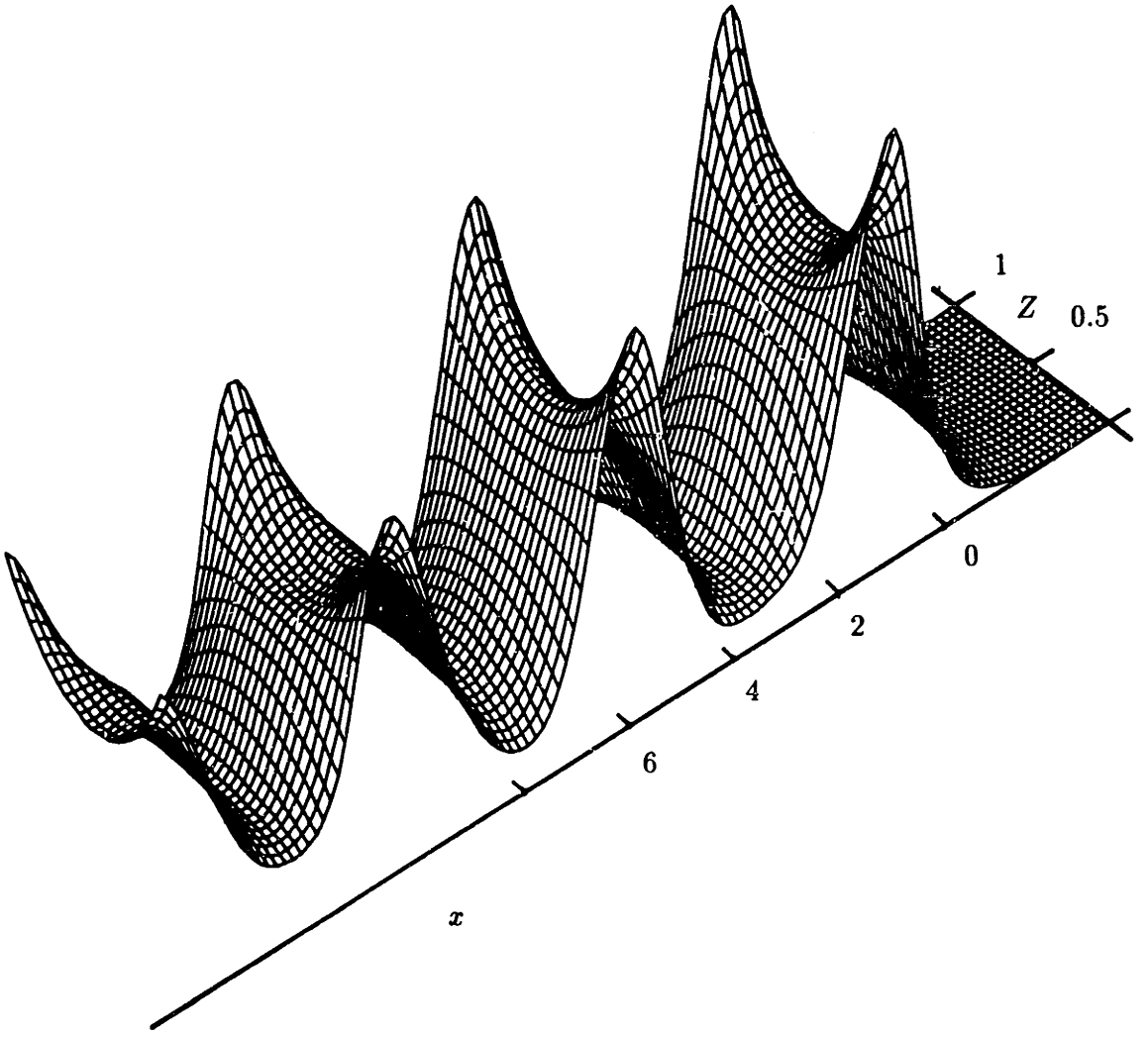

FIGURE 2.2 Computed free surface of the head of undular bores in channels with sloping sidewalls. (*a*) $\theta = \frac{1}{4}\pi$, $\eta_\infty = 1.08$, $T = 12.5$; (*b*) $\theta = \frac{1}{3}\pi$, $\eta_\infty = 1.13$, $T = 9.5$.

same elevation as the undisturbed region far upstream; after this point, the changes occur slowly. The rate at which these waves mature increases with η_∞ as also the wave steepness. In these respects, the development of the bore in a channel with sloping sidewalls is similar to that in a channel with vertical sidewalls, but, as can be seen in figures 2.2*a* and 2.2*b*, a considerable three-dimensional structure is now present: wave crests are curved across the channel and steeper close to the sidewalls, where wave breaking is more likely to occur; some of the individual wave undulations tend to form a double-hump structure, having two crests separated by a shallow trough in the middle. There is, at least qualitatively, a resemblance to the photographs from the experiments of Sandover & Taylor (1962). Also it is interesting to note that changing $\mathcal{A}$ from 0.5 to 0.866 causes the wave pattern to become more uniform; this feature will be discussed more thoroughly later (see §2.5), in connection with waves of permanent form.

Turning now to a quantitative comparison of theory with experiment, figure 2.3 shows a plot of the leading-wave-crest height at the channel centerline as a function of Q. For both values of θ, the theoretical predictions are in good agreement with experiment, until Q is large enough for wave breaking to occur in the experiment, which is, of course, not taken into account in the theory; wave breaking was first observed at $Q \approx 1.5$ for $\theta = \frac{1}{4}\pi$ and at $Q \approx 1.15$ for $\theta = \frac{1}{3}\pi$, as is evident from the sudden dip of the experimental data points in figure 2.3, near those values of Q. Figures 2.4*a* and 2.4*b* show comparisons of the theoretical with the experimental profiles of the leading wave crest along the channel centerline, for $\theta = \frac{1}{4}\pi$, $\frac{1}{3}\pi$, respectively, and at the same $Q = 1.13$. Again, the agreement between theory and experiment is very good; in fact, this provides a rather severe test of the theory because, as is clear from experimental observations, changing θ from $\frac{1}{4}\pi$ to $\frac{1}{3}\pi$ alters the wave profile quite significantly. It should also be kept in mind that, in the experiments of Sandover & Taylor (1962), the channel geometry does not suggest a very thin boundary region with a wide core region, as postulated in the model—the values of ϵ are only moderately small. On the other hand, the good agreement between theory and experiment indicates that the channel is wide enough for three-dimensional effects to be important.

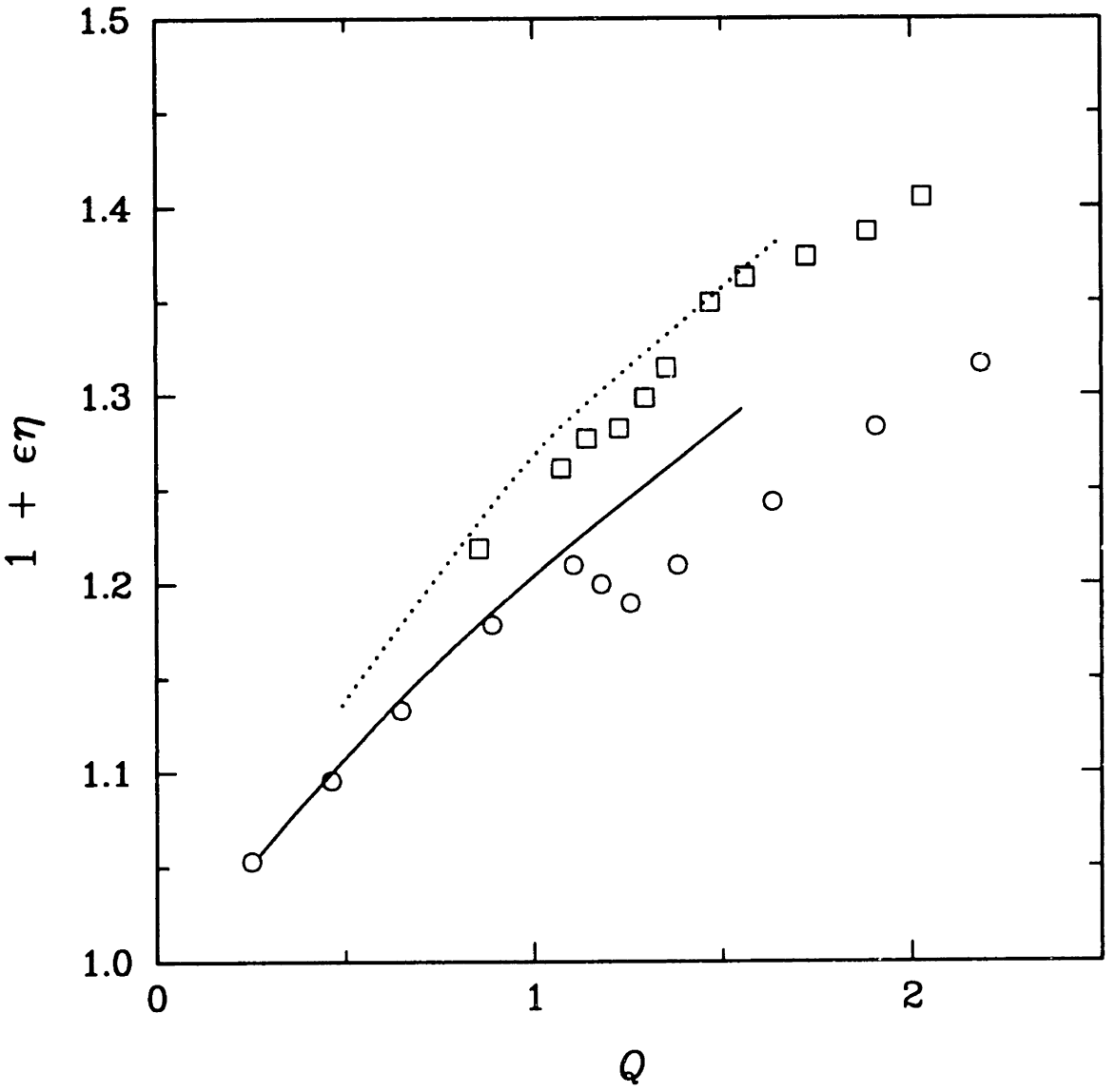

FIGURE 2.3 Variation of wave height of the leading crest (at the centerline) of undular bores with discharge; comparison of theory with experiments of Sandover & Taylor (1962), for two sidewall inclinations θ; ····· : theory, $\theta = \pi/4$; □: experiment, $\theta = \pi/4$; ——: theory, $\theta = \pi/3$; o: experiment, $\theta = \pi/3$.

(*a*)

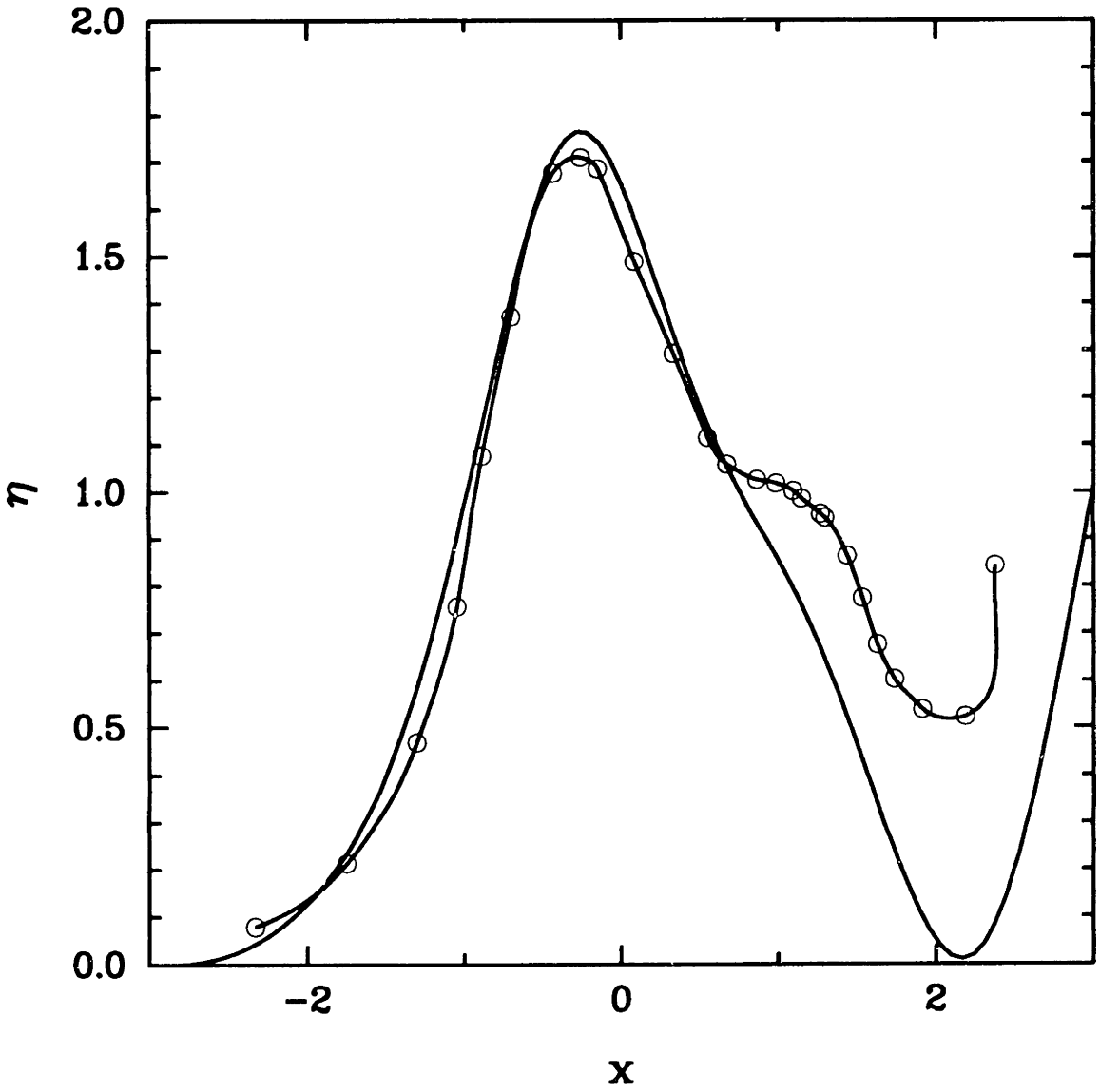

FIGURE 2.4 *a* (*for caption, see following page*)

(*b*)

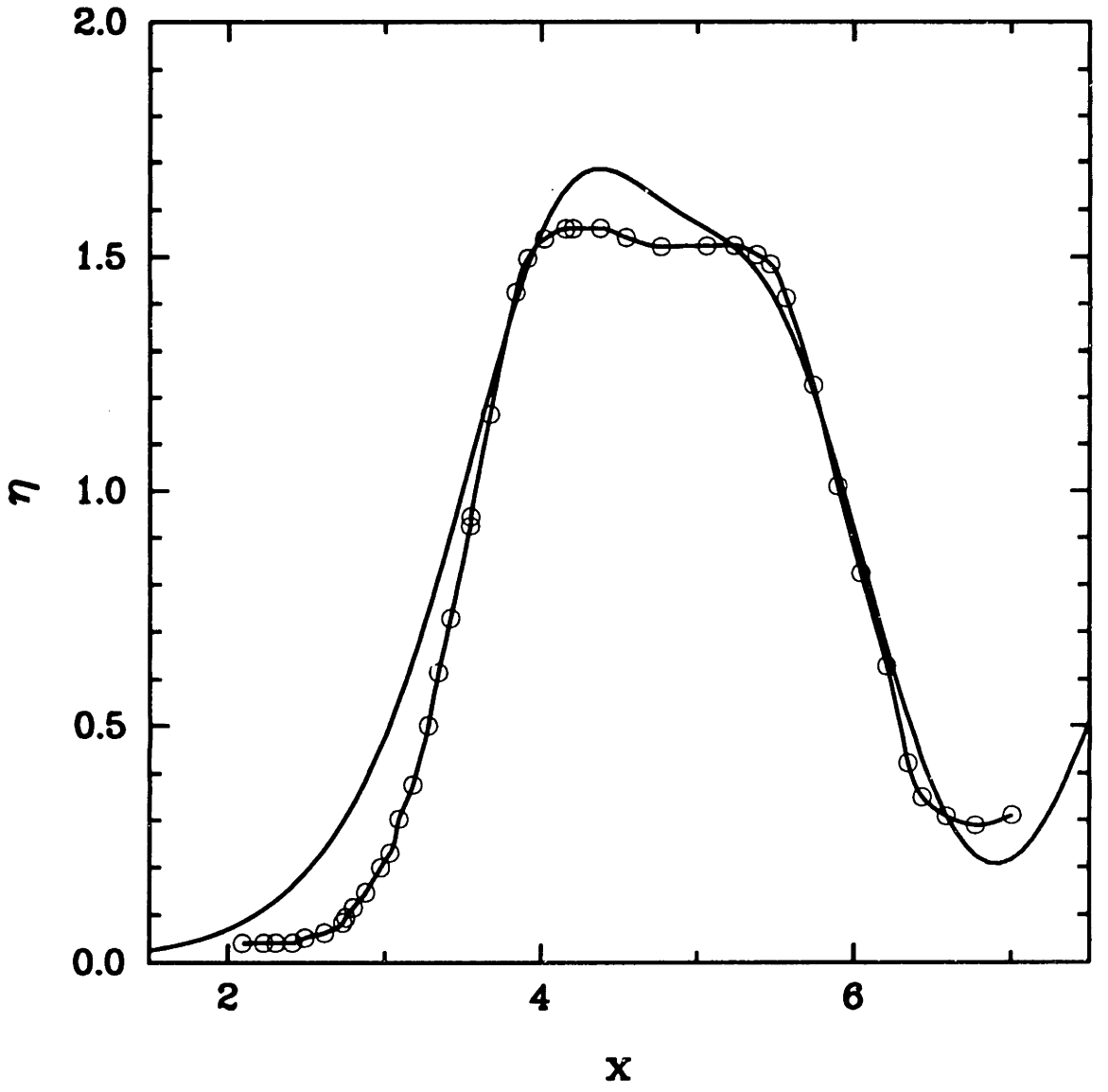

FIGURE 2.4 Profiles of leading waves (along the centerline) of undular bores; comparison of theory with experiments of Sandover & Taylor (1962); ——: theory,—⊖—: experiment. (a) $\theta = \frac{1}{4}\pi$, $T = 12.5$; (b) $\theta = \frac{1}{3}\pi$, $T = 9.5$

2.4 Upstream response due to transcritical forcing

Consider now the wave pattern generated by a pressure distribut moving at transcritical speed ($F \approx 1$). As remarked in chapter 1, this is an intriguing phenomenon and, for a channel with vertical sidewalls, it is now known (see Wu 1987, Akylas 1988) that, regardless of the shape of the forcing, there is a strong upstream response which consists of a uniform train of straight-crested KdV solitary waves. These waves are supercritical and travel ahead of the forcing; they are also localized, and after one separates from the forcing the state of the upstream free surface is very nearly like the initial undisturbed state so that the process can repeat continuously. Of course, it is the presence of vertical sidewalls that allows these particular waves to form—KdV solitary waves have no spanwise variations, so the channel sidewalls have to be vertical—and in the context of the present model, it is of interest to examine the extent to which the upstream disturbance is affected by sloping sidewalls.

The pressure distribution is assumed to move along the channel centerline and is taken to have a Gaussian form along x and to be localized in the spanwise direction:

$$p(x,Z) = \pi^{\frac{1}{2}} p_0 \exp(-x^2)\, \delta(Z-W), \tag{2.40}$$

where p_0 is a constant proportional to the total force exerted by the applied pressure and δ is the Dirac delta function. (The characteristic area covered by the pressure distribution (2.40) is π, and $p_0\pi$ is the total force exerted by the distributed pressure over an infinite plane.) Assuming, furthermore, that the channel is symmetric and the forcing is turned on impulsively, equations (2.7), (2.16) and (2.40) then lead to the following initial-boundary-value problem:

$$\eta_{Tx} + \lambda\eta_{xx} - \tfrac{3}{4}(\eta^2)_{xx} - \tfrac{1}{6}\eta_{xxxx} - \tfrac{1}{2}\eta_{ZZ} = 0 \quad (-\infty < x < \infty,\ 0 < Z < W), \tag{2.41}$$

$$\eta_Z = \mathcal{A}\eta_{xx} \quad (Z = 0), \tag{2.42a}$$

$$\eta_Z = \tfrac{1}{2}\pi^{\frac{1}{2}}\, p_0(\exp(-x^2))_{xx} \quad (Z = W), \tag{2.42b}$$

$$\eta = 0 \quad (T = 0). \tag{2.43}$$

The above problem is solved numerically using the method of Katsis & Akylas (1987*a*) with the same resolution as in the bore problem discussed in §2.3, and by normalizing the channel width $2W$ to unity. Again, the constraint (2.36), which ensures mass conservation, was satisfied to within a few percent (see Appendix A, for details).

Computations show the development of the upstream response to follow a simple (overall) pattern: initially, the upstream free surface rises in an arc swept back about the forcing that has been applied along the channel centerline, and spreads continuously until the channel sidewalls are met. Then, the sidewalls appear to support the further growth of the upstream disturbance into, almost, a wave of elevation which eventually separates from the forcing. This process repeats and a wave train can be seen travelling upstream, while a continuously elongating trough appears immediately behind the forcing corresponding to the mass that has been transferred to form the upstream waves.

Several parameters alter the specific appearance of the upstream response, some more profoundly than others. As the objective of the present study was to understand how sloping sidewalls affect the upstream response, the dependence of the new parameter $\mathcal{A}$—quite significant—will be discussed in detail below, but the influence of other parameters is worth noting. (The details of the excitation mechanism are complicated, but a few qualitative observations can be made.) The intensity of the forcing, p_0, affects both the rate at which upstream waves are generated as well as their amplitudes. This can be understood as follows: we can think of the excitation process as consisting of the forcing transferring mass upstream and the latter forming into, more or less, a free wave that can travel faster than the forcing. Lowering the intensity of the applied pressure lowers the rate at which mass is transferred upstream, so the rate of wave generation decreases. At the same time, the waves that form can have lower speeds, be of smaller amplitudes, and still separate from the forcing; in the calculations reported here, $p_0 = 10$.

The Froude number F is the speed of the forcing, and since upstream waves are those that travel faster than the forcing, wave speed and simultaneously wave amplitude is seen to increase with F; also, it takes longer for a wave of larger amplitude to form and detach.

The considerable changes in the upstream disturbance that result with changes in $\mathcal{A}$ are not sensitive to the exact value of the Froude number or its equivalent in the present formulation, λ. However, as can be seen from linear theory, the phase speed of long waves decreases as $\mathcal{A}$ is increased; therefore, maintaining a constant value of λ, say $\lambda = 0$, causes the resulting upstream waves to be increasingly steeper with some possible loss of accuracy, since this corresponds to the more severe supercritical forcing. Accordingly, the speed of the forcing was prescribed as the phase speed of linear long waves; when the non-rectangular shape of the channel cross-section is accounted for, the long-wave speed, measured in the laboratory reference frame, can be written as (Lamb 1945, §169)

$$\hat{c} = \left(1 - \frac{\epsilon\mathcal{A}}{W}\right)^{\frac{1}{2}} = 1 - \frac{\epsilon\mathcal{A}}{2W} + \cdots. \tag{2.44}$$

It follows then that, setting $F = \hat{c}$ and normalizing the channel width $2W$ to unity gives

$$\lambda = -\mathcal{A}.$$

Numerical solutions suggest that the nature of the upstream response depends crucially on the value of $\mathcal{A}$. For small $\mathcal{A}$ (≈ 0.1), the individual upstream waves remain straight while wave crests climb and troughs dip near the sidewalls, as expected from the wall boundary condition (2.42*a*). On increasing $\mathcal{A}$ further, the upstream wave disturbance loses its periodic appearance entirely and becomes quite disordered. Figure 2.5*a* shows the response for $\mathcal{A}$ = 0.5 ($\lambda = -0.5$) at $T = 4$. Note that the individual waves are quite different from each other and that there are large spanwise variations. Quite remarkably, as $\mathcal{A}$ approaches 1, consecutive pairs of upstream waves appear to coalesce at the sidewalls and the uniformity of the wavetrain is regained. As shown in figure 2.5*b* for $\mathcal{A} = 1$ ($\lambda = -1$) at $T = 4$, each of the upstream waves has sharp crests at the walls that split into two humps towards the centerline, and the troughs are nearly flat and broad with very little interaction between neighbouring waves. A similar tendency for the wave pattern to become more regular can be observed in the development of a bore also, when $\mathcal{A}$ is changed from 0.5 to 0.866 (figures 2.3*a* and 2.3*b*). In the following section, it will be shown that this change in wave pattern is related to the shapes of periodic waves of permanent form.

(*a*)

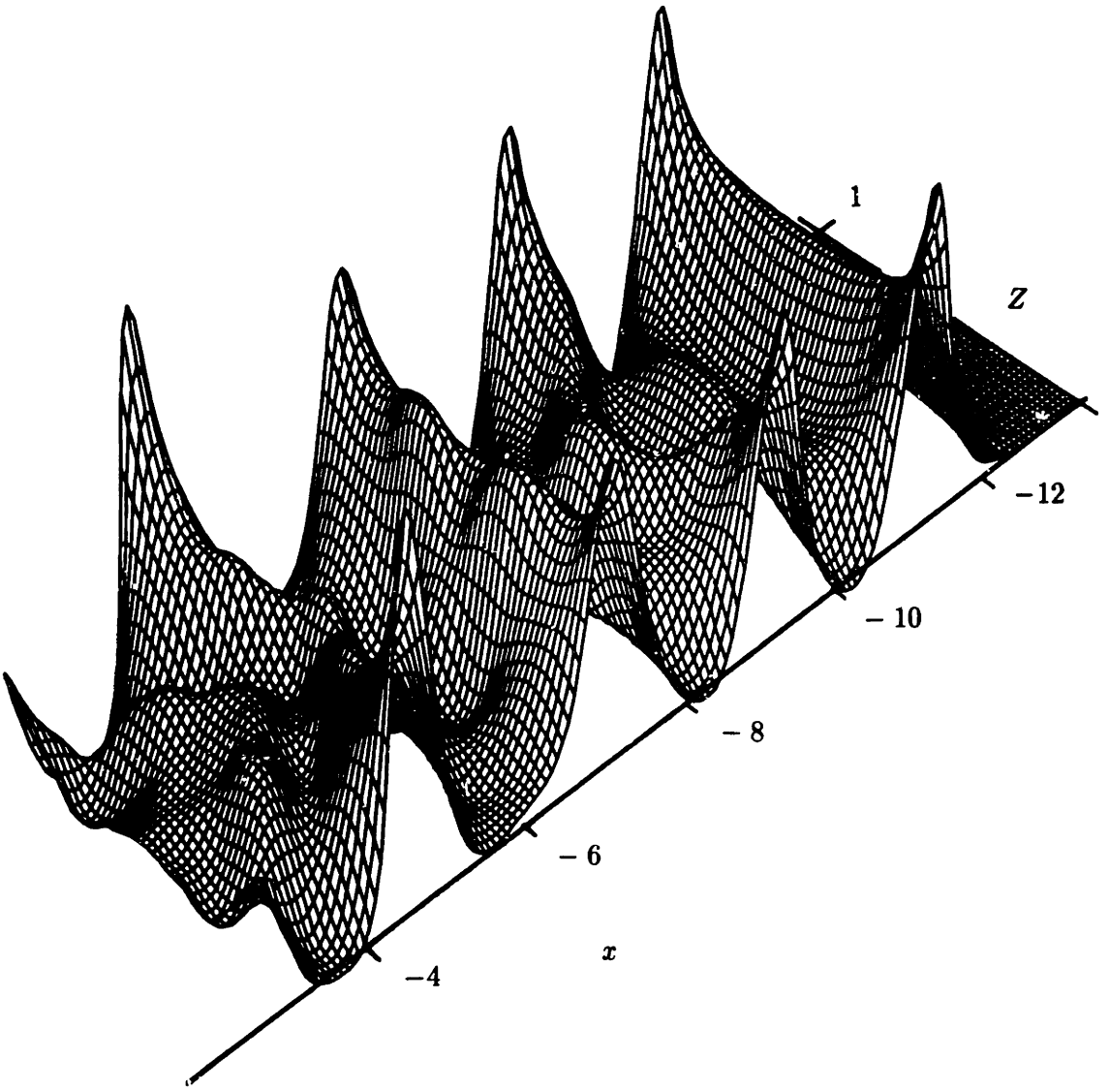

FIGURE 2.5*a* (*for caption, see following page*)

(*b*)

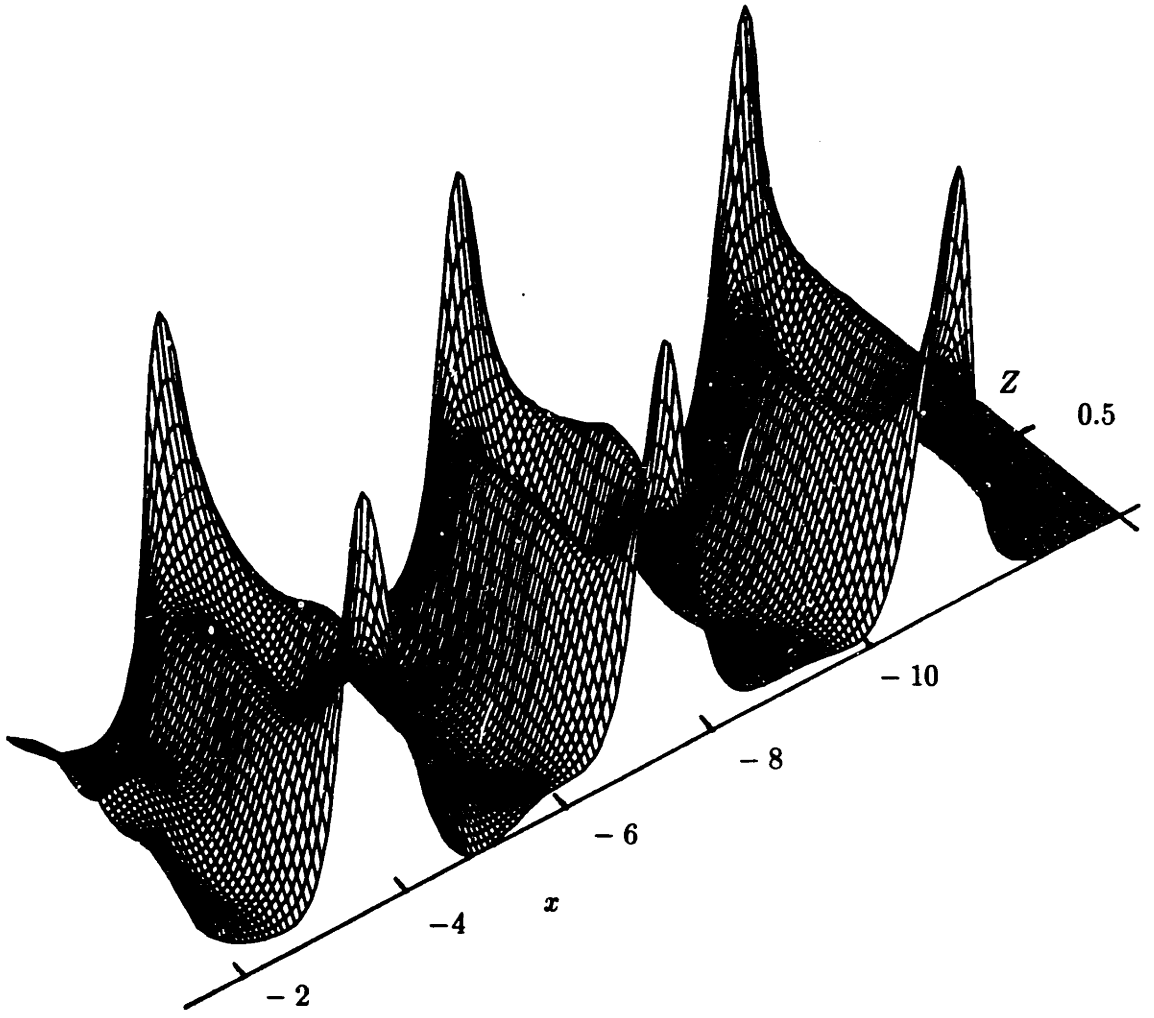

FIGURE 2.5 Upstream waves excited by transcritical forcing in channels with sloping sidewalls, at $T = 4$ and $p_0 = 10$. (*a*) $\mathcal{A} = 0.5$, $\lambda = -0.5$, (*b*) $\mathcal{A} = 1$, $\lambda = -1$.

(*a*)

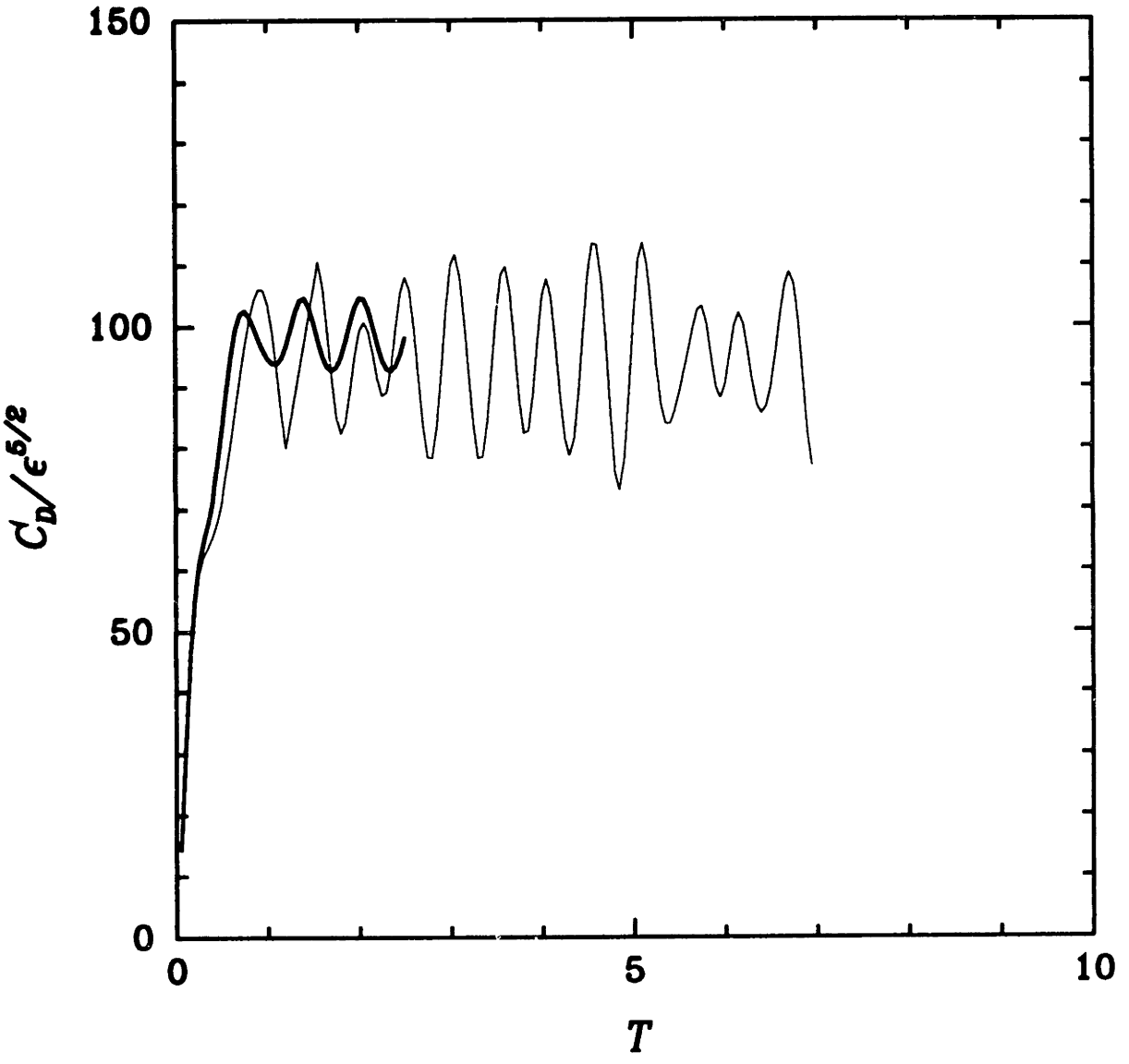

FIGURE 2.6 *a* (*for caption, see following page*)

(*b*)

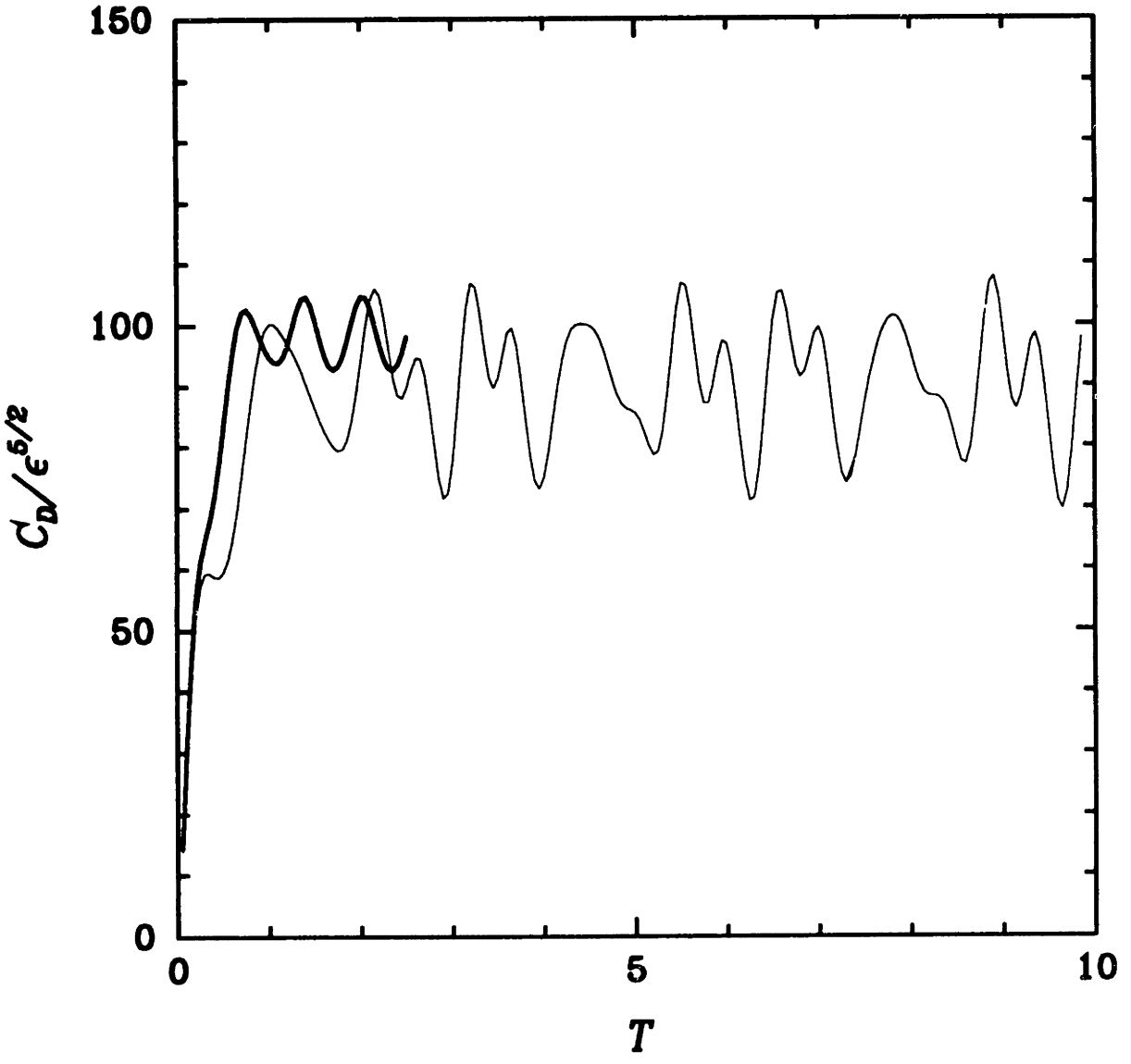

FIGURE 2.6 Variation of wave-resistance coefficient C_D with time T for $p_0 = 10$.
(*a*) —— : $\mathcal{A} = 0$; —— : $\mathcal{A} = 0.5$ ($\lambda = -0.5$). (*b*) —— : $\mathcal{A} = 0$; —— : $\mathcal{A} = 1$ ($\lambda = -1$).

Despite the seemingly disordered appearance of the upstream disturbance that results for intermediate values of $\mathcal{A}$, as can be seen in figure 2.5*a*, it seemed plausible that some average measure such as the wave resistance might be regular and periodic. The wave resistance D_w, is the integral

$$D_w = -\iint p\hat{\mathbf{x}} \cdot \mathrm{d}\mathbf{S},$$

where dS is an area element on the free surface with the normal directed out of the fluid, and $\hat{\mathbf{x}}$ is the unit vector along the x-axis. A wave-resistance coefficient, C_D can be defined by normalizing D_w with $\rho c_0^2 L h_0$, since L and h_0 are the characteristic lengths of the assumed pressure distribution. Using (2.40) and transferring the integration over the free surface to integration over the projected area in the xZ-plane gives

$$C_D = -\epsilon^{\frac{5}{2}} \pi^{\frac{1}{2}} p_0 \int_{-\infty}^{\infty} \exp(-x^2) \frac{\partial \eta}{\partial x} \, \mathrm{d}x. \tag{2.45}$$

Figures 2.6*a* and 2.6*b* show the variation of the wave resistance coefficient with time T for $\mathcal{A} = 0.5$ ($\lambda = -0.5$) and $\mathcal{A} = 1$ ($\lambda = -1$) respectively. In each figure, as a reference, the curve corresponding to channels with vertical sidewalls, $\mathcal{A} = 0$ ($\lambda = 0$), has been included; however, as the variation in C_D is very nearly sinusoidal when $\mathcal{A} = 0$, only a few cycles have been shown. When $\mathcal{A} = 0.5$, a fundamental period can be seen, but the modulation follows no simply discernible pattern. On the other hand, when $\mathcal{A} = 1$, a pattern of repetitive changes in C_D can be observed easily, though it is far from being simple. It is concluded that this average measure is not significantly more ordered than the appearance of the upstream disturbance. There is, however, a more important observation: as can be seen in figures 2.6*a* and 2.6*b* the wave resistance fluctuates by two to three times that experienced in a channel with vertical sidewalls; the mean value decreases, but only slightly.

2.5 Waves of permanent form

As remarked earlier, in a channel with vertical sidewalls, there is a close relation between the development of an undular bore and periodic waves of permanent form (cnoidal waves), which, in fact, can be used to construct approximate solutions based on modulation theory

(Gurevich & Pitaevskii 1974; Fornberg & Whitham 1978); this also turns out to be the case for the upstream response due to near-resonant forcing, as pointed out recently by Smyth (1987). Accordingly, in order to gain some insight into these wave phenomena in the presence of sloping sidewalls—in particular the crucial dependence on $\mathcal{A}$ noted in §§2.3, 2.4—here we look for periodic waves of permanent form. To this end, η is assumed to depend on $\xi = x + cT$, c being the phase speed, and on using (2.7) (with $p = 0$, $\lambda = 0$), (2.16) and taking the channel to be symmetric, one has

$$-c\eta_{\xi\xi} + \tfrac{3}{4}(\eta^2)_{\xi\xi} + \tfrac{1}{6}\eta_{\xi\xi\xi\xi} + \tfrac{1}{2}\eta_{ZZ} = 0 \quad (-\xi_0 < \xi < \xi_0,\ 0 < Z < W), \tag{2.46}$$

$$\eta_Z = \mathcal{A}\eta_{\xi\xi} \quad (Z = 0), \tag{2.47a}$$

$$\eta_Z = 0 \quad (Z = W), \tag{2.47b}$$

where $2\xi_0$ is the period; furthermore, the water depth is fixed by setting $\eta(\xi = \xi_0, Z = 0) = 0$. When $\mathcal{A} = 0$, cnoidal waves with no Z-variations are solutions of the above system, and the KdV solitary wave is obtained as a limiting case as the period is increased. Our goal here is to examine the effect of $\mathcal{A}$ on these known wave solutions.

2.5 *a Numerical results*

Equations (2.46), (2.47) are solved numerically using a combination of spectral and finite-difference methods. Assuming that waves are symmetric about $\xi = 0$, Fourier, spectral differentiation is used to calculate derivatives with respect to ξ, while derivatives with respect to Z are approximated by second-order finite differences. Thus for given values of the speed c, slope parameter $\mathcal{A}$, and half-period ξ_0, equation (2.46) and the boundary conditions (2.47) yield a nonlinear algebraic system for the unknown values of η at the grid points, which is solved through Newton's method. As a check, these numerical solutions were verified against results obtained independently from a second technique, using a shooting procedure. The basis for discretization is the same as in the first method—Fourier expansion in ξ and second-order, finite differences in Z; but the desired solution is found by starting with guessed values for η at the centerline $Z = W$, where (2.47b) is applied, and then

marching along lines of constant ξ towards the sloping wall at $Z = 0$. The assumed values of η at $Z = W$ are systematically corrected through Newton iteration and the marching procedure is repeated until the wall condition (2.47 *a*) is also met. Furthermore, for periodic waves, the constraint analogous to (2.36) is that

$$\int_{-\xi_0}^{\xi_0} \eta(\xi, Z)\, \mathrm{d}\xi$$

is independent of Z; the numerical solutions were checked against this constraint (see Appendix B for further details).

Starting with the known cnoidal-wave solution at $\mathcal{A} = 0$, continuation in $\mathcal{A}$ was used to compute solution families for $\mathcal{A} > 0$ and for a range of phase speeds, $0.5 \leq c \leq 2.5$ (the upstream waves shown in figure 2.5 *b* travel with a speed of, approximately, 2.5). The channel width $2W$ is normalized to unity in all cases discussed below, though the waves seem to be relatively insensitive to changes in W. The period $2\xi_0$ is taken to be 2π; cnoidal waves having this period and $0.5 \leq c \leq 2.5$ appear essentially as a series of KdV solitary waves, with very little interaction between individual crests. Numerical computations indicate that, as the speed c is increased for fixed $\mathcal{A}$, the wave structure remains qualitatively the same but, as one would expect, wave crests become steeper and three-dimensional features such as crest curvature, both in plan and elevation, become more pronounced. On the other hand, varying $\mathcal{A}$ gives rise to more dramatic effects: for small values of $\mathcal{A} > 0$, there appear small oscillatory tails and the crest acquires a depression near the centerline. Figure 2.7 *a* shows a perspective view of the free surface corresponding to $c = 2.5$ and $\mathcal{A} = 0.5$, at which point these effects have become quite strong and the wave has a fairly complicated three-dimensional structure. With further increase in $\mathcal{A}$, however, the oscillations at the tails tend to subside resulting in broad, nearly flat troughs for values of $\mathcal{A}$ around 1, as shown in figure 2.7 *b*. These computations were carried out using a resolution of 33 grid points in $0 \leq \xi \leq \pi$; in the spanwise direction, $0 \leq Z \leq 0.5$, 31 grid points were used in the first case, and 21 points in the second case.

Based on the above numerical calculations of steady waves, it is now possible to explain certain features of the unsteady wave patterns noted earlier. In particular, there is a strik-

(*a*)

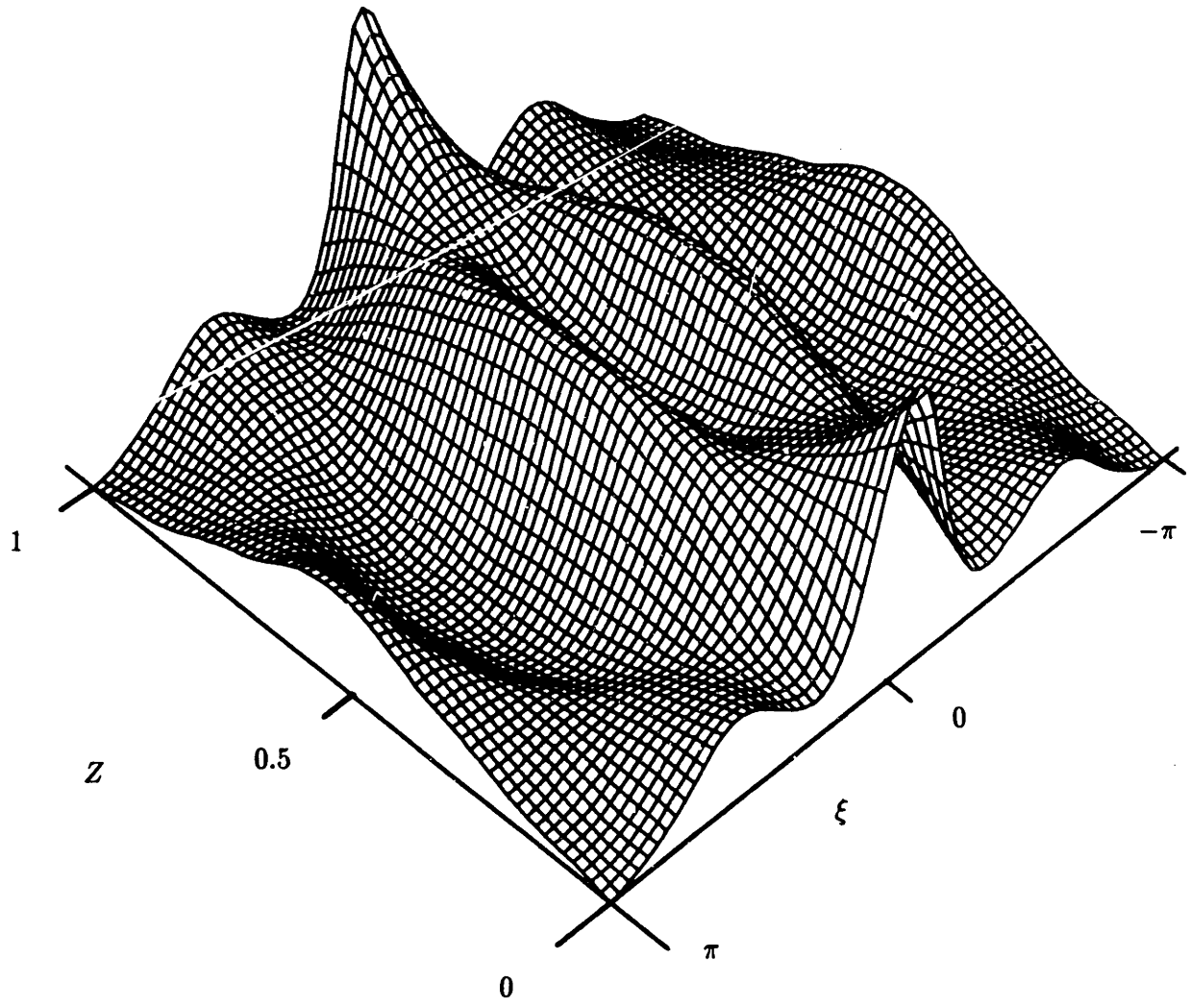

FIGURE 2.7 *a* (*for caption, see following page*)

(*b*)

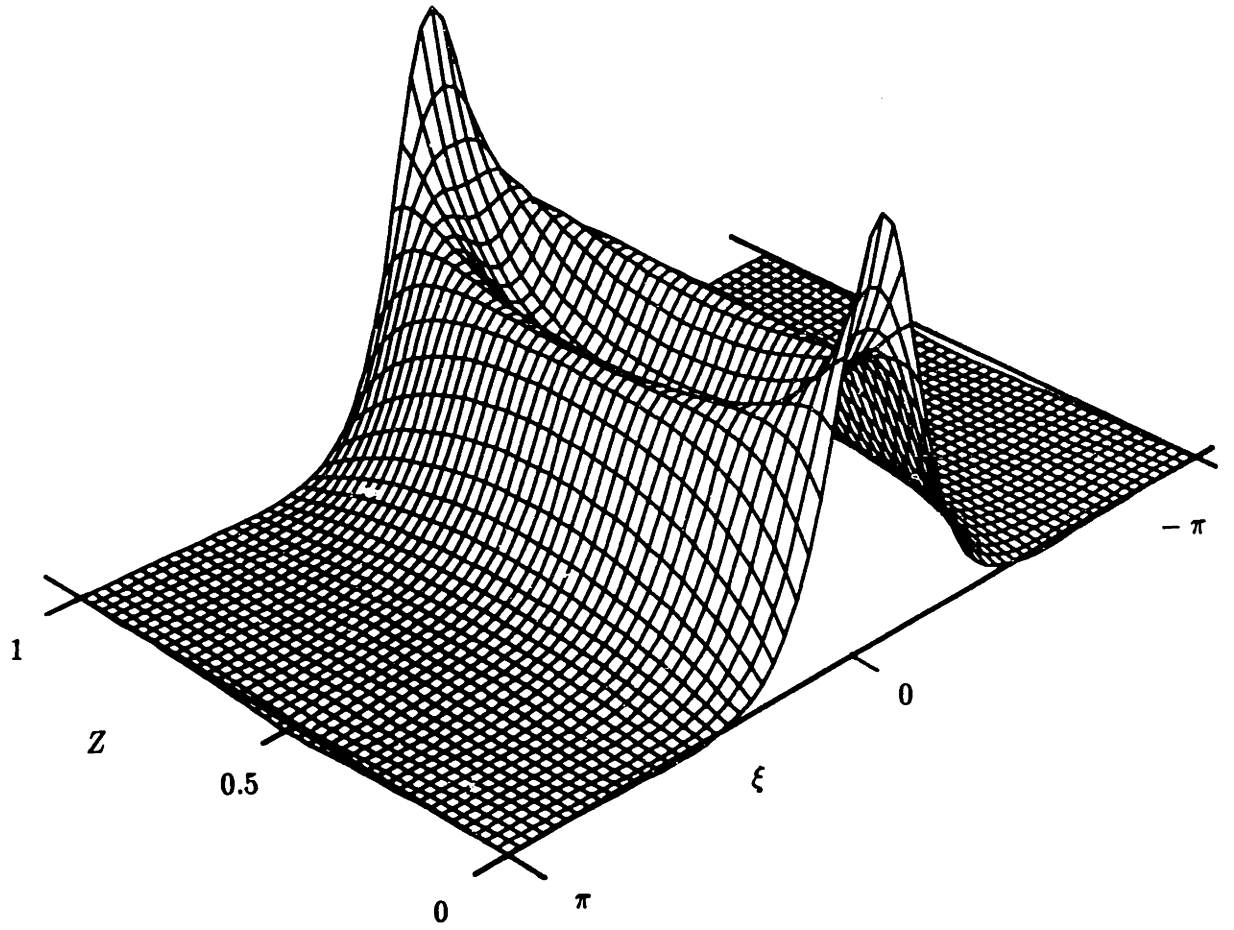

FIGURE 2.7 Periodic waves of permanent form of period $2\xi_0 = 2\pi$, speed $c = 2.5$ and channel width $2W = 1$. (a) $\mathcal{A} = 0.5$; (b) $\mathcal{A} = 1.0$.

ing similarity between the waves with the double-hump structure found in the upstream response for $\mathcal{A} = 1$ (see figure 2.5*b*), and the steady waves shown in figure 2.7*b* for the same value of $\mathcal{A}$. Figure 2.7*b* also suggests that there is little interaction between waves in neighbouring periods, so that each of these waves is expected to propagate more or less as a separate entity; the upstream response shown in figure 2.5*b*, which consists of a series of these waves, seems to support this claim. On the other hand, the relatively non-uniform appearance of the upstream response for $\mathcal{A} = 0.5$ (see figure 2.5*a*) is probably due to the large spanwise variations at the tails of the steady waves shown in figure 2.7*a*, which cause individual waves to interact in a complicated way. The same reasoning also seems to provide an explanation for the more uniform appearance of the undular bore for $\mathcal{A} = 0.866$ as compared to that for $\mathcal{A} = 0.5$ (figures 2.2*a* and 2.2*b*).

A question that has not been addressed so far, is whether solitary waves exist for $\mathcal{A} > 0$. Assuming that solitary waves can be obtained from periodic waves in the limit that the wave period becomes large, one could use continuation in ξ_0 to search for possible solitary waves numerically; this is a computationally expensive task and will not be pursued here. Another approach is to use perturbation theory for $\mathcal{A} \ll 1$, as discussed below.

2.5*b* *Perturbation theory for* $\mathcal{A} \ll 1$

Assuming that $\mathcal{A} \ll 1$, η is expanded in powers of $\mathcal{A}$:

$$\eta(\xi, Z) = \eta^{(0)}(\xi) + \mathcal{A}\eta^{(1)}(\xi, Z) + \mathcal{A}^2\eta^{(2)}(\xi, Z) + \cdots, \tag{2.48}$$

where $\eta^{(0)}$ is the KdV solitary wave,

$$\eta^{(0)} = a_0 \operatorname{sech}^2 \alpha\xi \tag{2.49a}$$

with
$$\alpha = (\tfrac{3}{4}a_0)^{\frac{1}{2}}, \quad c = \alpha/2. \tag{2.49b}$$

Upon substitution of (2.48), (2.49) into (2.46), (2.47), it is found that $\eta^{(1)}$ satisfies a linear inhomogeneous problem. It proves convenient to write

$$\eta^{(1)} = \frac{2W}{\pi}\eta^{(0)}_{\xi\xi} \sin\frac{\pi Z}{2W} + \tilde{\eta}(\xi, Z),$$

so that $\tilde{\eta}$ satisfies a problem with homogeneous boundary conditions:

$$(-c\tilde{\eta} + \tfrac{3}{2}\eta^{(0)}\tilde{\eta} + \tfrac{1}{6}\tilde{\eta})_{\xi\xi} + \tfrac{1}{2}\tilde{\eta}_{ZZ} = \mathcal{R}, \tag{2.50}$$

$$\tilde{\eta}_Z = 0 \quad (Z = 0,\ W), \tag{2.51}$$

where

$$\mathcal{R} = \left\{ c\eta^{(0)} + \frac{W}{\pi}\sin\frac{\pi Z}{2W}\left[3(\eta_\xi^{(0)})^2 + \left(\frac{\pi}{2W}\right)^2 \eta^{(0)}\right]\right\}_{\xi\xi}.$$

The solution of (2.50), (2.51) is posed as a Fourier series

$$\tilde{\eta} = \sum_{n=0}^{\infty} G^{(n)}(\xi)\cos\frac{n\pi Z}{W}$$

which meets the boundary conditions (2.51) automatically. The Fourier coefficients are to be determined by solving a sequence of ordinary differential equations:

$$\left[-cG^{(n)} + \tfrac{3}{2}\eta^{(0)}G^{(n)} + \tfrac{1}{6}G^{(n)}_{\xi\xi}\right]_{\xi\xi} - \tfrac{1}{2}\left(\frac{n\pi}{W}\right)^2 G^{(n)} = \mathcal{R}^{(n)} \quad (n = 0,1,2,\ldots), \tag{2.52}$$

where

$$\mathcal{R}^{(0)} = \left[\frac{6W}{\pi^2}(\eta_\xi^{(0)})^2 + \frac{1}{2W}\eta^{(0)}\right]_{\xi\xi},$$

and

$$\mathcal{R}^{(n)} = \frac{4W}{\pi^2(1-4n^2)}\left[(3\eta_\xi^{(0)})^2 + \left(\frac{\pi}{2W}\right)^2 \eta^{(0)}\right]_{\xi\xi} \quad (n = 1,2,3,\ldots).$$

Furthermore, for η to remain localized in the x-direction, we require

$$G^{(n)}(\xi) \to 0 \quad (\xi \to \pm\infty) \tag{2.53}$$

for all n.

Now the solution of (2.52) subject to (2.53) can be readily found for $n = 0$:

$$G^{(0)} = \frac{6W}{\pi^2}a_0^2(3S^4 - 2S^2) + \frac{1}{W}(S^2 - \alpha\xi RS^2), \tag{2.54}$$

where $S \equiv \operatorname{sech}\alpha\xi$, $R \equiv \tanh\alpha\xi$. The last term in (2.54) is secular and makes the expansion (2.48) non-uniform as $\xi \to \pm\infty$; however, noting that

$$\frac{\partial}{\partial a_0}(a_0 S^2) = S^2 - \alpha\xi RS^2,$$

this non-uniformity can be interpreted as a slight change in the amplitude, a_0, of the KdV solitary wave (2.49). On the other hand, we argue that, in general, one cannot find a solution of (2.52) that satisfies (2.53) for $n \geq 1$: as $|\xi| \to \infty$, the four homogeneous solutions of (2.52) behave like

$$\exp(\pm q\xi), \quad \exp(\pm ir\xi), \tag{2.55}$$

where $$q^2 = 3c + \left[9c^2 + 3\left(\tfrac{n\pi}{W}\right)^2\right]^{\frac{1}{2}}, \quad r^2 = -3c + \left[9c^2 + 3\left(\tfrac{n\pi}{W}\right)^2\right]^{\frac{1}{2}},$$

and only one of these solutions is consistent with (2.53). Accordingly, in order to find a smooth solution of the inhomogeneous equation (2.52), one needs to include a contribution from the homogeneous solutions (2.55) with oscillating behaviour as well, thus violating (2.53). Therefore, it is concluded that no solitary waves are possible for $\mathcal{A} \ll 1$; this seems to be consistent with our numerical calculations which indicate that small-amplitude oscillations, owing to cross modes corresponding to $n \geq 1$ in (2.52), appear at the tails when $\mathcal{A}$ is small. It is interesting to note that, in this respect, there is an analogy with long-wave propagation in a slowly rotating channel: solitary waves do not seem to exist in this case either, owing to the radiation of Poincaré waves which are the corresponding cross modes (Katsis & Akylas 1987*b*, Melville, Tomasson & Renouard 1989). Of course, as the perturbation theory is expected to be valid only for $\mathcal{A} \ll 1$, it is still possible that solitary waves may exist for other parameter values; for example, figure 2.7*b* suggests that perhaps such waves could be found for values of $\mathcal{A}$ around 1.

2.6 The case $\mathcal{A} < 0$

Now that different aspects of wave propagation in channels with cross-sections characterized by $\mathcal{A} > 0$ have been discussed, the corresponding studies for $\mathcal{A} < 0$ can be presented briefly.

The wavetrain that develops at the head of undular bores is similar to the disturbance that appears upstream of a forcing travelling with transcritical speeds in a channel; so, for negative values of $\mathcal{A}$, only the latter initial-value problem, equations (2.41)–(2.43), was studied. As in the previous case (§2.4), we choose $\lambda = -\mathcal{A}$ and $p_0 = 10$ and the response

is computed over the range $-1 \leq \mathcal{A} \leq 0$. For small negative values of $\mathcal{A}$, the upstream response consists of a train of waves of elevation with wave crests that dip and troughs that climb at the sidewalls as expected from wall boundary condition (2.42a); with further decrease in $\mathcal{A}$, the spanwise curvature of these waves become more exaggerated. In figure 2.8a, the upstream response for $\mathcal{A} = -0.5$ at $T = 4$, is seen to exhibit some lack of uniformity and successive crests differ slightly from one another. However, these variations are mild compared with the disordered appearance of the free surface for positive values of $\mathcal{A}$ (see figure 2.5a). In figure 2.8b for $\mathcal{A} = -1$ ($T = 4$), even the small irregularities of the wavetrain have completely disappeared. Note that the wavetrain is quite uniform but the troughs are not flat and though there may be interactions at the tails between waves in successive periods, the uniform development of the upstream waves is not disrupted. It would appear then that localized solutions (solitary waves) are not essential for a strong and uniform response to occur.

As the changes in the response discussed above were mild compared with those for positive values $\mathcal{A}$, the wave resistance results were not surprising. Figure 2.9 shows the variation of the wave resistance coefficient, C_D, defined in (2.45), for $\mathcal{A} = -1$.

Periodic waves were computed over the range $-1 \leq \mathcal{A} \leq 0$, similar to the solutions of §2.5; here, the period $2\xi_0 = 2\pi$, phase speed $c = 1.5$ and channel width $2W = 1$. The change in wave shape over this range is gradual; the strong variations that develop for positive values of $\mathcal{A}$ (figure 2.7a) do not occur. Figure 2.10 shows the solution at $\mathcal{A} = -1$. Note that the wave is not very steep, even though a wave of the same phase speed and period at $\mathcal{A} = 0$ resembles a solitary wave, having a relatively sharp, narrow crest and a broad flat trough. The decrease in steepness suggests a lessening of the effect of nonlinearity which can be understood as follows. Long, linear, two-dimensional periodic waves in channels with $\mathcal{A} = -1$ and $2W = 1$ would have a phase speed $c = 1$ according to (2.44). So as $\mathcal{A}$ decreases, to obtain steep nonlinear waves, it is necessary to increase the phase speed as well. By choosing a larger phase speed, say 3.5, it should be possible to reproduce a periodic wave of shape similar to the individual waves in the upstream response shown in

(*a*)

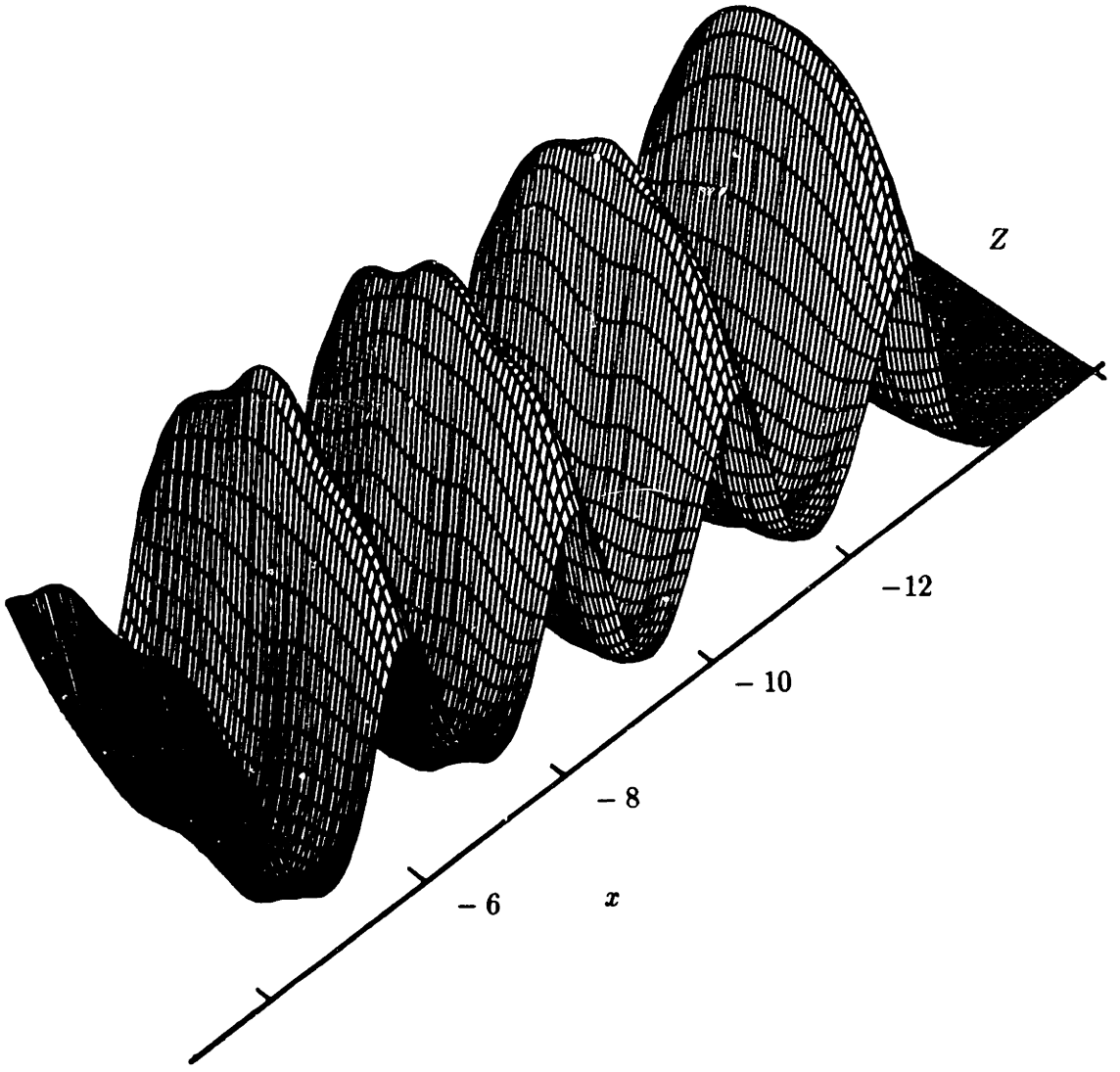

FIGURE 2.8*a* *(for caption, see following page)*

(*b*)

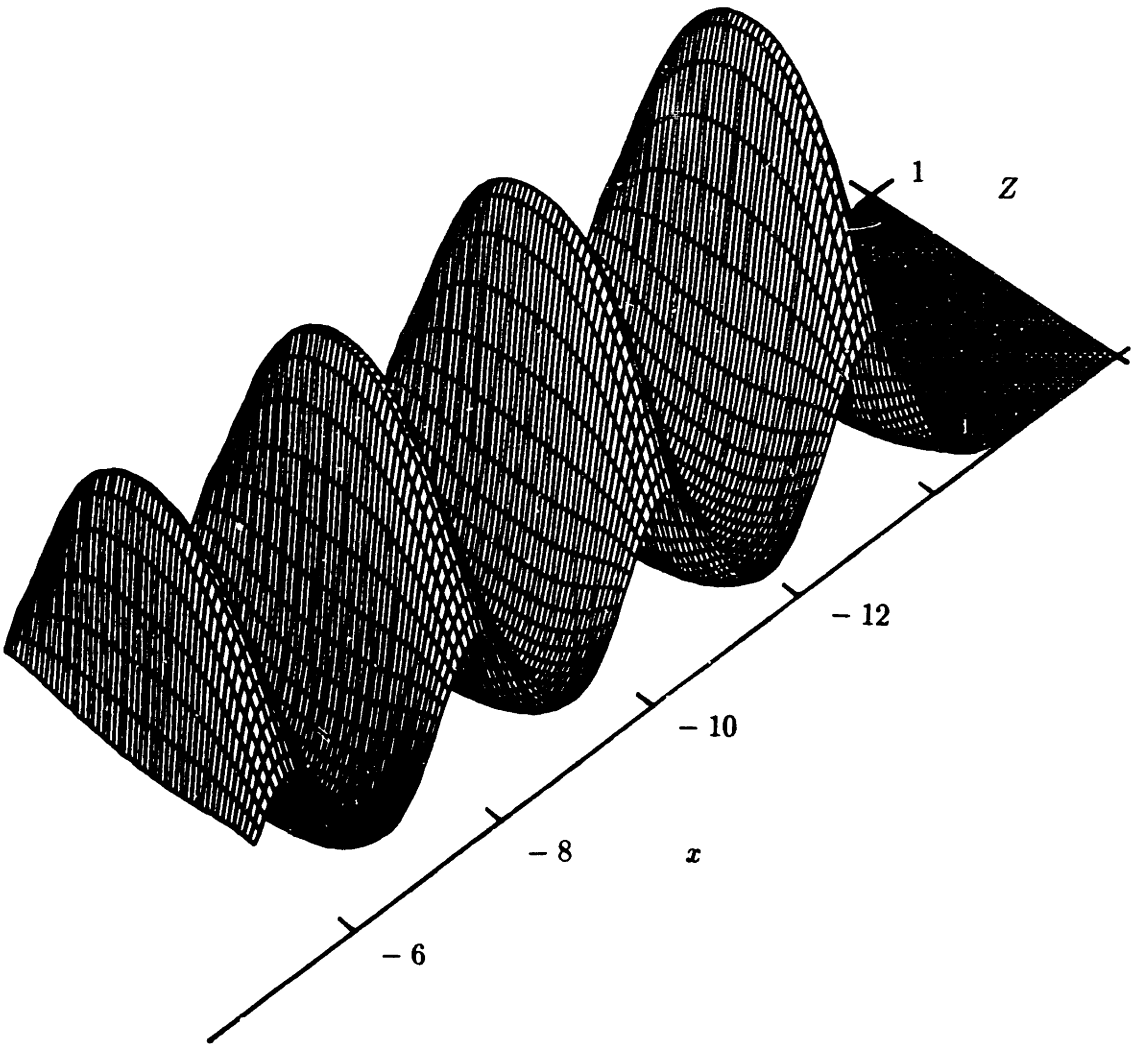

FIGURE 2.8 Upstream waves excited by transcritical forcing in channels with sloping sidewalls, at $T = 4$ and $p_0 = 10$. (*a*) $\mathcal{A} = -0.5$, $\lambda = 0.5$, (*b*) $\mathcal{A} = -1$, $\lambda = 1$.

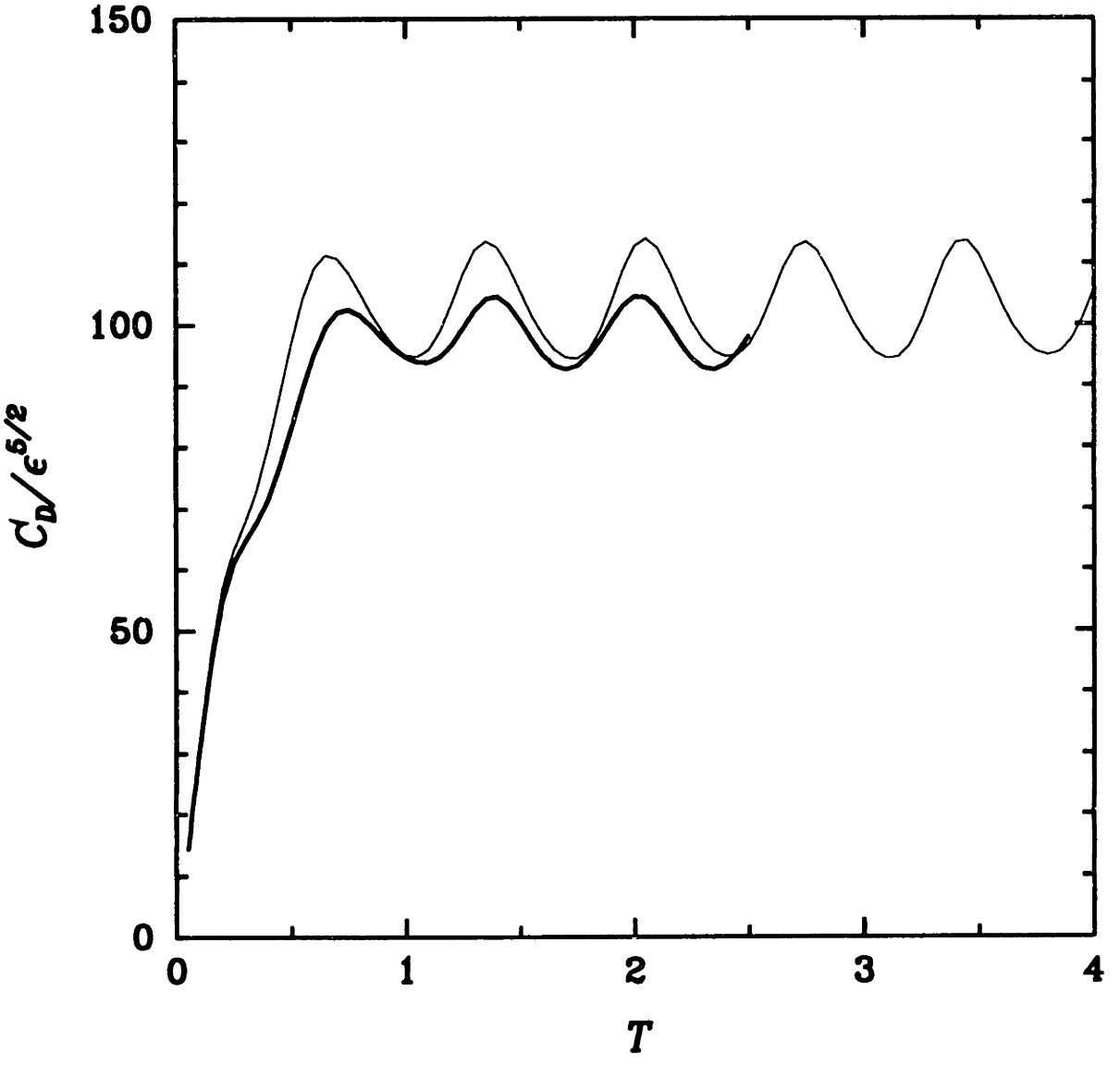

FIGURE 2.9 Variation of wave-resistance coefficient C_D with time T for $p_0 = 10$; —— : $\mathcal{A} = 0$; —— : $\mathcal{A} = -1$ ($\lambda = 1$).

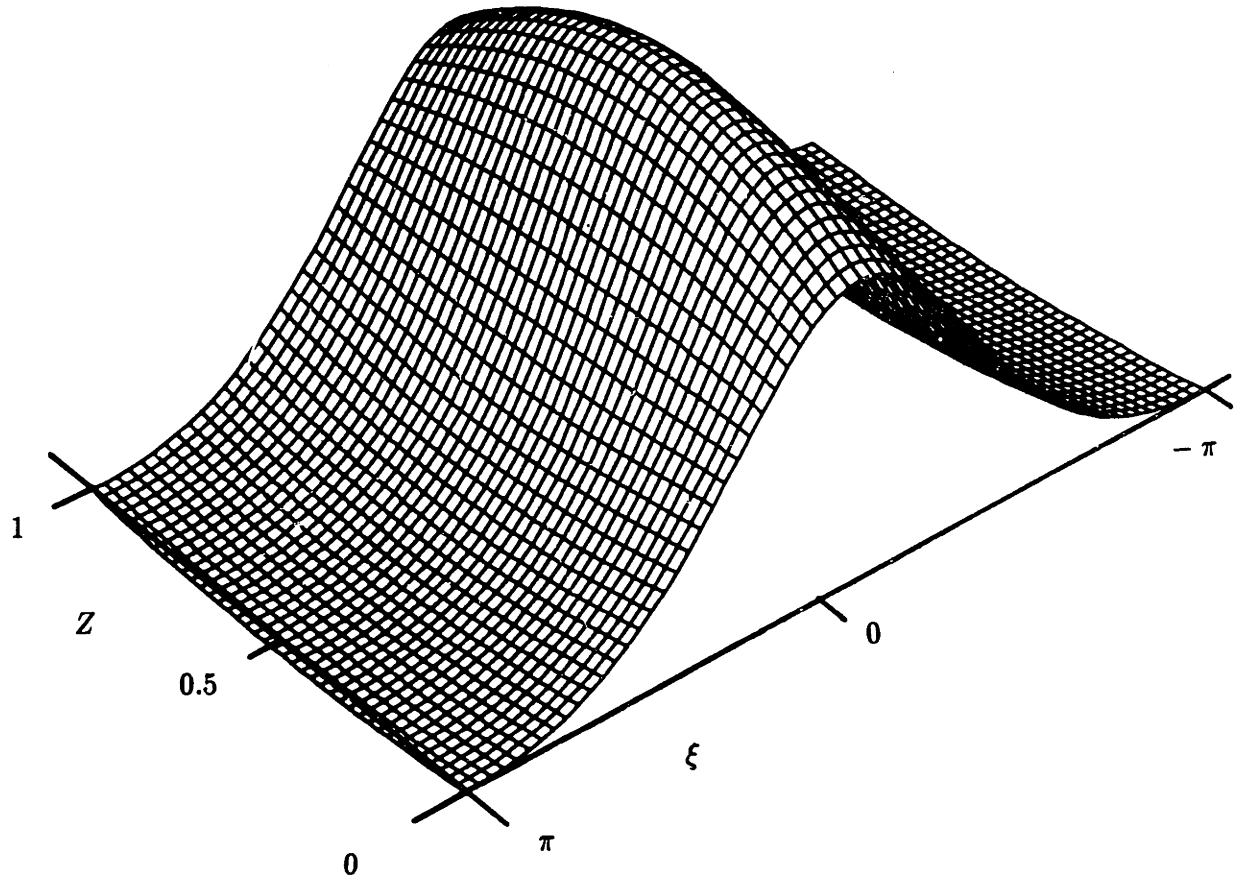

FIGURE 2.10 Wave of permanent form of period $2\xi_0 = 2\pi$, speed $c = 1.5$, channel width $2W = 1$ and $\mathcal{A} = -1$.

figure 2.8*b*. However, our goal in computing the periodic waves was less an end and more to understand the upstream response, so these calculations were not pursued further.

Finally, we note that Sandover & Taylor (1962) raised the concern, based on their experiments in channels with trapezoidal cross-sections (where $\mathcal{A}$ was positive), that the large spanwise variations in wave elevation require channel depth to be significantly larger than the mean water depth. In view of the appearance of the response in figure 2.9*b*, it is perhaps of interest in channel design that waves travelling in a channel whose cross-section is characterized by $\mathcal{A} < 0$—a simple criterion—are less likely to spill over the sidewalls.

CHAPTER 3

RADIATION DAMPING OF FINITE-AMPLITUDE PROGRESSIVE EDGE WAVES

3.1 Introduction

Edge waves are trapped waves that propagate along the shoreline of a beach and whose amplitude decays in the offshore direction. The first known solution is due to Stokes (1846; see Lamb 1945, §260) for a beach of uniform slope. Later, Ursell (1952) pointed out that additional edge-wave modes are possible depending on the slope angle α; a new mode appears as α drops below certain critical values. More recently, Whitham (1976) studied nonlinear effects in the Stokes edge wave using perturbation expansions in the amplitude. Carrying out the expansion up to third order, he found the main effect of nonlinearity to be the usual amplitude dependence in the dispersion relation, and the corrections to the edge wave to be exponentially decaying far from the shore. The fundamental mode (the Stokes edge wave), however, turns out to be exceptional: generally, weakly nonlinear periodic edge waves are expected to be attenuated by radiating oblique waves out to sea. This mechanism of radiation from travelling edge waves due to nonlinear self-interactions and the consequent radiation damping is the subject of this chapter.

To understand how edge waves can radiate oblique waves owing to finite-amplitude effects, it is useful to discuss in qualitative terms the asymptotic form far out to sea of nonlinear corrections to a linear periodic edge wave, according to a small-amplitude expansion. As usual, at each order in the expansion, a linear inhomogeneous problem needs to be solved. The forcing arises due to nonlinear interactions of the fundamental harmonic and in general includes higher harmonics which move with the wave phase speed. Accordingly, nonlinear corrections have the same harmonic behaviour as the forcing along the shoreline; to determine the offshore dependence, one then has to solve a forced boundary-value problem for each harmonic, where the forcing is trapped in the offshore direction. Far from

the shoreline, the corresponding solution, in general, consists of a particular integral that is likewise trapped, and a homogeneous solution. So the behaviour out to sea of nonlinear corrections to an edge wave depends on whether free waves, with the phase speed and longshore wavenumber of each harmonic comprising the forcing, are evanescent or propagating in the offshore direction; in the latter case, the nonlinear corrections represent oblique waves propagating away from the shoreline. Conditions under which this can be expected to occur can be readily determined by examining the dispersion relation for edge waves and that for free waves far from the shoreline. In §3.2, a few examples are considered for which edge-wave dispersion relations are known in closed form, and the appropriate conditions for radiation are derived. Of course, these are only necessary conditions and one has to examine the corresponding boundary-value problems in detail, in order to establish that radiation indeed takes place. In particular, for the Stokes edge wave on a uniformly sloping beach, studied by Whitham (1976), the forcing of the second and third harmonics, due to quadratic and cubic nonlinear interactions, happens to vanish, and therefore radiation does not occur up to third order. However, for the second edge-wave mode, quadratic nonlinear interactions lead to non-zero second-harmonic forcing and radiation occurs for the range of beach slopes $\frac{1}{18}\pi < \alpha < \frac{1}{6}\pi$. In §3.3, the amplitude of the radiated oblique wave and the decay rate of the edge wave are calculated explicitly for beach slopes in this range.

It is worth noting that, instead of the full water-wave formulation, the simpler shallow-water equations have frequently been used in previous studies of edge waves on a uniformly sloping beach on the physical grounds that these waves are confined to the vicinity of the shore where, indeed, the water depth is small. Comparisons with results from the full theory have usually supported this view; for example, even though there are discrepancies in the behaviour of nonlinear corrections far from the shore, where the water is not shallow, the amplitude dependence in the dispersion relation, predicted by the two approaches for the Stokes edge wave, is the same in the small-beach-slope limit, $\alpha \ll 1$ (Whitham 1976). Also, energy transfer from standing edge waves to waves propagating normally away from the shore, which occurs for all beach slopes, has been demonstrated in shallow water-theory

(Guza & Bowen 1976; Rockliff 1978) and validated in the full theory (Minzoni & Whitham 1977). On the other hand, as shown in §3.2, radiation of oblique waves from progressive finite-amplitude edge waves is possible only for certain ranges of finite beach slopes, and cannot be discussed using the shallow-water equations; this is an important limitation of shallow-water theory.

Earlier work (Bowen & Inman 1969; Guza & Bowen 1976; Minzoni & Whitham 1977) has demonstrated, both theoretically and experimentally, that normally incident and reflected waves on a beach are unstable to subharmonic standing edge-wave perturbations; this instability is closely related to the radiation damping of standing edge waves, mentioned above, and has been proposed as a mechanism for the generation of standing edge waves in coastal waters, which in turn lead to longshore periodic beach forms. Along similar lines, it is pointed out here that a nonlinear mechanism, reciprocal to that involved in the radiation damping of finite-amplitude edge waves, can feed energy from obliquely incident and reflected waves to progressive subharmonic edge waves. In §3.4, the details of this process are given within the framework of a shallow-water model for seas of finite depth.

3.2 Condition for radiation

A Cartesian coordinate system is chosen such that x is the offshore, y is the vertically upward and z is the longshore coordinate. All quantities are cast in dimensionless form using a typical wavelength L as the length scale, and $(L/g)^{\frac{1}{2}}$ as the time scale, g being the gravitational acceleration. The water depth, $h = h(x)$ varies in the offshore direction only and tends to a constant h_0 as $x \to \infty$. Assuming that a linear edge-wave mode exists, the corresponding velocity potential takes the form

$$F(x, y) \exp[\mathrm{i}(kz - \omega t)] + \text{c.c.}, \tag{3.1}$$

where k is the longshore wavenumber, ω is the frequency and c.c. denotes 'complex conjugate.' The dispersion relation for this trapped mode, $\omega = \omega(k)$, depends on the details of the particular beach profile; however, far out to sea ($x \to \infty$), the edge-wave mode must

also satisfy asymptotically the water-wave equations for constant depth and in particular the dispersion relation

$$\omega^2 = (k^2 + q^2)^{\frac{1}{2}} \tanh(k^2 + q^2)^{\frac{1}{2}} h_0; \tag{3.2}$$

here q is the offshore wavenumber, and, since this is a trapped mode, q is imaginary and $\omega^2 < k \tanh kh_0$. In addition to edge waves, there is also a continuous spectrum, consisting of waves that propagate far from the shoreline ($x \to \infty$), so that the corresponding offshore wavenumber is real and $\omega^2 > k \tanh kh_0$.

Now consider the problem of finding nonlinear corrections to the edge wave (3.1) by perturbation expansions in the amplitude. As noted earlier, a sequence of linear inhomogeneous boundary-value problems arises. The corresponding forcing terms are generated by nonlinear self-interactions of the edge wave and are proportional to some harmonic of the linear phase, $kz - \omega t$; for example, at second order, quadratic nonlinear interactions give rise to a second harmonic term, proportional to $\exp[i(2kz - 2\omega t)]$. The solutions of these inhomogeneous problems have the same longshore phase as the corresponding forcings so that, for the nth harmonic, say, the appropriate forced solution can be written as

$$S^{(n)}(x, y) \exp[in(kz - \omega t)] + \text{c.c.}.$$

Moreover, since the forcing is trapped close to the shoreline, this solution also has to satisfy as $x \to \infty$ (where the water depth is uniform) a dispersion relation of the form (3.2):

$$(n\omega)^2 = ((nk)^2 + q^2)^{\frac{1}{2}} \tanh((nk)^2 + q^2)^{\frac{1}{2}} h_0. \tag{3.3}$$

So, the necessary condition for radiation to occur at the nth order of the perturbation expansion (where the nth harmonic first appears) is simply that the offshore wavenumber q in (3.3) be real or, equivalently, q^2 be positive.

We now turn to a few specific examples for which analytical edge-wave solutions are known and the above condition for radiation can be made more explicit.

3.2*a* *Uniformly sloping beach*

For the classical problem of a uniformly sloping beach, Ursell (1952) found the edge-wave dispersion relation to be

$$\omega^2 = k\sin(2m+1)\alpha, \quad (m = 0, 1, 2, \ldots), \tag{3.4}$$

where α is the beach slope and the mth mode is possible if

$$\alpha < \frac{\pi}{2(2m+1)}. \tag{3.5}$$

In this case, the water depth is large out to sea, so that (3.3) becomes

$$(n\omega)^2 = ((nk)^2 + q^2)^{\frac{1}{2}}. \tag{3.6}$$

Therefore, combining (3.4)–(3.6), it is concluded that the nth harmonic is propagating in deep water ($q^2 > 0$) when the beach slope is in the range

$$\frac{\sin^{-1}(\frac{1}{n})}{2m+1} < \alpha < \frac{\pi}{2(2m+1)}. \tag{3.7}$$

According to (3.7), for any given edge-wave mode and beach slope, radiation is possible at some order in the expansion. However, as α is decreased for fixed mode number m, the order of the harmonic that first leaks energy out to sea increases and the effect is weaker. On the other hand, given α, however small, a certain harmonic can be made to radiate by increasing m. This explains the difficulty of shallow-water theory, which is expected to be a useful approximation as $\alpha \to 0$ for m fixed, in describing this radiation phenomenon.

It is important to note that (3.7) provides only a necessary condition for radiation. In particular, (3.7) indicates that the second harmonic ($n = 2$) of the fundamental edge wave ($m = 0$) can radiate to deep water when $\frac{1}{6}\pi < \alpha < \frac{1}{2}\pi$ but, as already remarked, the corresponding forcing term in the perturbation expansion vanishes and the same happens to be true for the third harmonic as well (Whitham 1976); so the Stokes edge wave remains trapped up to third order. On the other hand, for the second edge-wave mode ($m = 1$), (3.7) suggests that the second harmonic can radiate when $\frac{1}{18}\pi < \alpha < \frac{1}{6}\pi$, and this is demonstrated in detail in §3.3.

3.2 *b Shallow water*

When the water depth remains finite and shallow everywhere such that $kh_0 \to 0$, Minzoni (1976) has shown that the difficulties associated with shallow-water theory for a uniformly sloping beach are no longer present. There is a finite, discrete spectrum of edge waves and a continuous spectrum corresponding to waves of oblique incidence. Furthermore, he shows that edge-wave frequencies are bounded:

$$\omega^2 < k^2 h_0. \tag{3.8}$$

In the shallow-water limit, (3.3) reduces to

$$(n\omega)^2 = ((nk)^2 + q^2)h_0$$

and, in view of (3.8), the offshore wavenumber q is always imaginary ($q^2 < 0$) so that all harmonics are trapped. Therefore, in uniformly shallow seas, assuming that dispersive effects can be neglected altogether, finite-amplitude edge waves do not radiate.

3.2 *c Finite small depth*

When the water depth is finite but small, $kh_0 \ll 1$, dispersive effects are weak and (3.3) can be approximated as

$$(n\omega)^2 = ((nk)^2 + q^2)h_0 \,[1 - \tfrac{1}{3}((nk)^2 + q^2)h_0^2]. \tag{3.9}$$

Grimshaw (1974) showed that the dispersion relation for long edge waves in oceans of finite depth, including leading-order dispersive effects, takes the form

$$\omega^2 = k^2 h_0[1 - (\mathcal{A}^2 + \tfrac{1}{3})k^2 h_0^2], \tag{3.10}$$

where

$$\mathcal{A} = \frac{1}{h_0^2}\int_0^\infty [h_0 - h(x)]\,\mathrm{d}x$$

is the area under the beach profile and is assumed to be $O(1)$. $\mathcal{A}$ is the same quantity that appears in the wall boundary condition (2.16), obtained by extending this long-wave model to include nonlinear effects. (The difference in form is due to the use of a single length scale

L in this chapter.) If now the edge-wave dispersion relation (3.10) is substituted into (3.9), it follows that radiation of the nth harmonic is possible ($q^2 > 0$) if

$$\mathcal{A}^2 < \frac{n^2 - 1}{3}. \tag{3.11}$$

Note that this condition is qualitatively similar to (3.7) which was obtained for a uniformly sloping beach: larger values of $\mathcal{A}$ correspond physically to smaller slope angles, and for any given beach (fixed $\mathcal{A}$) radiation can occur at some order in the expansion. Radiation of oblique waves and the reciprocal mechanism of excitation of progressive edge waves by incident oblique waves will be demonstrated in detail for this case in §3.4, using the nonlinear model derived in §2.2

3.3 The second edge-wave mode

The discussion is now confined to the second edge-wave mode on a uniformly sloping beach of slope α. Assuming inviscid, irrotational flow, the governing equations, correct to second order in wave amplitude, for the velocity potential $\epsilon\Phi(x, y, z, t)$ read

$$\Phi_{xx} + \Phi_{yy} + \Phi_{zz} = 0 \quad (x \geq 0, -x\tan\alpha < y < 0), \tag{3.12}$$

$$\Phi_y + \Phi_{tt} = -\epsilon\,|\nabla\Phi|_t^2 + \epsilon\left[(\Phi_y + \Phi_{tt})\Phi_t\right]_y \quad (y = 0), \tag{3.13a}$$

$$\Phi_x \sin\alpha + \Phi_y \cos\alpha = 0 \quad (y = -x\tan\alpha), \tag{3.13b}$$

where ϵ ($\ll 1$) is a measure of wave amplitude.

In linear theory ($\epsilon = 0$), wave solutions of the form $\Phi = \Psi(x, y)\exp[\mathrm{i}(\kappa z - \omega t)]$ satisfy the eigenvalue problem

$$\Psi_{xx} + \Psi_{yy} - \kappa^2\Psi = 0 \quad (x \geq 0, -x\tan\alpha < y < 0), \tag{3.14}$$

$$\Psi_y - \omega^2\Psi = 0 \quad (y = 0), \tag{3.15a}$$

$$\Psi_x \sin\alpha + \Psi_y \cos\alpha = 0 \quad (y = -x\tan\alpha), \tag{3.15b}$$

where κ is the longshore wavenumber and ω is the frequency. It is known (see Whitham 1979, for details) that there are two kinds of eigensolutions: first, there is a discrete spectrum

consisting of a finite number of edge waves, determined by condition (3.5) on the beach slope, that satisfy the dispersion relations (3.4); the corresponding eigenfunctions can be expressed as finite sums of exponentials that decay out to sea (Ursell 1952). In particular, the second edge-wave mode for $\kappa = k$ takes the form $\Phi = F(x,y)\exp[\mathrm{i}(kz - \omega t)] + \text{c.c.}$, where

$$F(x,y) = \frac{\tan^2\alpha - 1}{4\omega\tan^2\alpha}[\exp(-kx\cos 3\alpha + ky\sin 3\alpha) + \exp(-kx\cos\alpha - ky\sin\alpha)] + \frac{1}{2\omega\tan^2\alpha}\exp(-kx\cos\alpha + ky\sin\alpha) \tag{3.16}$$

and obeys the dispersion relation $\omega^2 = k\sin 3\alpha$ with $\alpha \leq \frac{1}{6}\pi$; here $F(x,y)$ has been normalized so that the amplitude of the free-surface elevation at the shoreline, $2\omega F(0,0)$, is unity. Apart from the edge waves, there is also a continuous spectrum of waves that are obliquely incident and reflected at the shoreline with

$$\omega^2 = (\kappa^2 + l^2)^{\frac{1}{2}} \quad (0 < l < \infty);$$

relatively simple expressions for the eigenfunctions in the continuous spectrum are known only for slope angles that are fractions of $\frac{1}{2}\pi$.

3.3*a* *Solution for the second harmonic*

In order to study finite-amplitude effects on the second edge-wave mode, the corresponding velocity potential is expanded in a perturbation series

$$\Phi(x,y,z,t) = \{A(T)F(x,y)\mathrm{e}^{\mathrm{i}\theta} + \text{c.c.}\} + \epsilon\{A^2(T)S(x,y)\mathrm{e}^{2\mathrm{i}\theta} + \text{c.c.}\} + \cdots$$

whose leading-order term is proportional to the linear eigensolution (3.16); here $\theta = kz - \omega t$, and $A(T)$ anticipates the evolution on a 'slow' time scale $T = \epsilon^2 t$ owing to finite-amplitude effects. Proceeding to $O(\epsilon)$, $S(x,y)$ satisfies an inhomogeneous boundary-value problem which consists of equation (3.14) with $\kappa = 2k$, subject to the forced free-surface condition

$$S_y - 4\omega^2 S = R(x) \quad (y = 0), \tag{3.17}$$

where

$$R(x) = \mathrm{i}\frac{k^2\cos 2\alpha}{2\omega\tan^2\alpha}\{3\exp(-2kx\cos\alpha) + (2-5\cos 2\alpha)\exp[-kx(\cos\alpha+\cos 3\alpha)]\}, \quad (3.18)$$

and to the bottom boundary condition (3.15b); the forcing $R(x)$ derives from quadratic interactions of the fundamental harmonic. This problem is solved by posing $S(x,y)$ as an expansion in terms of the eigenfunctions of the discrete ($\hat{\Psi}_m(x,y)$) and the continuous spectrum ($\Psi_l(x,y)$) of the eigenvalue problem (3.14), (3.15) for $\kappa = 2k$:

$$S(x,y) = \sum_m \hat{c}_m\hat{\Psi}_m(x,y) + \int_0^\infty c_l\Psi_l(x,y)\,\mathrm{d}l; \quad (3.19)$$

thus, (3.14) and (3.15b) are satisfied automatically, and it remains to determine the coefficients $\hat{c}_m$, c_l such that (3.17) is met as well. To this end, $R(x)$ is expanded in terms of the reduced eigenfunctions $\{\hat{\Psi}_m(x,0), \Psi_l(x,0)\}$:

$$R(x) = \sum_m \hat{r}_m\hat{\Psi}_m(x,0) + \int_0^\infty r_l\Psi_l(x,0)\,\mathrm{d}l; \quad (3.20a)$$

using Green's theorem, it can be shown that these eigenfunctions form an orthogonal set,

$$\int_0^\infty \hat{\Psi}_m(x,0)\hat{\Psi}_j(x,0)\,\mathrm{d}x = \hat{P}_m\delta_{mj},$$

$$\int_0^\infty \Psi_l(x,0)\Psi_j(x,0)\,\mathrm{d}x = P_l\delta(l-j),$$

$$\int_0^\infty \hat{\Psi}_m(x,0)\Psi_l(x,0)\,\mathrm{d}x = 0,$$

$\hat{P}_m$, P_l being normalization constants, so that

$$\hat{r}_m = \frac{1}{\hat{P}_m}\int_0^\infty R(x)\hat{\Psi}_m(x,0)\,\mathrm{d}x, \quad r_l = \frac{1}{P_l}\int_0^\infty R(x)\Psi_l(x,0)\,\mathrm{d}x. \quad (3.20b)$$

Thus, substituting (3.19) and (3.20) into (3.17) and equating coefficients, $\hat{c}_m$, c_l are determined, and a formal expression for $S(x,y)$ is obtained:

$$S(x,y) = \sum_m \frac{\hat{r}_m\hat{\Psi}_m(x,y)}{2k\sin(2m+1)\alpha - 4\omega^2} + \int_0^\infty \frac{r_l\Psi_l(x,y)}{(4k^2+l^2)^{\frac{1}{2}} - 4\omega^2}\,\mathrm{d}l. \quad (3.21)$$

Attention is now focussed on the above solution in order to discuss the asymptotic behaviour of $S(x,y)$ out to sea ($x \to \infty$). To begin with, it is important to note that the integrand in (3.21) can have a pole on the real l-axis at

$$l = l_0 \equiv 2k(4\sin^2 3\alpha - 1)^{\frac{1}{2}}$$

when $$(4k^2 + l^2)^{\frac{1}{2}} = 4\omega^2 = 4k \sin 3\alpha$$

and this is possible if $\alpha > \frac{1}{18}\pi$, which is precisely the condition, derived in §3.2 *a*, for the second harmonic of the second edge-wave mode to radiate. Assuming then that $\alpha > \frac{1}{18}\pi$, the path of integration in (3.21) has to be suitably deformed around the pole at $l = l_0$ so that energy is radiated away from the shoreline. The choice of integration path, consistent with this radiation condition, is made by considering the asymptotic form of the eigenfunctions of the continuous spectrum, $\Psi_l(x, y)$, as $x \to \infty$. As already indicated, for $\alpha = \frac{\pi}{2N}$, there is a relatively simple expression for $\Psi_l(x, y)$ in terms of contour integrals (Whitham 1979; §7.6) and, using the residue theorem, one has

$$\Psi_l(x, y) = \sum_{j=1}^{N} \mathcal{H}_j^{\pm} \exp(\sigma_j^{\pm} x + \tau_j^{\pm} y) + \text{c.c.}, \tag{3.22}$$

where $$\mathcal{H}_j^{\pm} = \pm \frac{(\lambda \pm l)^N}{D_j^{\pm}},$$

with

$$D_j^{\pm} = 4lw^{2j} \prod_{\substack{p=1 \\ p \neq j}}^{N} (w^j - w^p) \left[\lambda(w^j - w^p) \pm l(w^j + w^p)\right],$$

$$\lambda = (4k^2 + l^2)^{\frac{1}{2}}, \quad w = \mathrm{e}^{\mathrm{i}\pi/N},$$

$$\sigma_j^{\pm} = -\lambda \sin \frac{j\pi}{N} \pm \mathrm{i}l \cos \frac{j\pi}{N}, \quad \tau_j^{\pm} = -\lambda \cos \frac{j\pi}{N} \mp \mathrm{i}l \sin \frac{j\pi}{N}.$$

Here $\Psi_l(x, y)$ has been normalized so that $\Psi_l(0, 0) = 1$ and the superscript $\pm$ indicates that both kinds of terms are to be included in the sum in (3.22). Therefore,

$$\Psi_l(x, y) \sim [\mathcal{H}_N^- + (\mathcal{H}_N^+)^*] \exp(\mathrm{i}lx + \lambda y) + \text{c.c.} \quad (x \to \infty).$$

Now, returning to (3.21), to ensure causality, the path of integration is indented below the pole at $l = l_0$, and, making use of the above asymptotic formula for $\Psi_l(x, y)$, the residue theorem yields

$$S(x, 0) \sim 2\pi\mathrm{i}[\mathcal{H}_N^- + (\mathcal{H}_N^+)^*] r_{l_0} \frac{4k \sin 3\alpha}{l_0} \exp(\mathrm{i}l_0 x) \quad (x \to \infty); \tag{3.23}$$

when combined with the phase function $\exp[2\mathrm{i}(kz - \omega t)]$, (3.23) indeed represents an oblique wave radiating to deep water. We remark here that the radiated wave is directed at an

angle $\tan^{-1}(4\sin^2 3\alpha - 1)^{\frac{1}{2}}$ to the shoreline, which is, curiously enough, independent of the longshore wavenumber. For more general depth variations, the direction of radiation is expected to depend on the wavenumber; for example, this is the case for the shallow-water model of §3.2*c* (see §3.4). An explicit expression for the amplitude of the free-surface elevation of the radiated wave in deep water, $\epsilon a = 4\epsilon\omega \mid S(x \to \infty, 0) \mid$, can be found by combining (3.18), (3.20*b*), (3.22) and (3.23):

$$a = 32(k\sin 3\alpha)^{\frac{3}{2}} N^{\frac{1}{2}} C \frac{\mid I^N(l_0) \mid}{l_0}, \tag{3.24}$$

where

$$C = \left[\frac{(1-(-1)^N\rho^N)(1-\rho)}{(1+(-1)^N\rho^N)(1+\rho)}\right]^{\frac{1}{2}}$$

with

$$\rho = \frac{\lambda_0 - l_0}{\lambda_0 + l_0}, \qquad \lambda_0 = (4k^2 + l_0^2)^{\frac{1}{2}},$$

and

$$\begin{aligned} I^N(l) &= \int_0^\infty R(x)\Psi_l(x,0)\,\mathrm{d}x \\ &= \mathrm{i}\frac{k^2}{2\omega}\cos 2\alpha \frac{(2-5\cos 2\alpha)}{\tan^2\alpha} \sum_{j=1}^{N} \frac{H_j^{\pm}}{k(\cos\alpha + \cos 3\alpha) - \sigma_j^{\pm}} + \text{c.c.} \end{aligned}$$

(The expression for $R(x)$ in (3.18) consists of two exponential terms but the first of them is proportional to the first edge-wave mode of wavenumber $2k$, $\hat{\Psi}_0(x,0)$, and does not contribute to $I^N(l)$ since the eigenfunctions are orthogonal.) Table 1 lists values of a for beach slopes in the range $\frac{1}{16}\pi \leq \alpha \leq \frac{1}{8}\pi$, corresponding to $8 \geq N \geq 4$, for $k = 1$; a is proportional to k. For $\alpha = \frac{1}{18}\pi$ ($N = 9$), the radiated wave is at cut-off conditions ($l_0 = 0$ so that the group velocity in the offshore direction vanishes) and, owing to a resonance phenomenon, a is infinite according to (3.24); of course, this difficulty can be remedied by allowing for slow variations of the radiated wave in the offshore direction, but the details will not be pursued here. Also, for $\alpha = \frac{1}{6}\pi$ ($N = 3$), the second edge-wave mode is at cut-off and a separate theory is needed in this case as well.

For $\alpha > \frac{1}{18}\pi$, when radiation is possible, the asymptotic behaviour of $S(x,y)$ is dominated by the contribution from the continuous spectrum (the integral in (3.21)), since the trapped modes comprising the sum in (3.21) decay exponentially out to sea. On the other

α	$a \times 10$	$\mu \times 10^3$
$\frac{1}{8}\pi$	0.920	0.71
$\frac{1}{10}\pi$	0.962	1.19
$\frac{1}{12}\pi$	0.895	1.19
$\frac{1}{14}\pi$	0.827	1.01
$\frac{1}{16}\pi$	0.814	0.80

TABLE 1. Amplitude of radiated wave a, and decay rate μ, for $k = 1$.

hand, according to the shallow-water theory, there is an infinite number of trapped modes (Eckart 1951) which form a complete set so that $S(x,0) \to 0$ as $x \to \infty$, precluding radiation for any beach slope. Of course, for fixed beach slope, the higher-order shallow-water trapped modes are not uniformly valid out to sea, and this theory cannot be used to discuss the radiation of oblique waves.

3.3*b* *Decay of edge-wave amplitude*

The finite-amplitude edge wave will be attenuated as energy is radiated out to sea. The associated decay rate can be determined by continuing the perturbation procedure to $O(\epsilon^2)$. The velocity potential at this order satisfies a linear inhomogeneous problem with forcing proportional to both the first and third harmonics. The solution to the third harmonic can be obtained in a manner similar to that employed for $S(x,y)$; radiation is now possible for still smaller slopes, $\alpha > \frac{1}{3}\sin^{-1}(\frac{1}{3})$, which condition is automatically met when the second harmonic radiates ($\alpha > \frac{1}{18}\pi$). Denoting the $O(\epsilon^2)$ correction to the first harmonic of the velocity potential as $\epsilon^2\{A^2A^*F^{(2)}(x,y)\exp(\mathrm{i}\theta) + \text{c.c.}\}$, $F^{(2)}(x,y)$ satisfies an inhomogeneous boundary value problem

$$F^{(2)}_{xx} + F^{(2)}_{yy} - k^2F^{(2)} = 0 \quad (x \geq 0, -x\tan\alpha < y < 0), \tag{3.25}$$

$$F^{(2)}_{y} - \omega^2F^{(2)} = G(x,T) \quad (y = 0), \tag{3.26a}$$

$$F^{(2)}_{x}\sin\alpha + F^{(2)}_{y}\cos\alpha = 0 \quad (y = -x\tan\alpha). \tag{3.26b}$$

The forcing $G(x,T)$ consists of three kinds of terms resulting from the slow evolution of the amplitude A_T, quadratic interactions of the basic edge-wave mode with the second harmonic, and cubic self-interactions of the edge-wave mode. In particular,

$$\begin{aligned} G(x,T) \;=\; & \frac{2\mathrm{i}\omega}{A^2A^*}A_TF + 2\mathrm{i}\omega[F_xS_x + F_yS_y + 2k^2FS] \\ & + \mathrm{i}\omega[F(S_{yy} - 4\omega^2S_y) - 2S(F_{yy} - \omega^2F_y) + RF_y] + C\{F\}, \end{aligned} \tag{3.27}$$

where $C\{F\}$ represents terms resulting from cubic interactions.

The forced problem (3.25)–(3.26) has a homogeneous eigensolution, $F(x,y)$, and, therefore, the forcing $G(x,T)$ has to satisfy an appropriate solvability condition for $F^{(2)}$ to be bounded as $x \to \infty$. Applying Green's theorem to the functions $F(x,y)$, $F^{(2)}(x,y)$ in the wedge $x \geq 0$, $-x\tan\alpha \leq y \leq 0$, this condition is found to be

$$\int_0^\infty G(x,T)F(x,0)\,\mathrm{d}x = 0, \tag{3.28}$$

and, using (3.27), leads to an evolution equation of the form

$$A_T + (\mu + \mathrm{i}\nu)A^2A^* = 0 \tag{3.29}$$

for the edge-wave amplitude $A(T)$, where μ, ν are real constants. If the second harmonic does not radiate energy to deep water as in the Stokes edge wave studied by Whitham (1976), $\mu = 0$, and ν determines the dependence of the linear dispersion relation on amplitude, but $|A|$ remains constant. On the other hand, in the presence of radiation μ is expected to be positive and the amplitude will decay according to

$$|A(T)| = \left(2\mu T + |A(0)|^{-2}\right)^{-\frac{1}{2}}. \tag{3.30}$$

Though a complete description of the evolution requires that both ν and μ be evaluated, the decay of the amplitude of the edge wave is dependent on μ only. In order to evaluate μ, note that the solution (3.21) for $S(x,y)$ is imaginary as long as the integrand in (3.21) does not have a pole on the real l-axis because $R(x)$ in (3.18), and consequently $\hat{r}_m$, r_l in (3.20*b*), are imaginary, so that the terms involving S in (3.27) are real. Furthermore, the terms resulting from cubic interactions, $C\{F\}$, in (3.27) turn out to be real as well, implying that $\mu = 0$ in the evolution equation (3.29). On the other hand, when there is a real pole and radiation occurs, the integral in (3.21) (with the integration path indented below the pole at $l = l_0$) may be split into

$$\mathrm{P}\int_0^\infty \frac{r_l\Psi_l(x,y)}{(4k^2+l^2)^{\frac{1}{2}} - 4\omega^2}\,\mathrm{d}l + \mathrm{i}\pi r_{l_0}\frac{4k\sin 3\alpha}{l_0}\Psi_{l_0}(x,y), \tag{3.31}$$

where P denotes the principal value of the integral. The first term in (3.31) is imaginary, but the second term which is the contribution from the pole is real (r_{l_0} is imaginary) and

gives rise to a non-zero value for μ. So, for the purpose of calculating μ, it suffices to take into account only the contribution of the pole in (3.31) to terms involving $S(x,y)$ in (3.27), and carry out the integration in (3.28). Since μ is proportional to $k^{\frac{5}{2}}$, in table 1 values of μ for $\frac{1}{16}\pi \leq \alpha \leq \frac{1}{8}\pi$ are given for $k = 1$. Indeed, μ turns out to be positive, consistent with the fact that the edge-wave amplitude decays by radiating oblique waves out to sea.

We remark here that the values of μ in table 1 are of the same order of magnitude as those found by Minzoni & Whitham (1977) for decay rates of standing Stokes edge waves. So, radiation damping of progressive edge waves can be expected to be about as significant as that of standing edge waves. In laboratory experiments, Yeh (1986) observed that viscous dissipation of standing edge waves completely overwhelms the expected radiation damping by nonlinear interactions; in fact, measured damping was significantly larger than that expected from theoretical considerations of viscous effects alone. A flux due to radiation was observed and moreover, Yeh (1986) notes that the damping rate diminishes gradually, suggesting that radiation contributes to damping during the initial stages of decay.

3.4 Shallow-water edge waves

We now return to the model for long waves in seas of finite depth, referred to in §3.2 *c*, and give details for the radiation damping of edge waves and the related mechanism of edge-wave excitation by obliquely incident waves.

The sea bed is assumed to have constant depth h_0 everywhere except in the vicinity of the shore. Weakly nonlinear, weakly dispersive waves that are essentially propagating along the shoreline may then be modelled by the Kadomtsev–Petviashvili equation (KP), as shown in §2.2, and, in a reference frame moving at the linear-long-wave speed in the longshore direction, the free-surface elevation $\eta(x,z,t)$ satisfies

$$\eta_{tz} + \tfrac{3}{4}(\eta^2)_{zz} + \tfrac{1}{6}\eta_{zzzz} + \tfrac{1}{2}\eta_{xx} = 0 \quad (x > 0). \tag{3.32}$$

When the beach slope is $O(1)$, the following boundary condition takes into account the effect of depth variation in the nearshore region:

$$\eta_x = \mathcal{A}\eta_{zz} \quad (x = 0), \tag{3.33}$$

where $\mathcal{A}$ is the area under the depth profile, defined in §2.3. Here variables have been scaled such that weak effects—nonlinearity, dispersion and three-dimensionality—are of equal importance. (See §2.2*a*, 2.2*b* for derivation. The difference in the sign of the first term in (3.32) and (2.7) is due to the choice of reference frames: in this instance, the reference frame travels at the linear-long-wave speed in the longshore direction; in §2.2 the reference frame is travelling at the same speed, but in the opposite direction.)

The system (3.32), (3.33) admits two kinds of linear-wave solutions of the form $\eta = H(x)\exp[\mathrm{i}(kz - \omega t)]$. There is a single edge wave

$$H = f(x) = \exp(-k^2\mathcal{A}x), \tag{3.34}$$

with the dispersion relation

$$\omega = -\tfrac{1}{2}k^3\left(\tfrac{1}{3} + \mathcal{A}^2\right). \tag{3.35}$$

In addition, there is a continuous spectrum of linear, obliquely incident and reflected waves

$$H = f_l(x) = \cos lx - \frac{k^2\mathcal{A}}{l}\sin lx, \tag{3.36}$$

with

$$\omega k = -\tfrac{1}{6}k^4 + \tfrac{1}{2}l^2 \quad (0 < l < \infty). \tag{3.37}$$

The dispersion relations (3.35), (3.37) are consistent with (3.10), (3.9) respectively, for slightly three-dimensional waves, propagating along the shoreline in a reference frame moving with the linear-long-wave speed.

3.4*a* *Radiation damping*

Following the perturbation procedure of §3.3, the free-surface elevation is expanded as

$$\eta = \epsilon\{A(T)f(x)\mathrm{e}^{\mathrm{i}\theta} + \text{c.c.}\} + \epsilon^2\{A^2 s(x)\mathrm{e}^{2\mathrm{i}\theta} + \text{c.c.}\} + \cdots. \tag{3.38}$$

The leading-order term is the linear edge-wave solution (3.34), (3.35) and, as before, $A(T)$ allows for evolution on the 'slow' time $T = \epsilon^2 t$, ϵ being a small amplitude parameter. At the next order, collecting terms proportional to $\exp(2\mathrm{i}\theta)$, it is found that $s(x)$ satisfies an inhomogeneous boundary-value problem:

$$\frac{\mathrm{d}^2 s}{\mathrm{d}x^2} + 4k^2(1 - \mathcal{A}^2)s = 6k^2\exp(-2k^2\mathcal{A}x) \quad (x > 0), \tag{3.39}$$

$$\frac{ds}{dx} = -4\mathcal{A}k^2 s \quad (x = 0) \tag{3.40}$$

with $s(x)$ bounded as $x \to \infty$. The appropriate solution to this problem is readily found to be

$$s(x) = \frac{3}{2k^2}\exp(-2k^2\mathcal{A}x) + \frac{3\mathcal{A}}{2k^2[\mathrm{i}(1-\mathcal{A}^2)^{\frac{1}{2}} - 2\mathcal{A}]}\exp[-2\mathrm{i}k^2(1-\mathcal{A}^2)^{\frac{1}{2}}x].$$

The first term is a particular integral with the same decaying behaviour as the forcing in (3.39) and the second term, which is a homogeneous solution, is added so that the boundary condition (3.40) is also met. This second term decays exponentially and the second harmonic remains trapped if $\mathcal{A} > 1$; otherwise, when combined with $\exp[2\mathrm{i}(kz - \omega t)]$, it represents an oblique wave propagating out to sea at an angle $\tan^{-1}[kh_0(1-\mathcal{A}^2)^{\frac{1}{2}}]$ to the shoreline. (Note that $kh_0 \ll 1$ in this theory and the radiated wave propagates at a very small angle to the shoreline, consistent with the assumption of weakly three-dimensional waves.) So the second harmonic radiates when $\mathcal{A} < 1$; this condition agrees with (3.11), which was deduced in §3.2*c* from heuristic arguments. Furthermore, unlike the radiation from edge waves over a uniformly sloping beach, the direction of the radiated oblique wave now depends on the longshore wavenumber k.

The evolution equation for $A(T)$ again takes the form (3.29). The coefficients μ, ν are determined by considering the inhomogeneous problem for the $O(\epsilon^3)$ correction to the first harmonic, and imposing a solvability condition. In particular, the corresponding forcing is

$$g(x,T) = \mathrm{i}\frac{1}{A^2A^*}A_T f(x) + \tfrac{3}{2}kf(x)s(x)$$

and the appropriate solvability condition, analogous to (3.28), is

$$\int_0^\infty g(x,T)f(x)\,dx = 0;$$

carrying out the integration yields

$$\mu = \frac{9}{4k}\frac{\mathcal{A}^3(1-\mathcal{A}^2)^{\frac{1}{2}}}{3\mathcal{A}^2+1}, \qquad \nu = -\frac{9}{8k}\frac{1+\mathcal{A}^2-2\mathcal{A}^4}{3\mathcal{A}^2+1}. \tag{3.41}$$

Note that, if $\mathcal{A} < 1$, $\mu > 0$ and $|A(T)|$ decays according to (3.30); on the other hand, if $\mathcal{A} > 1$, μ is imaginary,

$$\mu = -\mathrm{i}\frac{9}{4k}\frac{\mathcal{A}^3(\mathcal{A}^2-1)^{\frac{1}{2}}}{3\mathcal{A}^2+1},$$

and, combined with $i\nu$, determines the amplitude correction to the linear dispersion relation (3.35), while $|A|$ remains constant.

3.4*b* *Excitation of edge waves*

As already noted, previous theoretical and experimental work (Bowen & Inman 1969; Guza & Bowen 1976; Minzoni & Whitham 1977; Rockliff 1978) has pointed out that normally incident and reflected waves on a beach are unstable to subharmonic standing edge-wave perturbations, and this provides a nonlinear mechanism for the generation of finite-amplitude standing edge waves. Here it is shown that, through a very similar nonlinear-interaction mechanism, an obliquely incident and reflected wave can generate a finite-amplitude subharmonic travelling edge wave. This is possible in general when the condition for radiation from a progressive edge wave, discussed in §3.2, is met, but it is easiest to work out the details in the context of the present shallow-water model.

Assuming that $\mathcal{A} < 1$, an obliquely incident and reflected wave of the form (3.36) having longshore wavenumber $2k$ and frequency 2ω, where ω, k are related through the edge-wave dispersion relation (3.35), turns out to be unstable to a travelling edge-wave perturbation of wavenumber k and frequency ω. At the initial stage of the instability, the edge-wave amplitude grows exponentially, but eventually this growth is limited by finite-amplitude effects and a steady state is reached; in particular, if the incoming-wave amplitude is $O(\epsilon^2)$, the steady-state edge-wave amplitude turns out to be $O(\epsilon)$. Accordingly, in order to trace the evolution of the edge wave, the expansion (3.38) is modified to include the $O(\epsilon^2)$ incident and reflected wave:

$$\eta = \epsilon\{A(T)f(x)e^{i\theta} + \text{c.c.}\} + \epsilon^2\{[A^2 s(x) + Bf_l(x)]e^{2i\theta} + \text{c.c.}\} + \cdots, \tag{3.42}$$

where $B = O(1)$ is constant, and $f_l(x)$ is given by (3.36) with $l = 2k^2(1 - \mathcal{A}^2)^{\frac{1}{2}}$ so that (3.37) is satisfied. With this change, when the perturbation procedure is carried out, the evolution equation for $A(T)$ takes the form of (3.29) with an additional term:

$$A_T + i\tfrac{3}{2}\mathcal{A}^2 kBA^* + (\mu + i\nu)A^2A^* = 0, \tag{3.43}$$

where μ, ν are still given by (3.41). The second term in (3.43) represents the interaction of the incident and reflected wave with the edge wave, and accounts for the initial instability: for $|\ A\ | \ll 1$, the third term in (3.43) may be neglected and it is found that the edge-wave perturbation grows exponentially with growth rate $\frac{3}{2}\mathcal{A}^2 kB$ by extracting energy from the incoming and reflected wave. Eventually, as the edge wave grows to finite amplitude, radiation of oblique waves out to sea comes into play, and a steady state obtains:

$$|A| = \left(\frac{3}{2}\frac{\mathcal{A}^2 kB}{|\ \mu + i\nu\ |}\right)^{\frac{1}{2}}.$$

CHAPTER 4

NONLINEAR SHALLOW-WATER EDGE WAVES

4.1 Introduction

Stokes used perturbation expansions in wave amplitude to show that nonlinear plane periodic waves are distorted by the presence of harmonics, and that their dispersion relation is amplitude dependent. He computed solutions correct to third order for water of finite depth and up to fifth order for water of infinite depth. Moreover, he argued that the limiting case of a wave of maximum amplitude would have a sharp crest with included angle $\frac{2}{3}\pi$ (see Whitham 1974, §13.13). In recent times, it has become possible to obtain very accurate descriptions of periodic waves of almost the limiting amplitude ($d/l \approx 0.14$; d is the trough-to-crest height and l is the wavelength) using numerical methods. The stability of these waves to two-dimensional (Longuett-Higgins 1978; Tanaka 1985; Saffman 1985) and three-dimensional (McLean 1982) disturbances has been studied extensively and unexpected bifurcations of these symmetric waves into new kinds of superharmonic, asymmetric waves have been detected (Chen & Saffman 1980) at large wave amplitudes. It seemed of interest then, to study a pure three-dimensional wave of finite amplitude.

The edge wave, introduced in the previous chapter, is a suitable candidate for studying the combined effects of nonlinearity and three-dimensionality. Although it is a three-dimensional wave, the edge wave is trapped close to the shore where the water depth is small, and the simpler shallow-water theory is applicable. This has been demonstrated by comparative studies of nearshore wave phenomena using both the shallow-water and full water-wave theories (Whitham 1976; Guza & Bowen 1976; Minzoni & Whitham 1977). There is also some indication that on increasing amplitude, edge-wave shape should undergo changes different from that predicted by perturbative solutions for small amplitudes: as has been noted earlier in §3.2, linear phase speeds for edge waves are less than that of plane waves propagating in the region far out at sea; so, if the phase speed continues to

increase with wave amplitude as suggested by the leading-order correction in the perturbation theory, eventually it will reach the long-wave speed. Simultaneously, the exponential decay far out at sea will vanish and there will no longer be an edge wave. In that case, far out at sea there should be a nonlinear shallow-water wave in water of constant depth, but, such a wave cannot remain of permanent form. It is of interest then, to determine whether edge waves merely cease to exist with some limiting amplitude without the phase speed reaching the long-wave speed, or whether, perhaps, there are turning points that allow the amplitude at the shoreline to grow while the phase speed retreats to smaller values. It is known (Whitham 1976) that a three-dimensional nonlinear wave that is not trapped (its elevation tends to a finite value far out at sea) can exist when the beach face is almost vertical. So a smooth transition of the nonlinear edge wave at large enough amplitudes to a similar non-trapped wave is plausible.

In §3.2*b*, it was shown that, according to shallow-water theory, radiative damping of edge waves does not occur when the beach remains shallow everywhere and dispersive effects are neglected altogether out to sea. Therefore, it is meaningful to search for periodic finite-amplitude shallow-water edge waves of permanent form on such a beach; here the beach with exponentially decaying slope, for which Ball (1967) found an analytical linear solution is used. In §4.2, the problem is formulated and the perturbation solution for small amplitudes is derived, and in §4.3 the results of a numerical study for higher amplitudes are presented. The numerical study was not completely successful as it could not be established that the failure in the computations, beyond a certain amplitude, occurred close to a physical limiting edge wave. This study preceded those presented in chapters 2 and 3.

4.2 Analytical results

A Cartesian coordinate system is chosen with x as the longshore, y as the vertically upward, and z as the offshore coordinate. A description of the flow field is sought in terms of a two-dimensional velocity potential $\phi(x, z, t)$—in the shallow-water limit, it is assumed that the vertical component of fluid velocity is relatively small—and the free-surface elevation

$y = \eta(x, z, t)$, on a beach of depth $h(z)$. The shallow-water equations are

$$\eta_t + [(h + \eta)\phi_x]_x + [(h + \eta)\phi_z]_z = 0, \tag{4.1}$$

and

$$\phi_t + \tfrac{1}{2}\phi_x^2 + \tfrac{1}{2}\phi_z^2 + \eta = 0; \tag{4.2}$$

here the length scale L and time scale $(g/L)^{\frac{1}{2}}$, where $2\pi L$ is the wavelength and g is the gravitational acceleration, have been used to make (4.1) and (4.2) dimensionless. Linear edge waves are found as eigenfunctions of the linearized form of (4.1) and (4.2), by requiring that the solutions be regular at the shoreline $z = 0$, and vanishing as $z \to \infty$.

It is important, for the nonlinear calculations that follow, to note that the shoreline is not the straight line $z = 0$; rather, the instantaneous shoreline is located at $z = \xi(x, t)$, and this location can be determined by observing that the water depth vanishes at the shoreline:

$$h(z) + \eta(x, z, t) = 0 \quad (z = \xi(x, t)), \tag{4.3}$$

from which it follows readily, in linear theory, that

$$\xi(x, t) = -\frac{\eta}{\mathrm{d}h/\mathrm{d}z} \quad (z = 0).$$

In formulating the nonlinear problem, the zero-thickness condition (4.3) is included with the field equations (4.1), (4.2) and the instantaneous shoreline is required to satisfy the kinematic boundary condition

$$\xi_t + \phi_x \xi_x = \phi_z \quad (z = \xi(x, t)). \tag{4.4}$$

The exponential beach profile

$$h(z) = H[1 - \exp(-\sigma z)] \tag{4.5}$$

is defined by two parameters

$$H = h_0/L, \quad \sigma = B/L,$$

h_0 being the water depth far from the shore attained over a distance $O(B)$; here $\sigma = O(1)$, and shallow-water theory remains valid as $z \to \infty$ if $H \ll 1$.

4.2*a* *Linear solution*

The linear edge-wave modes for the exponential beach (4.5) were given by Ball (1967). We begin by mapping the semi-infinite region $0 \leq z < \infty$ on to a finite strip $0 \leq s \leq 1$ according to

$$s = 1 - \exp(-\sigma z), \tag{4.6}$$

so that the shoreline is at $s = 0$ and $s \to 1$ as $z \to \infty$, and look for periodic waves $\phi(s,\theta)$, $\eta(s,\theta)$ that have a phase $\theta = x - c_0 t$ with a phase speed c_0. Equations (4.1) and (4.2) are linearized assuming ϕ and η to be small, and combined by eliminating η to obtain, in the transformed variables

$$s(1-s)^2\phi_{ss} + (1-s)(1-2s)\phi_s + \frac{1}{\sigma^2}(s - \frac{c_0^2}{H})\phi_{\theta\theta} = 0. \tag{4.7}$$

The solution to (4.7) that remains bounded at the shore ($s = 0$) and vanishes as $s \to 1$ is

$$\phi(s,\theta) = (1-s)^p G(s)\sin\theta, \tag{4.8a}$$

with

$$p = \frac{1}{\sigma}\left(1 - \frac{c_0^2}{H}\right)^{\frac{1}{2}}; \tag{4.8b}$$

$G(s)$ satisfies a standard hypergeometric equation whose solution that is regular at $s = 0$ is (Abramowitz & Stegun 1964 p. 563)

$$G(s) = F(a_+; a_-; 1; s),$$

$$a_\pm = \frac{2p+1}{2} \pm \tfrac{1}{2}(1 + \frac{4}{\sigma^2})^{\frac{1}{2}},$$

and a physically acceptable solution ($G(s)$ bounded at $s = 1$) requires that

$$a_- = -n \quad (n = 0, 1, 2, \ldots).$$

Each n labels an edge wave mode and there are but a finite number of modes for a given σ, such that $p > 0$. Here, only the fundamental mode ($n = 0$, $G(s) = 1$) is needed which, on reverting to physical space, is

$$\phi(x,z,t) = \exp(-p\sigma z)\sin(x - c_0 t), \tag{4.9a}$$

$$\eta(x,z,t) = -c_0 \exp(-p\sigma z)\cos(x - c_0 t), \tag{4.9b}$$

with phase speed
$$c_0^2 = H\sigma^2 p \tag{4.9c}$$

and
$$p = \tfrac{1}{2}(1 + \frac{4}{\sigma^2})^{\frac{1}{2}} - \tfrac{1}{2}. \tag{4.9d}$$

4.2b *Weakly nonlinear solution*

As mentioned in chapter 3, weakly nonlinear effects in the fundamental edge wave over a uniformly sloping beach were studied by Whitham (1976) using both shallow-water theory and the full theory. The discrepancies noted in the shallow-water solutions were then shown to disappear by Minzoni (1976) for general beaches that remain shallow everywhere. Here, the main steps in obtaining finite-amplitude corrections to the fundamental edge wave (4.9) are presented, specializing Minzoni's (1976) analysis to the exponential beach (4.5). To begin with, let

$$\phi(z,\theta) = \epsilon\phi^{(1)}(z,\theta) + \epsilon^2\phi^{(2)}(z,\theta) + \epsilon^3\phi^{(3)}(z,\theta) + \cdots, \tag{4.10a}$$

$$\eta(z,\theta) = \epsilon\eta^{(1)}(z,\theta) + \epsilon^2\eta^{(2)}(z,\theta) + \epsilon^3\eta^{(3)}(z,\theta) + \cdots, \tag{4.10b}$$

and
$$c = c_0(1 + \epsilon^2 c_2 + \cdots) \tag{4.10c}$$

where, ϵ ($\ll 1$) is a measure of wave amplitude. The $O(\epsilon)$ correction term to the phase speed in (4.10c) is omitted as it is easily shown to be absent, while the run-up variable $\xi(x,t)$ can be found, once ϕ and η are known, using Taylor expansions of (4.3); since the solutions are perturbations to the linear problem, the domain remains $0 \leq s \leq 1$ and corrections to ξ do not affect ϕ and η.

The expansions (4.10) are substituted into (4.1) and (4.2) and, as usual, a sequence of linear problems is extracted; at each stage the pair of equations may be reduced to one for $\phi^{(n)}$ by eliminating the corresponding $\eta^{(n)}$. The leading order terms $(\phi^{(1)}, \eta^{(1)})$ are taken to be the fundamental edge-wave mode (4.9a, b). At the next order, $\phi^{(2)}$ satisfies an inhomogeneous problem with forcing proportional to the second harmonic; a solution of the

same form can be found,

$$\phi^{(2)}(z,\theta) = S(z)\sin 2\theta,$$

where $S(z)$ satisfies

$$(hS_z)_z + 4(c_0^2 - h)S = \tfrac{3}{2}[1 - (p\sigma)^2]\exp(-2p\sigma z) \quad (0 < z < \infty). \tag{4.11}$$

The solution $S(z)$ was found numerically, but the details will be postponed to the next section. It is pointed out that, for radiation (discussed in chapter 3) to occur, the homogeneous solutions of (4.11) should be oscillatory as $z \to \infty$; here $c_0^2 < H$ (p is real in (4.8)) and radiation does not occur.

Proceeding to $O(\epsilon^2)$, the inhomogeneous problem for $\phi^{(3)}$ is forced by terms proportional to both the fundamental and third harmonics. The part of the solution proportional to the fundamental harmonic will be secular unless the forcing satisfies an orthogonality condition:

$$\int_0^\infty R(z;c_2)\exp(-p\sigma z)\,\mathrm{d}z = 0. \tag{4.12}$$

The forcing proportional to the first harmonic at this order, $R(z;c2)$, contains the free parameter c_2 which ensures that condition (4.12) is satisfied, and this gives anticipated amplitude correction to the phase speed.

The perturbation method becomes increasingly difficult beyond this point, but it has been taken far enough to know how the nonlinear solution should behave at small amplitudes, as well as provide a non-singular starting point for the nonlinear calculations. There is one additional feature of these three-dimensional waves that must be noted here. The solution to $\phi^{(3)}$ that is proportional to the fundamental harmonic will be nonuniform as $z \to \infty$; Whitham (1976), and Minzoni (1976) for uniformly shallow beaches, point out that this non-uniformity can be remedied by recognizing the $O(\epsilon^2)$ correction to the fundamental mode as a Taylor expansion which can then be reversed to give a slight amplitude-dependent modification to the exponential decay. This decay rate can, however, be predicted directly from the phase speed correction: far out at sea, since the solutions are exponentially decaying, linear theory is sufficient, but waves travel at the *nonlinear* phase speed. For the linear

edge wave (4.9), the exponential decay rate is

$$p\sigma = (1 - \frac{c_0^2}{H})^{\frac{1}{2}}; \tag{4.13}$$

the decay rate, correct to $O(\epsilon^2)$, for the nonlinear problem is found by substituting the nonlinear phase speed c (from 4.10c) in (4.13):

$$p^N\sigma = (1 - \frac{c^2}{H})^{\frac{1}{2}} = p\sigma(1 - \frac{c_2 c_0^2}{Hp\sigma}\epsilon^2), \tag{4.14}$$

where the p^N is the nonlinear counterpart of p.

4.3 Numerical results

The nonlinear edge wave is found as the trapped periodic solution of (4.1)–(4.4) for the beach (4.5). A suitable form of the governing equations will be solved numerically by fixing some measure of wave amplitude, leaving the phase speed as an unknown quantity.

4.3*a* *Coordinate transformation*

The functions ϕ and η are periodic with a phase $\theta = x - ct$, where c is the phase speed of the nonlinear wave. So it is natural to turn to a Fourier spectral method to describe the dependence on θ since this would allow for the expected increase in participation of higher harmonics with increasing wave amplitude. While spectral methods may be devised for taking derivatives with respect to z also, it is simpler to use finite-difference methods. The exponential decay of the linear solution in the offshore direction indicates that a uniform grid in z is far from efficient; an efficient distribution would follow the solution more closely, with more grid points in the region of the more rapid changes. Furthermore, the offshore region is infinite in extent, $\xi(\theta) \leq z < \infty$, and has an unknown left boundary. Therefore, a coordinate transformation of the type

$$s = 1 - \exp[-p^*\sigma(z - \xi(\theta))], \tag{4.15}$$

which is more general than (4.6), is very attractive; here p^* is a free parameter that allows some control over the mapping. The region is now finite and fixed: $0 \leq s \leq 1$. Also, if $\xi(\theta)$

is dropped from the transformation (4.15), which is consistent in linear theory (infinitesimal waves), the linear edge-wave mode (4.8) becomes

$$\phi(s,\theta) = (1-s)^{p/p^*} G(s) \sin\theta.$$

If $p^* = p$, this solution varies linearly with s and any finite-difference discretization will obtain the solution accurately. We choose p^* to be slightly smaller than p, which is obtained from (4.9*d*). Then the linear solution in terms of s has a finite derivative as $s \to 1$ and, as long as the behaviour of the nonlinear wave is not very different, finite differences can be expected to represent the solution accurately.

The eigenvalue c_0 whose exact value is known from the analytical solution could be computed very accurately using the mapping (4.15) (omitting $\xi(\theta)$) and centred, second-order finite-difference formulae over a uniform grid. The mapping (4.15) with a uniform grid was then used to integrate (4.11) and subsequently (4.12), to determine the leading phase-speed correction as well as the initial guess for the full nonlinear calculations that follow.

4.3*b* *Discretization*

As indicated above, it is natural to turn to a Fourier spectral method to describe the periodic longshore behaviour, while, in the transformed coordinates, finite differences can be used in the offshore direction. The method is therefore quite similar to that used for periodic waves of the KP (§2.5) and is discussed in Appendix B. First, equations (4.1)–(4.5) are written in terms of the new coordinates θ and s. Then, η is eliminated from the mass conservation equation (4.1) and the zero-thickness condition (4.3), using the momentum equation (4.2) and its derivatives. We look for symmetric waves over one-half the period ($0 \le \theta \le \pi$) and fix the phase by specifying ϕ to be an odd function of θ; ξ and η are then even functions of θ.

On discretizing, there results a system of nonlinear algebraic equations consisting of a field equation at interior grid points $0 < \theta_i < \pi$ ($i = 0, 1, \ldots N$), $0 < s_j < 1$ ($j = 0, 1, \ldots M$),

the zero-thickness condition (4.3) and kinematic condition (4.4) applied at shoreline grid points $0 \leq \theta_i \leq \pi$, and the condition $\phi = 0$ at $s = 1$. This last condition can be incorporated into the field equations to reduce the number of unknowns. Alternately, since these are trapped waves and the amplitude is small as $s \to 1$, the exponential decay with rate $p^N\sigma$ given by (4.14) can be used to apply an asymptotic boundary condition at $s = 1 - \Delta s$, instead of the field equations:

$$\phi(\theta_i, 1 - \Delta s) = \phi(\theta_i, 1 - 2\Delta s)2^{-p^N/p^*}.$$

Both types of offshore boundary conditions were tried and found to give similar results.

A modification was introduced in order to locate a few grid points far from the shoreline, since the offshore behaviour had exhibited non-uniformities in the analytical solutions. Accordingly, the computational region was divided into three regions with different intervals between grid points, Δs_1, Δs_2 and Δs_3 given by

$$\Delta s_1 = \frac{1}{M_1} \quad (0 \leq s_j \leq 1 - \Delta s_1,\ j = 0, 1 \ldots M_1),$$

$$\Delta s_2 = \frac{s_1}{M_2} \quad (1 - \Delta s_1 < s_j \leq 1 - \Delta s_2,\ j = 1, 2 \ldots M_2),$$

$$\Delta s_3 = \frac{s_2}{M_3} \quad (1 - \Delta s_2 < s_j \leq 1,\ j = 1, 2 \ldots M_3).$$

An additional equation specifying some measure of wave amplitude is also needed. In the weakly nonlinear solution (§4.2*b*), the amplitude of the fundamental harmonic of the velocity potential, at the shoreline, is ϵ; here, this quantity ϵ is held fixed and ϕ, ξ and the phase speed c are obtained using Newton's method.

4.3*c* *Results*

According to the results for weakly nonlinear waves, the phase speed increases with wave-amplitude and the leading-order correction, from (4.10*c*), is proportional to ϵ^2. Beginning with this solution as an initial guess, numerical solutions for edge waves of higher amplitudes were calculated by Newton iteration and continuation in ϵ. At small amplitudes, the number of grid points in the θ-direction, N, can be small. At higher amplitudes, as higher

harmonics begin to participate, N must be increased to obtain an acceptable solution—one that remains smooth and does not change appreciably on increasing N.

Nonlinear edge waves were computed for two beach profiles, $\sigma = 0.5$ and 0.1, with H set to 0.1 in order to be consistent with the assumption of shallow beaches. Figures 4.1*a* and 4.1*b* show the variation in phase speed as the amplitude is increased for $\sigma = 0.5$ and 0.1 respectively; the straight lines (dotted) are the perturbation solutions correct to $O(\epsilon^2)$ and the continuous lines are the results of the numerical calculations. In both cases, there is agreement at small amplitudes, vindicating the numerical scheme, and a smooth departure with increasing amplitudes. The graphs show the maximum amplitudes upto which smooth solutions could be obtained; for $\sigma = 0.5$, this maximum amplitude is $\epsilon = 5.37 \times 10^{-2}$ obtained using $N = 25$, $M_1 = 30$, $M_2 = 10$, $M_3 = 5$, and for $\sigma = 0.5$, it is is $\epsilon = 3.18 \times 10^{-2}$ with $N = 24$, $M_1 = 30$, $M_2 = 10$, $M_3 = 5$. The free-surface elevation η corresponding to these maximum amplitudes are shown in figures 4.2*a* and 4.2*b* by drawing intersections of the wave with planes of constant s (these are not planes of constant z) at equal increments Δs_1, for one-half the period, $0 \leq \theta \leq \pi$; only a few such profiles, beginning with that at the shoreline, $s = 0$, have been shown. Clearly, the sharpening of crests and broadening of troughs, anticipated from observations of similar distortions for plane waves (Schwartz 1974), have occurred, the distortions being greatest at the shoreline where wave amplitudes are the largest. It could not be established, however, whether these solutions were close to an edge wave of maximum elevation analogous to the known limiting form for plane waves. Augmenting the algebraic system of equations with a pseudo-arc-length equation (Keller 1977) and continuation in the arc-length variable was not sufficient to negotiate past the point at which the computations failed to give a smooth solution.

The breakdown of the computations are signalled by the appearance of oscillations in the solutions at the shoreline grid points, which is known to occur when spectral schemes attempt to represent discontinuous functions (Gibb's phenomenon). This could occur, for example, as a cusp develops as in the case of plane waves, or when there is a discontinuity in the derivative which is suggested by the solution shown in figure 4.2*a*.

(*a*)

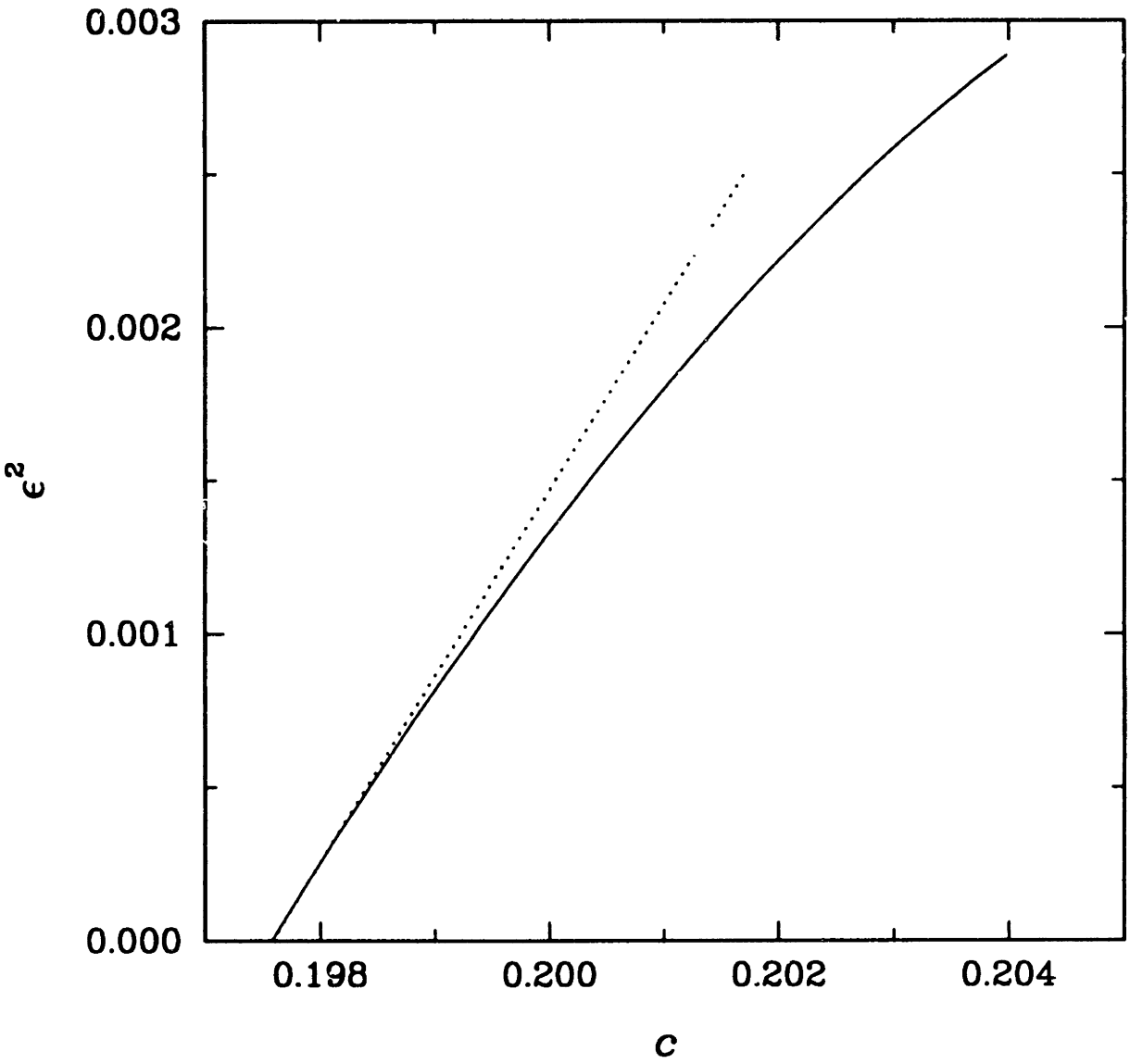

FIGURE 4.1 *a* (*for caption, see following page*)

(b)

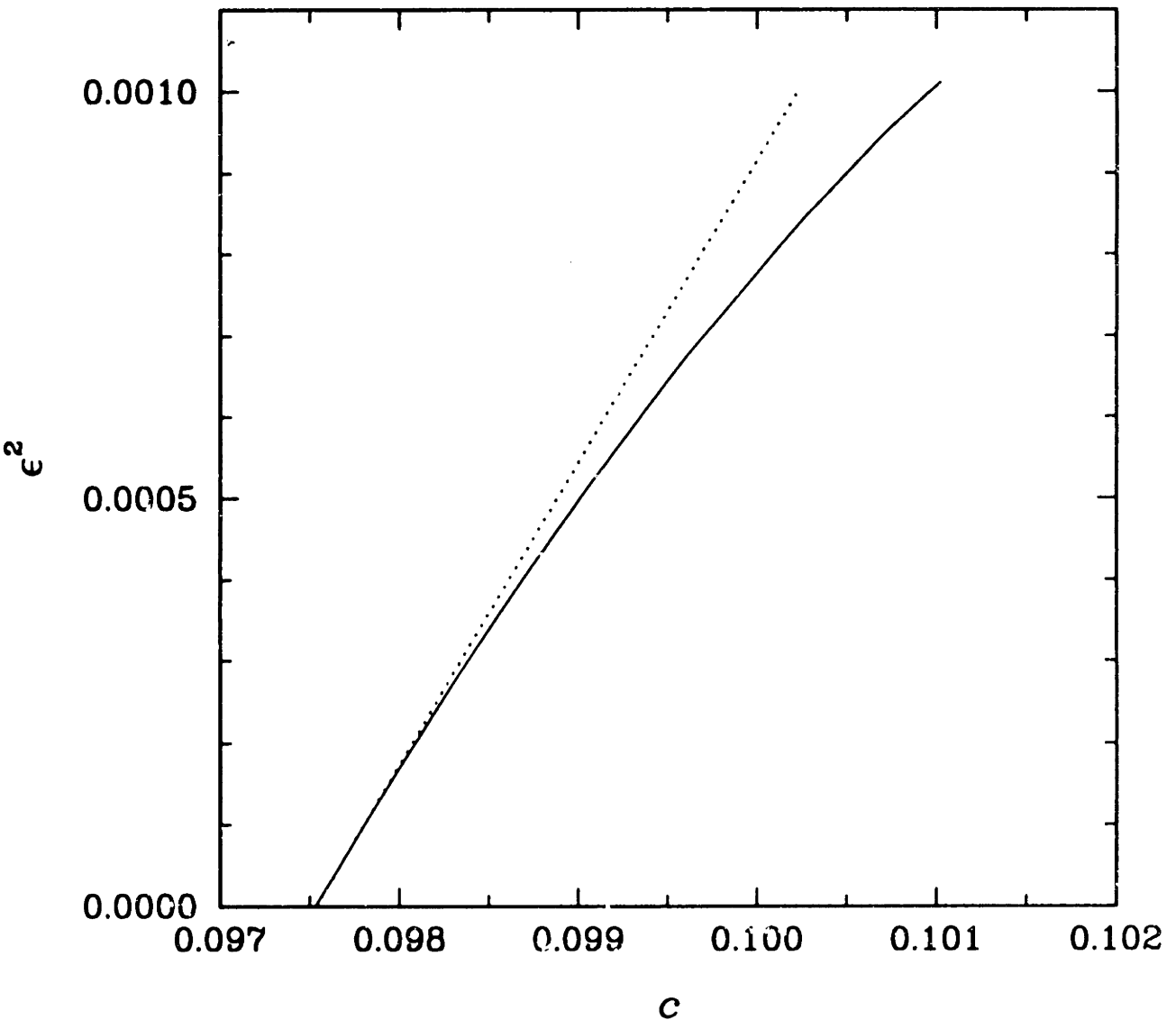

FIGURE 4.1 Variation of phase speed c with amplitude ϵ of nonlinear edge waves; ····· : analytical (weakly nonlinear), ——-: numerical. (a) $\sigma = 0.5$; (b) $\sigma = 0.1$.

(*a*)

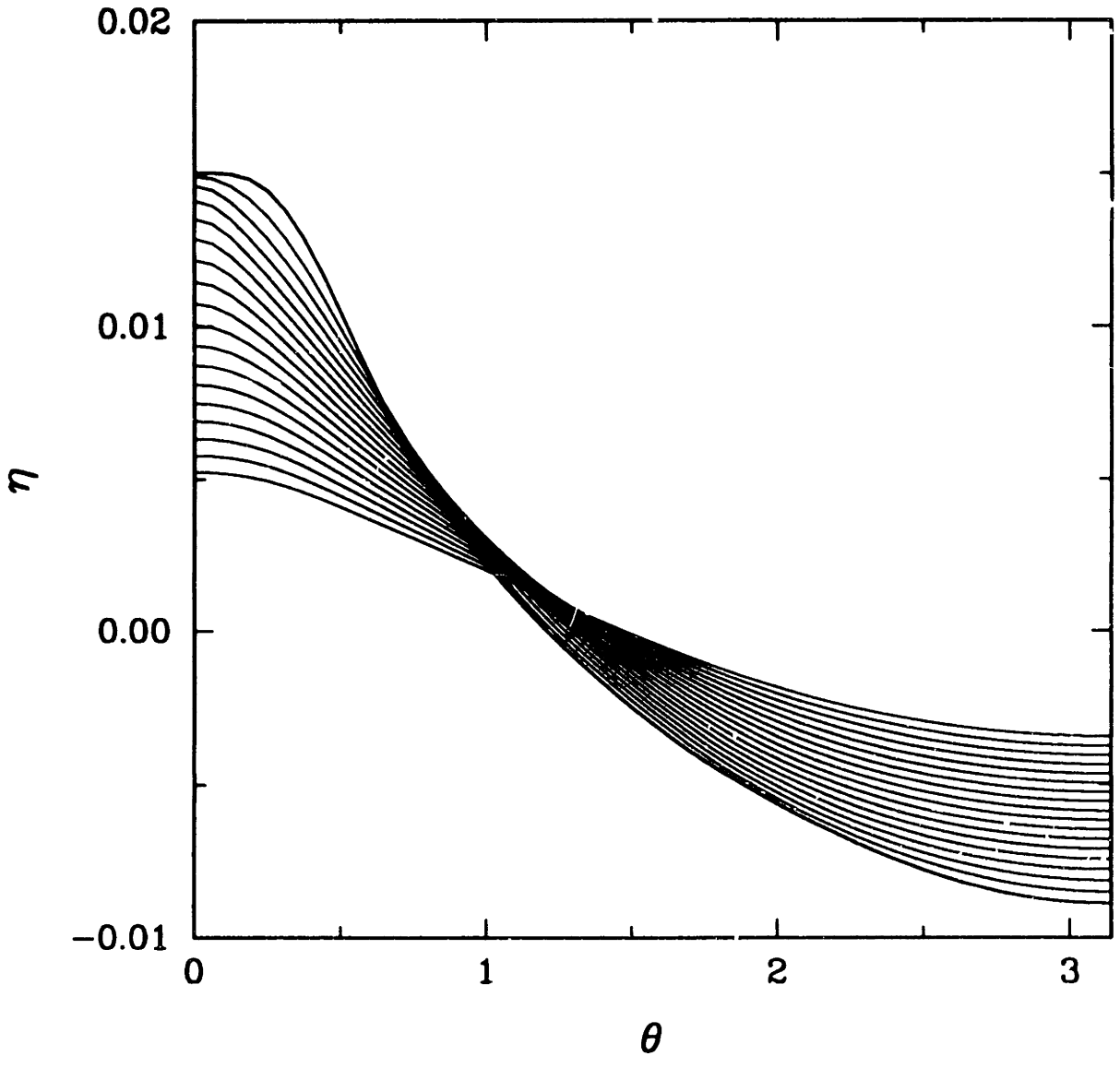

FIGURE 4.2*a* (*for caption, see following page*)

(*b*)

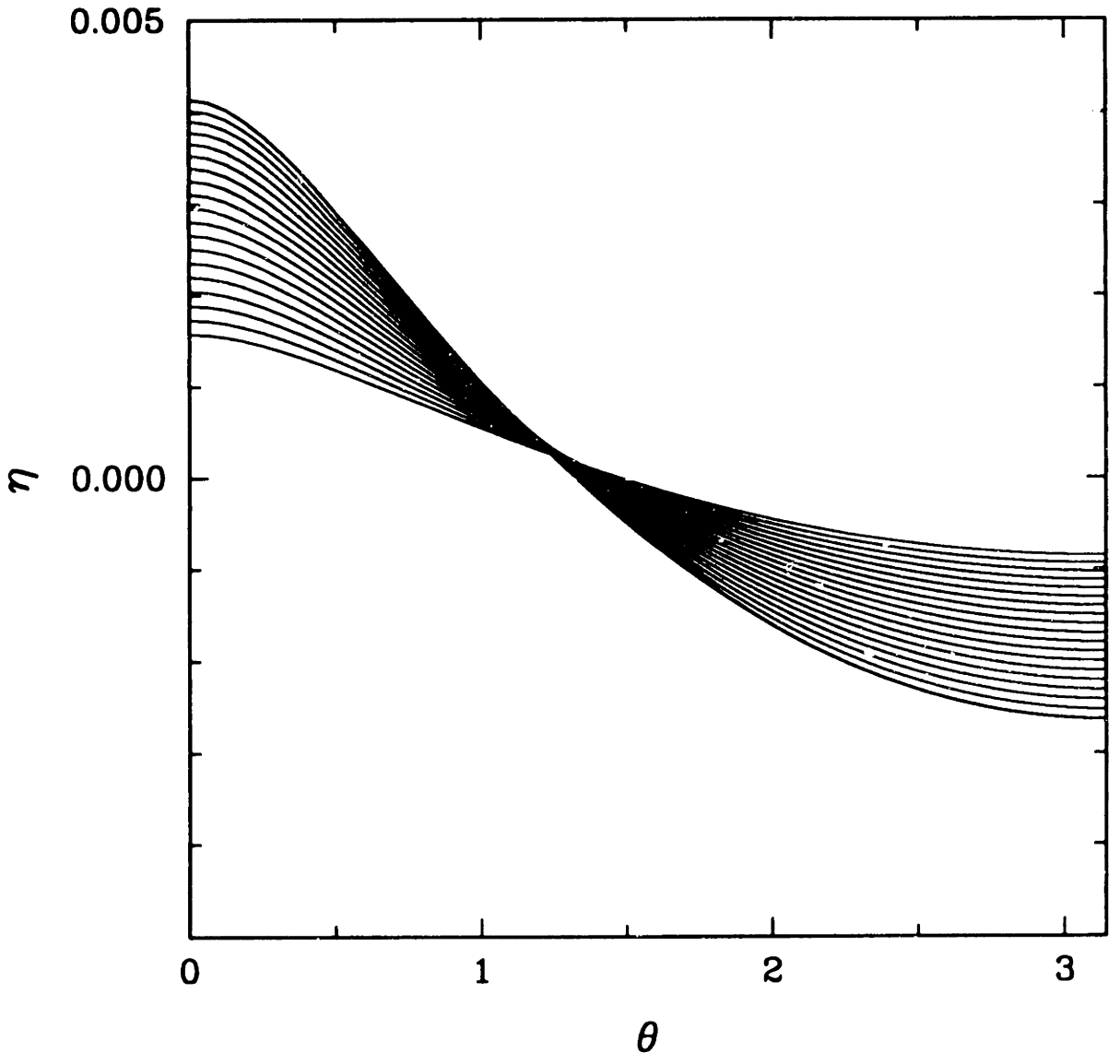

FIGURE 4.2 Intersections of the free-surface elevation of the computed nonlinear edge wave with planes of constant s. (a) $H = 0.1$, $\sigma = 0.5$, $\epsilon = 5.37 \times 10^{-2}$; (b) $H = 0.1$, $\sigma = 0.1$, $\epsilon = 3.18 \times 10^{-2}$;

CHAPTER 5

CONCLUDING REMARKS

A study has been undertaken to understand some of the ways in which nonlinear, three-dimensional waves that arise in water of varying depth distinguish themselves from their simpler counterparts: nonlinear, two-dimensional and linear three-dimensional water waves.

A relatively simple theoretical model was developed to discuss the propagation of waves in wide channels with sloping sidewalls, in the special limit that weak nonlinear, dispersive and three-dimensional effects attain a balance. In this limit, the full water-wave theory is reduced to a simpler problem (KP) with boundary conditions that prescribe the effect of depth variation at the sidewalls. In particular, when sidewall slopes are $O(1)$, the theory states that the ensuing waves are insensitive to the details of sidewall depth variations; a single parameter, $\mathcal{A}$, which is obtained from the cross-sectional area, is sufficient to characterize the effect of depth variations.

The theory was tested against previous experimental studies of undular bores and found to predict qualitative wavetrain features (such as the plateau formation near the centerline as $\mathcal{A}$ increases, and crest curvature) and to be in close quantitative agreement in the comparisons of the leading crest. Furthermore, the theory assumes channel width to be large compared with water depth and the region near sidewalls where water depth varies to be thin compared with channel width. In the experiments, the channel widths were but six to seven times the water depth and changes in depth occurred over a region that is one third to slightly less than one half the channel width. Yet, remarkably, the predictions of the theory are quite good, making it useful and indicating that three-dimensional effects become important even in channels of moderate width.

In channels of rectangular cross-section, a strong response upstream of a forcing travelling at transcritical speeds had been observed in several earlier experimental and theoretical studies. It has been supposed that the continual growth of the upstream disturbance owes to the existence of solitary waves (stable and localized solutions) of the KdV which can be supported by vertical sidewalls. Computations using the present theory show that even

in the absence of solitary wave solutions (from perturbation theory for $\mathcal{A} \ll 1$) a strong upstream response is present. Moreover, the nature of these disturbances (as well as that at the head of undular bores) depend crucially on $\mathcal{A}$; in particular, the upstream disturbance loses its uniformity as $\mathcal{A}$ is increased and then regains it as $\mathcal{A}$ approaches 1. However, the individual waves for $\mathcal{A} = 1$ are quite novel in appearance, having crests that split into a double hump towards the channel centre and possessing broad and nearly flat troughs. These changes in the response turn out to be closely related to the structure of the corresponding waves of permanent form. Also, the rather flat, broad trough of the long-period wave of permanent form for $\mathcal{A} = 1$ suggests that a three-dimensional solitary wave might exist for some special combination of channel width and phase speed with $\mathcal{A} \approx 1$.

Clearly, the theory developed here is a suitable basis for experimental studies of nonlinear three-dimensional water waves. It would be of interest, for example, to examine whether the rather sharp change in waveform that occurs as $\mathcal{A}$ approaches unity can be observed.

Although the wall boundary condition for milder slopes ($\beta = O(\epsilon^{\frac{1}{2}})$) was derived, the solutions for this case were not studied. The form of the boundary condition is intriguing. According to (2.31), the spectral components $\hat{\eta}(k, Z = 0)$ are small as $\epsilon \to 0$ unless k is close to the zeroes of the profile function $K(k)$. This is in contrast to the boundary condition (2.16) for $O(1)$ sidewall slopes, where no component $\hat{\eta}(k, Z = 0)$ is, *a priori*, vanishingly small.

Of engineering interest in the design of open channels could be the simple criterion of ensuring that $\mathcal{A}$ remains negative for the cross-section over the expected range of flows. When $\mathcal{A} = -1$, wave crests are much higher at the centerline, and since it is the integral $\mathcal{A}$ that influences wave shape and not the precise slope at the walls, structurally sound cross-sections with $\mathcal{A} < 0$ can be achieved by, for example, making the water depth at the sidewalls slightly larger than that in the central part of the channel.

From previous studies, it has been established that finite-amplitude standing edge waves are attenuated by the radiation of a second harmonic component directed normally out to sea. In the present study, it was shown using finite-amplitude expansions that progressive

edge waves can be attenuated by radiation of oblique waves out to sea, provided that a certain condition is met. According to this condition, for the case of a uniformly sloping beach, however small the beach slope, radiation from any particular edge-wave mode can occur at a sufficiently high order. So, even though the Stokes edge wave remains trapped up to third order, at the fourth or higher order radiation is expected to occur. On the other hand, radiation at a particular order, say the second order for which the effect is strongest, can occur for a sufficiently high edge-wave mode. This was demonstrated in detail for the second edge-wave mode. Radiation damping of progressive edge waves is, in this respect as well, a more complicated mechanism than in the case of standing edge waves.

In laboratory experiments of damping of standing edge waves (Yeh 1986), it was observed that the damping rates far exceeded the expected rates from theoretical considerations alone. Nonetheless, the mechanism was shown to be present from measurements of the associated flux. As mentioned in §3.3*a*, the flux associated with radiation from progressive edge waves on a uniformly sloping beach is directed at an angle that is independent of the longshore wavenumber. It is presumed, therefore, that it will be possible to detect the flux from finite-amplitude progressive edge waves even though the attenuation is likely to be masked by viscous dissipation.

It was also demonstrated explicitly, using the KP model for long edge waves on beaches that remain shallow everywhere, that a mechanism reciprocal to that involved in radiation damping can lead to the excitation and growth of a travelling subharmonic edge wave by waves obliquely incident and reflected on the beach. It should be possible to detect this in the laboratory and perhaps, in field experiments also.

The mechanism of radiation owing to self-interactions of a travelling trapped wave is not necessarily restricted to edge waves on beaches. It could arise in other contexts where there is a mixed spectrum of trapped and continuous modes and harmonics of the trapped mode are resonant with propagating modes. It is then useful to note that the possibility of radiation damping can be diagnosed easily from the linear dispersion relations for the trapped mode and that of waves far out at 'sea.'

APPENDIX A

NUMERICAL SCHEME FOR THE INITIAL-VALUE PROBLEMS

The initial-boundary-value problems of chapter 2 for the development of an undular bore and the excitation of upstream waves by an applied pressure, equations (2.33)–(2.35) and (2.41)–(2.44), respectively, were integrated numerically using a Lax-Wendroff-type scheme used previously by Katsis & Akylas (1987a) for channels of rectangular cross-section. The essential difference here is in the treatment of the wall boundary condition. We begin by writing $\eta(x, Z; T + \Delta T)$ as a Taylor expansion

$$\eta(x, Z; T + \Delta T) = \eta(x, Z; T) + \Delta T \eta_T(x, Z; T) + \frac{\Delta T^2}{2!}\eta_{TT}(x, z; T) + \cdots, \qquad (A.1)$$

and then use the differential equation to represent η_T and η_{TT} in terms of spatial derivatives alone, evaluated at T, so that (A.1) is an explicit formula for $\eta(x, Z; T + \Delta T)$. In order to find η_T, the KP (2.41) is integrated once with respect to x,

$$\eta_T = -\lambda\eta_x + \tfrac{3}{4}(\eta^2)_x + \tfrac{1}{6}\eta_{xxx} + \tfrac{1}{2}\int_{-\infty}^{x} \eta_{ZZ}(x_1, Z, T)\, \mathrm{d}x_1 \qquad (A.2)$$

using the conditions that far upstream ($x \to -\infty$) there are no disturbances for all $T > 0$. Next, by differentiating (A.2) with respect to T and then using (A.2) to eliminate η_T in the resulting equation, η_{TT} can be written in terms of spatial derivatives. Centred, second-order finite-difference formulae were used to represent these spatial derivatives of η, and the integrals, such as the one in (A.2), were evaluated using the trapezoidal rule. At all interior grid points, (A.1) is applied to obtain the solution at $T + \Delta T$, and this solution is used to update the boundary values at $Z = 0, W$ to complete the cycle of calculations at each time step.

The centerline boundary conditions (2.34*b*) and (2.42*b*) were represented using one-sided, second-order finite-difference formulae:

$$\eta(W, T + \Delta T) = \frac{1}{3}\left\{4\eta(W - \Delta Z, T) - \eta(W - 2\Delta Z, T) + \pi^{\frac{1}{2}} p_0[\exp(-x^2)]_{xx}\Delta Z\right\}, \quad (A.3)$$

setting $p_0 = 0$ for (2.34 *b*). However, the wall boundary condition (2.34 *a*) required a slightly different treatment. Since,

$$\eta_{xx}(Z = 0) = \eta_{xx}(Z = \Delta Z) - \Delta Z \eta_{xxZ}(Z = \Delta Z) + O(\Delta Z^2)$$

it is consistent to write the boundary condition (2.34 *a*) as

$$\frac{1}{\Delta Z}[\eta(Z = \Delta Z) - \eta(Z = 0)] = \mathcal{A}\eta_{xx}(Z = \Delta Z), \tag{A.4}$$

where η and η_{xx} at the interior points $Z = \Delta Z$ are known at $T + \Delta T$ from the discrete interior equations, and the truncation error is $O(\Delta Z)$. Equation (A.4) can then be used to update boundary values $\eta(Z = 0)$. Implementing the wall boundary condition in a manner analogous to (A.3) led to unstable growth of the solution. For the linearized interior equations, from von Neumann analysis, Katsis & Akylas (1987 *a*) find stability requirements to be

$$\frac{\Delta T}{\Delta x^3} < O(1), \quad \frac{\Delta T \Delta x}{\Delta Z^2} < O(1),$$

and this is a good estimate for the nonlinear computations too.

A.1 *Undular bore*

As noted in §2.3 *a*, the upstream boundary that exists owing to the finite extent of computational domain presents little difficulty, while the *ad hoc* treatment of the downstream boundary—holding η fixed as η_∞—was deemed adequate because the resulting contamination appears to be confined to a small region close to the downstream boundary. Katsis (1986) reached this conclusion based on comparisons of numerical solutions with analytical solutions; here, a representative example from the study of undular bores is given.

The calculations used to compare theory with experiments of Sandover & Taylor (1962), in §2.3 *b*, were obtained with the downstream boundary located at $x = 17.5$. In figure A.1, the change in solution, $\Delta\eta$ that results when this boundary is located at $x = 26.25$ is shown for a typical case: $\mathcal{A} = 0.5, \eta_\infty = 1.0, T = 5$. Clearly, significant errors remain confined close to the downstream boundary so that the comparisons of leading-crest properties are

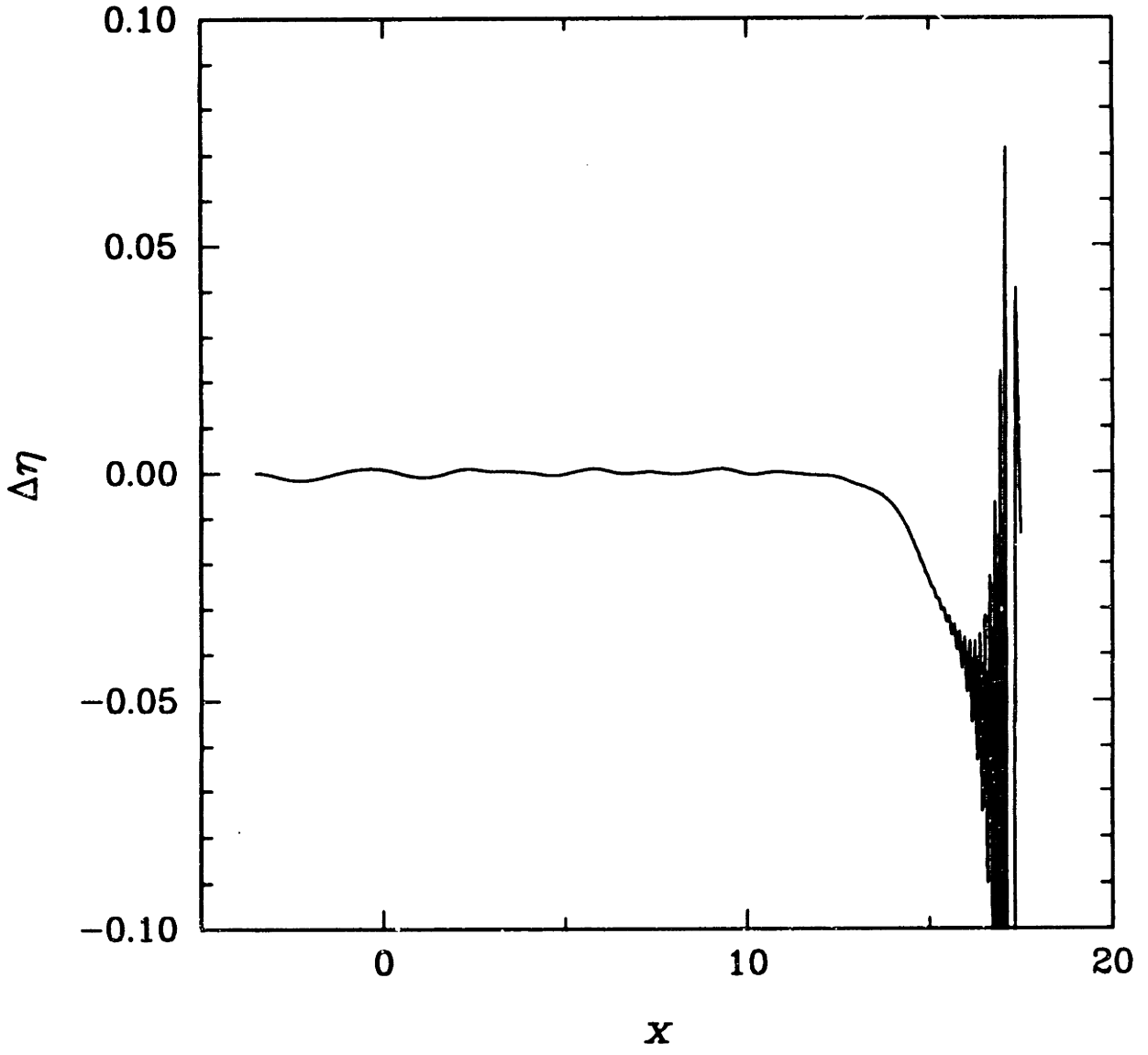

FIGURE A.1 Contamination at the downstream boundary at $T = 5$ for $A = 0.5$ and $\eta_\infty = 1$.

A	η_∞	T	$e_1 \times 10^2$	$e_2 \times 10^2$
0.5	0.75	13	6.5	0.5
0.5	1.08	12.5	1.1	0.5
0.866	0.75	10	19	0.9
0.866	1.13	9.5	4.4	1.0

TABLE 2. Variation of I_1 across channel

valid; for the case shown, the second crest occurs at $x = 7.35$. Moreover, the solutions were checked against the integral constraint (2.36). Let

$$I = \int_{x_{-\infty}}^{x_{\infty}} \eta(x, Z, T)\, \mathrm{d}x \tag{A.5}$$

and $I_0 \equiv I(T = 0)$. If $x_{\pm\infty}$ are chosen to be very large, then it follows from (2.36) that $I - I_0$ must remain small for all time and be independent of Z. In the computations, since the domain was held fixed, eventually $I - I_0$ will grow large. In table A.1, this quantity, normalized suitably by defining

$$e_1 = \max_{0 \le Z \le W} \left\{ \frac{I - I_0}{I_0} \right\}$$

is listed for a few of the cases used for the comparisons with experiments (§2.3*b*). Though e_1 is not very small, its variation across the channel does remain very small. Table A.1 lists a second quantity that measures this variation,

$$e_2 = \frac{I_{max} - I_{min}}{I_{max}},$$

where the subscripts max and min denote the maximum and minimum values that I takes across the channel.

A.2 *Forced upstream waves*

In the study of waves excited upstream by a forcing travelling at transcritical speeds, once again, errors arising from the artificial downstream boundary conditions—setting η and its derivatives equal to zero at $x = x_{\infty}$—do not significantly contaminate the upstream solution. The solutions consist of upstream waves of elevation connected by a trough, corresponding to the mass transferred upstream, to trailing small-amplitude waves (in the two-dimensional case these are modulated cnoidal waves). So, the computational domain must include at least a portion of the trailing waves as well. A criterion based on mass conservation was used to extend the downstream boundary, $x = x_{\infty}$. Since, initially, the free-surface elevation η is everywhere zero, the integral of η over the entire domain should vanish always. Beginning with a threshold value of 10^{-4} and checking every 100 time steps,

x_∞ was increased by $2\Delta x$ each time the integral of η exceeded the threshold value by more than 1%; the threshold value was then reset to the higher value. While this procedure is somewhat arbitrary, it was found to be adequate.

In this case, as the domain is extended during the course of the computations, one can expect the integral (A.5) to remain small. A slightly different measure of the error is now defined, since I_0 is zero. We take

$$\hat{\epsilon} = \max_{0 \le Z \le W} \left\{ \frac{I}{\hat{I}} \right\}$$

where $\hat{I} \equiv I(x_\infty = 0)$ so that $\hat{I}$ consists of the upstream disturbances present at time T. For the cases discussed in §2.4, $\hat{\epsilon} = 3 \times 10^{-2}$ ($\mathcal{A} = 0.5, T = 4$) and 3.4×10^{-2} ($\mathcal{A} = 1.0, T = 4$).

APPENDIX B

NUMERICAL SCHEME FOR PERIODIC WAVES

The periodic waves of the KP discussed in §2.5 and the shallow-water edge waves (§4.2) were computed using variants of a mixed Fourier spectral and finite difference scheme. In each case, the velocity potential and free-surface elevation are defined over a finite region in the spanwise coordinate Z (or s in §4.2) and is periodic in the other coordinate ξ (or θ) (in the discussion here, the period is assumed to be 2π for convenience). Second-order centred finite-difference formulae were used for derivatives with respect to Z and Fourier spectral methods for derivatives with respect to θ. The solutions were obtained over one half the period by assuming waves to be symmetrical and the phase was fixed by prescribing, for example, η to be an even function of ξ. Denoting the restriction of η on the grid as

$$\eta_{ij} = \eta(\xi_i, Z_j)$$

with

$$\xi_i = \frac{i}{N}\pi \quad (i = 0, 1, \ldots N),$$
$$Z_j = \frac{j}{M}W \quad (j = 0, 1, \ldots M),$$

derivatives with respect to ξ at ξ_n can be written as

$$\frac{\partial \eta}{\partial \xi}(\xi_n, Z_j) = \sum_{i=0}^{N} \boldsymbol{D}^{e}_{ni}\eta_{ij},$$

where $\boldsymbol{D}^{e}_{ni}$ is an $(N+1) \times (N+1)$ matrix constructed from trigonometric relations; the superscript 'e' indicates that the matrix operates on an even function. Similarly, a matrix $\boldsymbol{D}^{o}$ can be constructed to obtain derivatives of odd functions. Higher-order derivatives can be taken with corresponding matrices derived directly or from suitable products of $\boldsymbol{D}^{e}$ and $\boldsymbol{D}^{o}$. For example, the matrix $\boldsymbol{D}^{2e}$ that is used to compute second derivatives of even functions is given by

$$\boldsymbol{D}^{2e}_{ni} = \boldsymbol{D}^{o}_{nl}\boldsymbol{D}^{e}_{li}.$$

Two methods were used to compute the periodic waves of the KP. Using the matrices defined above and second-order, centred finite-difference formulae, a nonlinear algebraic system of equations was obtained from the discretization of the KP at each interior grid

point in $0 \leq \xi \leq \pi$, $0 < Z < W$ or $0 \leq i \leq N$, $1 \leq j \leq M-1$, the wall boundary condition (2.47a) at $Z = 0$ or $0 \leq i \leq N-1$, $j = 0$ and the centerline condition (2.47b) at $Z = W$ or $0 \leq i \leq N$, $j = M$. The reference level is fixed by setting $\eta = 0$ at $\xi = \pi$, $Z = 0$. In order to solve the equations by Newton's method, the Jacobian was evaluated numerically. The calculations were begun from the cnoidal waves of the KdV, which are exact solutions when $\mathcal{A} = 0$ and can be computed accurately using a Runge-Kutta integration; continuation in $\mathcal{A}$ then gives the other solutions. The shooting procedure used to verify these solutions uses the same kinds of discretizations but, instead of the matrices ($\boldsymbol{D}^e, \boldsymbol{D}^o \ldots$), fast Fourier transforms were used for computing derivatives.

The basic difference between the scheme described above and that used for the shallow-water edge wave of chapter 4 is that, in implementing Newton iteration for solving the nonlinear system, which results from discretization, the Jacobian was constructed analytically. This is, of course, the chief reason for using the matrices, $\boldsymbol{D}^e$ and $\boldsymbol{D}^o$, rather than fast Fourier transforms.

REFERENCES

ABRAMOWITZ, M. & STEGUN, I. A. 1964 *Handbook of Mathematical Functions.* Washington, D. C. National Bureau of Standards.

ABLOWITZ, M. J. & SEGUR, H. 1981 *Solitons and the Inverse Scattering Transform.* Philadelphia, SIAM.

AKYLAS, T. R. 1984 On the excitation of long nonlinear water waves by a moving pressure distribution. *J. Fluid Mech.* **141**, 455–466.

AKYLAS, T. R. 1988 Nonlinear forced wave phenomena. In *Nonlinear Wave Interactions in Fluids* (ed. R. W. Miksad, T. R. Akylas & T. Herbert) ASME AMD–Vol. 87 p. 157.

BALL, F. K. 1967 Edge waves in an ocean of finite depth. *Deep-Sea Res.* **14**, 79–88.

BOWEN, A. J. & INMAN, D. L. 1969 Rip currents II. Laboratory and field observations. *J. Geophys. Res.* **74**, 5479–5490.

BOWEN, A. J. & INMAN, D. L. 1971 Edge waves and crescentic bars. *J. Geophys. Res.* **76**, 8662–8671.

CHEN, B. & SAFFMAN, P. G. 1980 Numerical evidence for the existence of new types of gravity waves of permanent form on deep water. *Stud. Appl. Math.* **62**, 1–21.

DAVID, D., LEVI, D. & WINTERNITZ, P. 1989 Solitons in shallow seas of variable depth and in marine straits. *Stud. Appl. Math.* **80**, 1–23.

ECKART, C. 1951 Surface waves in water of variable depth. *Marine Physical Lab. Scripps Inst. Ocean Wave Report* 100-99.

FOTEKIN, R. C., WEBSTER, W. C. & WEHAUSEN, J. V. 1984 Ship-generated solitons. *Proc. 15th Symp. Naval Hydrodyn., Hamburg*, 347–364.

FENTON, J. D. 1973 Cnoidal waves and bores in uniform channels of arbitrary cross-section. *J. Fluid Mech.* **58**, 417–434.

FORNBERG, B. & WHITHAM, G. B. 1978 A numerical and theoretical study of certain nonlinear wave phenomena. *Phil. Trans. R. Soc. Lond.* A **289**, 373–404.

GRIMSHAW, R. 1974 Edge waves: a long-wave theory for oceans of finite depth. *J. Fluid Mech.* **62**, 775–791.

GUREVICH, A. V. & PITAEVSKII, L. P. 1974 Nonstationary structure of a collisionless shock wave. *Sov. Phys.-JETP.* **38**, No. 2, 291–297.

GUZA, R. T. & BOWEN, A. J. 1976 Finite amplitude edge waves. *J. Mar. Res.* **34**, 269–293.

GUZA, R. T. & INMAN, D. L. 1975 Edge waves and beach cusps. *J. Geophys. Res.* **80** 2997–3012.

KATSIS, C. 1986 An analytical and numerical study of certain three-dimensional nonlinear wave phenomena. Ph. D. thesis, Department of Mechanical Engineering, MIT.

KATSIS, C. & AKYLAS, T. R. 1987*a* On the excitation of long nonlinear water waves by a moving pressure distribution. Part 2. Three-dimensional effects. *J. Fluid Mech.* **177**, 49–65.

KATSIS, C. & AKYLAS, T. R. 1987*b* Solitary internal waves in a rotating channel: A numerical study. *Phys. Fluids* **30**, 297–301.

KIRBY, J. T., PHILIP, R. & VENGAYIL, P. 1987 One-dimensional and weakly two-dimensional waves in varying channels: numerical examples. In *Nonlinear Water Waves.* (ed. K. Horikawa & H. Maruo) pp. 357–364, Springer–Verlag.

LAMB, H. 1945 *Hydrodynamics.* Dover.

LEE, S. J., YATES, G. T. & WU, T. Y. 1989 Experiments and analyses of upstream-advancing solitary waves generated by moving disturbances. *J. Fluid Mech.* **199**, 569–593.

LIGHTHILL, M. J. 1978 *Waves in Fluids.* Cambridge University Press.

LONGUETT-HIGGINS, M. S. 1978 The instabilities of gravity waves of finite amplitude in deep water. I. Superharmonics. *Proc. R. Soc. Lond.* A **360**, 471–488.

MCLEAN, J. W. 1982 Instabilities of finite-amplitude water waves. *J. Fluid Mech.* **114**, 315–330.

MELVILLE, W. K., TOMASSON, G. G. & RENOUARD, D. P. 1989 On the stability of Kelvin waves. *J. Fluid Mech.* **206**, 1–23.

MINZONI, A. A. 1976 Nonlinear edge waves and shallow-water theory. *J. Fluid Mech.* **74**, 369–374.

MINZONI, A. A. & WHITHAM, G. B. 1977 On the excitation of edge waves on beaches. *J. Fluid Mech.* **79**, 273-287.

MUNK, W., SNODGRASS, F. & CARRIER, G. 1956 Edge waves on the continental shelf. *Science* **123**, 127–132.

PEREGRINE, D. H. 1966 Calculations of the development of an undular bore. *J. Fluid Mech.* **25**, 321–330.

PEREGRINE, D. H. 1968 Long waves in a uniform channel of arbitrary cross-section. *J. Fluid Mech.* **32**, 353–365.

PEREGRINE, D. H. 1969 Solitary waves in trapezoidal channels. *J. Fluid Mech.* **35**, 1–6.

ROCKLIFF, N. 1978 Finite amplitude effects in free and forced edge waves. *Math. Proc. Camb. Phil. Soc.* **83**, 463–479.

SAFFMAN, P. G. 1985 The superharmonic instability of finite-amplitude water waves. *J. Fluid Mech.* **159**, 169–174.

SANDOVER, J. A. & TAYLOR, C. 1962 Cnoidal waves and bores. *La Houille Blanche* **17**, 443–455.

SCHWARTZ, L. W. 1974 Computer extension and analytic continuation of Stokes' expansion for gravity waves. *J. Fluid Mech.* **62**, 553–578.

SMYTH, N. F. 1986 Modulation theory solution for resonant flow over topography. *Proc. R. Soc. Lond.* A **409**, 79–97.

TANAKA, M. 1985 The stability of steep gravity waves. *J. Fluid Mech.* **156**, 281–289.

URSELL, F. 1952 Edge waves on a sloping beach. *Proc. R. Soc.* A **214**, 347-358.

WHITHAM, G. B. 1974 *Linear and Nonlinear Waves.* Wiley–Interscience.

WHITHAM, G. B. 1976 Nonlinear effects in edge waves. *J. Fluid Mech.* **74**, 353–368.

WHITHAM, G. B. 1979 *Lectures on Wave Propagation*, Tata Institute of Fundamental Research, Bombay, Springer.

Wu, T. Y. 1987 Generation of upstream advancing solitons by moving disturbances. *J. Fluid Mech.* **184**, 75–99.

Yeh, H. H. 1986 Experimental study of standing edge waves. *J. Fluid Mech.* **168**, 291–304.